

Final Report

AE3200 DSE

Airlifting Containers



Final Report

AE3200 DSE

by

Airlifting Containers

H. Aalbers	(1361635)	J.Q. Star	(4235061)
A.D. Doedijns	(1384430)	F.P. van Steijn	(4229622)
S.C.M. Dutrieux	(4139615)	R.P.M. van der Sommen	(4187040)
J.A.M. van Kester	(1507249)	A.J. Tluk	(4111613)
H.H. Krijnen	(1361686)	R.A.A. Wiskie	(4228936)
K.B.E. Nieuwenhuisen	(4205405)		

January 26, 2016

Assignment by the Royal Netherlands Air Force



Group:	02 - Airlifting Containers	
Project duration:	November 9, 2015 – February 1, 2016	
Supervisors:	Ir. J.A Melkert,	Chairman/principal tutor
	D.S. Blom,	Coach
	J. Krishnasamy	Coach

Preface

This is the final report of group 2 – Airlifting Containers as a part of the the Design Synthesis Exercise. The Design Synthesis Exercise is the final bachelor project conducted by students at the faculty of Aerospace Engineering of TU Delft. In ten weeks time, a conceptual and preliminary design for a real aerospace project is conducted by a group of eleven students. The purpose of this exercise is to gain experience with all steps and aspects of a design project. Furthermore, the engineering and system engineering skills learnt and knowledge gained during the bachelor study are applied and shown to be of adequate level to the supervisors.

The assignment for this Design Synthesis Exercise is to design an unmanned and autonomous military cargo container transportation system for the Royal Netherlands Air Force (RNLAf). This assignment comes from the Aerospace Cluster, which combines the resources of the RNLAf, TU Delft, NLR, aerospace companies and research institutes. This cluster focuses on knowledge development, production & application in the field of (military) Aerospace.

This report is intended to finalise the project and present the final concept to the Aerospace Cluster. Knowledge of prior reports is recommended, but not a prerequisite to understand the main points. To give a short summary of the previous reports, specifically the different concepts explored and the final trade-off, a chapter has been included to bring everyone up to speed. Also, basic (aerospace) engineering knowledge can be advantageous to understand all details.

We would like to express our gratitude to our principal tutor Ir. J.A. Melkert for answering our questions and our coaches D.S. Blom and J. Krishnasamy for their guidance during this Design Synthesis Exercise project. Finally, we want to thank the Royal Netherlands Air Force for this challenging design problem and their cooperation and guidance over the course of the project.

*Airlifting Containers
Delft, January 2016*

Harm Aalbers

Bram Doedijns

Sarah Dutrieux

Jethro van Kester

Hielke Krijnen

Kyle Nieuwenhuisen

Quinten Star

Floris van Steijn

Régis van der Sommen

Alexander Tluk

Rodney Wiskie

Summary

During military operations in foreign countries, supplies like provisions, spare parts and equipment are needed. The transportation of all these goods is a major undertaking for armed forces. It is rendered even more difficult as military bases are often situated far from airports or docks. The territory might be hostile and the areas hard to reach. The majority of the goods is transported in standard 20 ft containers. These containers are shipped by boat to the nearest dock or by plane to the nearest airport. From there the containers are transported in a convoy of trucks. These trucks usually take multiple days to cover 150 km. This way of transport is inefficient and costly. Also, during this time the goods, military equipment, but most importantly personnel can be subjected to hostile attacks. Therefore, the Royal Netherlands Air Force (RNLAf) is looking for an autonomous, unmanned aviation solution. Such a solution would improve the transportation time and increase the safety. The main requirements that are set by the RNLAf for this aviation solution are that the vehicle shall be unmanned, autonomous and able to take-off and land vertically. It shall deliver a payload of 5,000 kg over a distance of at least 250 km and return without fuelling. This should be realised for a unit cost of € 500,000 and an operational cost of 0.25 €/kg/100 km.

In compliance with the requirements, several design options were considered. The toughest requirement turned out to be the unit cost. Market analysis showed that a more realistic unit price was in the range of several millions. This led to several unorthodox concept designs, of which the best one was selected by a trade-off. The winning concept entered the detailed design phase and was worked out further. The resulting design is the HELLCAT: a helicopter with eight rotors, driven by eight General Motor LT4 V8 Small-Block engines. The LT4's are high performance car engines generating 485 kW of power each and 851 Nm of torque while having a mass of 300 kg. The engines are pushed to their limits during take-off and landing and thus maintenance is vital.

Given the power and torque from the engine, the optimal number of rotor blades can be determined. All rotors have two blades with a radius of 4 m. All forces acting on the rotor blades are calculated using blade element theory. The blades are linearly twisted and composed of two different airfoils for optimal lift production. The HELLCAT can be controlled by changing the collective pitch of the blades. The drag of the structure is larger than the drag caused by the container. Therefore, the structure is optimised for drag by creating non load bearing ultra light fairings.

The HELLCAT has a cruise speed of 42 m/s and has a service ceiling of 4,450 m (14,600 ft). The power required is highest during vertical take-off, which limits the rate of climb to 2 m/s. The rate of climb increases as the forward speed increases. With a forward velocity of 4 m/s, the rate of climb becomes 8 m/s. The fuel needed for the mission is calculated to be 2,000 kg, which leads to a fuel cost of 0.09 €/kg/100 km. The total operational cost then becomes 0.20 €/kg/100 km. The distance the HELLCAT can travel without payload is 700 km, which is called the ferry range.

The structure is designed to be as simple and light as possible. The structure only has to connect the rotors with the container as the HELLCAT is unmanned. The main structure consists of four rectangular beams of aluminium, creating a tic-tac-toe like structure. The beams are placed on top of each other and the container is connected by cables to the four intersections.

Using the equations of motion the stability of the HELLCAT is calculated and a control system was designed. The craft creates a forward velocity by increasing the pitch on the aft rotors and thus pitching the thrust vector forward. The roll is controlled by changing the pitch of the rotor blades on the left or right side. Yaw is controlled by pitching only the anticlockwise or clockwise rotating rotors and thus creating a change in angular momentum about the vertical axis. The engine is the most unreliable element of the craft. The design is such that even for the highest load case an engine can fail without the loss of the cargo or the HELLCAT.

The biggest challenge during the design phase was keeping the weight under 16,000 kg, as the powerplants are not capable of producing more lift. Especially due to the large amount of engines, the costs and weight increases fast, because all engines need the same systems. Another challenge is to get the engines certified for aviation standards, because the engines are made for cars. The HELLCAT is the first of its kind. Therefore, getting the control and stability correct and working with only changing the collective pitch was a risk. A first analysis shows promising results, but still remains a risk in further development.

The next step should be the testing of the engine, as the design strongly depends on this. At the same time a more detailed research in the stability and control should start. The HELLCAT could possibly be used by other countries who face the same problem. Even some harbours or companies involved in transporting containers could be interested. The next phase would be ordering and manufacturing the parts, test and assemble the craft. Finally, the HELLCAT should be tested and certified.

Contents

Preface	iii
Summary	v
List of Abbreviations	ix
List of Symbols	xi
1 Introduction	1
2 Summary Previous Reports	3
2.1 Requirements	3
2.2 Design Options	4
2.3 Design Concept Trade-Off	5
3 Mission Analysis	7
3.1 Functional Flow Diagram	7
3.2 Functional Breakdown Structure	10
3.3 Operation Logistics	13
3.4 Ground Operations	14
3.5 Typical Mission Profile	14
3.6 Flight Operations	15
3.6.1 Following the Flight Plan	15
3.6.2 Precision Landing and Take-Off	15
4 Propulsion and Power	17
4.1 Power Plant System	17
4.1.1 Recommendations	20
4.2 Performance	22
4.2.1 Power Calculations	22
4.2.2 Service Ceiling	25
4.2.3 Fuel Calculations	25
4.2.4 Verification and Validation of the Performance Model	26
5 Structures	27
5.1 Overall Rotor and Structure Configuration	27
5.2 Attachment System	28
5.3 Material Selection	30
5.3.1 Material Selection Process	30
5.3.2 Beam Material Selection	31
5.3.3 Landing Gear Material Selection	33
5.3.4 Aerodynamic Fairing Material Selection	33
5.4 Structural Analysis and Design	34
5.4.1 Assumptions, Notes and Failure Modes	34
5.4.2 Structural Analysis Tool	36
5.4.3 Design of the Main Structure	39
5.4.4 Design of the Landing Gear	46
5.4.5 Design of Landing Pads	49
5.4.6 Shock Dampers	51
5.5 Production Plan	51
5.6 Results	53
5.7 Recommendations	55

6	Aerodynamics	57
6.1	Rotor Characteristics	57
6.1.1	Airfoil Selection	57
6.1.2	Optimum Twist	58
6.1.3	Cost Estimation	60
6.1.4	Rotor System Design	62
6.2	Blade Element Theory	64
6.2.1	Calculating the Blade and Free Stream Air Angles and Velocities	64
6.2.2	Lift, power and drag determination at varying pitch angles	65
6.2.3	Speed Limitations for the Rotor	66
6.2.4	Influence of azimuth variations on the performance of the blade	66
6.3	Parasitic Drag Calculations	69
6.3.1	Main Structure Drag	69
6.3.2	Cable Drag	71
6.3.3	Container Drag	71
6.3.4	Engine Drag	71
6.3.5	Vertical Drag Estimation in Hover	72
6.4	Aerodynamic Moments	73
6.5	Verification and Validation	74
6.6	Recommendations	75
7	System, Control & Operations	77
7.1	Equations of Motion of the HELLCAT	77
7.1.1	Reference Frames	77
7.1.2	Rotational Equations of Motion	77
7.1.3	Translational Equations of Motion	78
7.1.4	Simplified Equations of Motion	78
7.2	Simulation	79
7.2.1	Physical Model	79
7.2.2	Physical Model Verification	79
7.3	Control of the UAV	80
7.3.1	Attitude Control	81
7.3.2	Verification Controller	83
7.3.3	Lateral Control	84
7.3.4	Engine Failure	84
7.3.5	Centre of Gravity Limits	84
7.4	Navigation and Avionics	86
7.4.1	Attitude and Accelerations	86
7.4.2	Navigation	86
7.4.3	Surrounding Awareness	87
7.4.4	Data Processing and Communication	87
7.4.5	Avionic Configuration	88
7.4.6	Deviations from Standard Procedures	88
7.4.7	Additional Avionic Systems	89
8	Interface Definition	91
8.1	Electric Block Diagram	91
8.2	Communication Flow Diagram	91
9	Risk Management	95
9.1	Risk Identification and Assessment	95
9.2	Risk mitigation	98
10	Sustainability	101
10.1	End of Life Disposal and Material Recyclability	101
10.2	Fuel Emissions	101
10.3	Noise	102

11 RAMS	103
11.1 Reliability	103
11.2 Availability.	103
11.3 Maintainability	103
11.4 Safety	104
11.5 Certification	104
12 Mass Breakdown of the UAV	105
12.1 Mass Breakdown of the Aerodynamic Subsystem	105
12.2 Mass Breakdown of the Propulsion and Power Subsystem	105
12.3 Mass Breakdown of the Control and Stability Subsystem	106
12.4 Mass breakdown of the UAV Structure	106
12.5 Mass Breakdown of the UAV per Subsystem	107
13 Cost Analysis	109
13.1 Cost Breakdown	109
13.2 Operational Cost	111
13.3 Development and Production Cost	111
13.4 Market Analysis.	113
14 Post DSE	115
14.1 Project Design Development Logic	115
14.2 Gantt Chart	115
15 Compliance Matrix and Feasibility Analysis	119
16 Conclusions	125
17 Recommendations	127
Bibliography	129

List of Abbreviations

Acronym	Description
2D	Two dimensional
3D	Three Dimensional
ACARS	Aircraft Communications Addressing and Reporting System
ALC	Air Lifting Container
ATB	Air Throttle Body
BET	Blade Element Theory
BR	Baseline Report
CAD	Computer Aided Design
CER	Cost Estimating Relationship
CFD	Computational Fluid Dynamics
CG	Centre of Gravity
CON	CONstraint
COS	COSt
CPDLC	Controller Pilot Data Link Communication
DAPCA	Development and Procurement Cost of Aircraft
DGPS	Differential Global Positioning System
DSE	Design Synthesis Exercise
EASA	European Aviation Safety Agency
ECU	Engine Control Unit
ENV	ENVironment
EO/IR	Electro-Optical/Infrared
EOL	End of Life Solution
EOM	Equation Of Motion
FAA	Federal Aviation Administration
FBD	Free Body Diagram
FBS	Functional Breakdown Structure
FC	Fuel Consumption
FCO	Flight Control & Operations
FFD	Functional Flow Diagram
FLC	FLight Control
FPE	Flight PErformance
FR	Final Report
FW	Fuel Weight
GIL	Gobal Interpreter Lock
GM	General Motors
GPS	Global positioning system
H	High
IED	Improvised Explosive Device
IGE	In-Ground-Effect
IMU	Inertial Measurement Unit
INDI	Incremental Non-linear Dynamic Inversion
IR	Infrared
ISA	International Standard Atmosphere
ISO	International Organization for Standardization
L	Low
LIDAR	Light Detection and Ranging
M	Medium
MT	Momentum Theory

MTOW	Maximum Take-Off Weight
MTR	Mid-Term Report
NAV	NAVigation
NDI	Non-linear Dynamic Inversion
NLR	Netherlands Aerospace Centre
OEW	Operational Empty Weight
OO	Object Oriented
PCF	Product Complexity Factor
PDF	Production Development Factor
PID	Proportional, Integral and Differential
PIDD	Proportional, Integral and Differential (2 nd derivative)
PLO	PayLOad
PP	Project Plan
PW	Payload Weight
RADALT	Radio Altimeter
RAM	Reliability, Availability, Maintainability and Safety
RAMS	Reliability, Availability, Maintainability and Safety
RDT&E	Research, Development, Test and Engineering
RNLAF	Royal Netherlands Air Force
RTK	Real Time Kinematic
SAE	Society of Automotive Engineers
SAF	SAFety
SD	Scenario Dependant
SFC	Specific Fuel Consumption
SONAR	Sound Navigation And Ranging
SST	SuSTainability
SYS	SYStem
TCAS	Traffic Alert and Collision Avoidance System
TDL	Tactical Data Link
TU Delft	Technische Universiteit Delft
UAV	Unmanned Aerial Vehicle
UHF	Ultra High Frequency
VH	Very High
VL	Very Low
VR	Vertol
VTOL	Vertical Take-Off and Landing
WEA	WEAther
WEI	WEIght

List of Symbols

Symbol	Description	Unit
a_{Blade}	Acceleration Blade	rad/s ²
$a_{Structure}$	Acceleration Blade	rad/s ²
A	Cross-sectional area	m ²
A_m	Enclosed area	m ²
B	Control matrix	—
b_{sk}	Width of plate	m
C	Constant	—
C_{DP}	Profile drag coefficient	—
c_m	Moment coefficient	N m
c_T	Thrust coefficient	N
d	Distance from origin	m
d_{Blade}	Diameter Blade	m
ds	Differential length ds	m
dx	Differential length dx	m
E	Young's modulus	N/m ²
f	Equivalent flat plate	m ²
g	Gravitational constant	m/s ²
H_s	Height between attachment drag strut and structure	m
I	Moment of Inertia	m ⁴
I_{yy}	Moment of Inertia around the yy-axis	m ⁴
I_{zz}	Moment of Inertia around the zz-axis	m ⁴
I_{Blade}	Moment of Inertia Blade	kg m ²
$I_{Structure}$	Moment of Inertia Structure	kg m ²
J	Matrix second mass moment of inertia	kg/m ⁴
J_r	Mass moment of inertia of the rotor	kg/m ⁴
k	Induced power factor	—
k	Spring constant	N/m
k	Effective length factor	—
L	Beam length	m
L_{Beam}	Beam length	m
$L_{rotorbeam}$	Length between rotors	m
$L_{perpendicularbeam}$	Length perpendicular beam	m
L	Moment around the x-axis	N m
M	Moment around the y-axis	N m
M	Figure of Merit	—
M_y	Moment around the y-axis	N m
M_z	Moment around the z-axis	N m
m	Mass	kg
m_{Beam}	Mass	kg
m_{Blade}	Mass	kg
N	Internal normal force	N
N_p	Number of points on the cross-section	—
N_{rot}	Number of rotors	—
N_x	Number of finite elements along beam span	—
n	Buckle mode	—
n_{max}	Maximum load factor	—
P_{climb}	Climbing power	W

P_{cr}	Critical buckle load	N
$P_{compressive}$	Compressive load	N
P_{engine}	Available power per engine	W
$P_{induced}$	Induced power	W
$P_{parasite}$	Parasite drag power	W
$P_{profile}$	Profile drag power	W
$P_{required}$	Power required to keep constant rotor RPM	kW
P_{tip}	Beam tip load	N
p	Aircraft roll angle in earth fixed frame	rad
p	Distance from web to shear centre	m
\dot{p}	Aircraft roll rate in earth fixed frame	rad/s
\ddot{p}	Angular acceleration in roll in earth fixed frame	rad/s ²
q	Aircraft pitch angle in earth fixed frame	rad
q_b	Open section shear flow	N/m
q_s	Closed section shear flow	N/m
\dot{q}	Aircraft pitch rate in earth fixed frame	rad/s
\ddot{q}	Angular acceleration in pitch in earth fixed frame	rad/s ²
R	Range	m
R_{blade}	Blade distance from rotor axle	m
R_{ferry}	Ferry Range	km
\mathbf{R}	Rotation matrix	—
r	Rotor disk radius	m
r	Aircraft yaw angle in earth fixed frame	rad
\dot{r}	Aircraft yaw rate in earth fixed frame	rad/s
\ddot{r}	Angular acceleration in yaw in earth fixed frame	rad/s ²
S_a	Allowable stress amplitude	N/m ²
$S_{a,0}$	Allowable stress amplitude required for fatigue failure	N/m ²
S_{blade}	Surface area of the blade element	m ²
S_m	Mean stress	N/m ²
S_u	Ultimate stress of the material	N/m ²
SF	Safety Factor	—
SFC	Specific Fuel Consumption	kg/s
s	Length around the cross-section	m
T	Thrust	N
T	Torsion	N m
$T_{Aerodynamic}$	Aerodynamic Torque	N m
T_{Engine}	Aerodynamic Torque	N m
T_{Net}	Aerodynamic Torque	N m
\mathbf{T}	Transformation matrix	—
t	Thickness of the cross-section	m
t_{sk}	Plate thickness	m
t_{top}	Top plate thickness	m
$t_{mission}$	Mission time	s
t_{web}	Web plate thickness	m
\mathbf{u}	Control input vector	—
V_{tip}	Blade tip velocity	m/s
V_y	Internal shear flow in y-direction	N
V_z	Internal shear flow in z-direction	N
v_{blade}	Blade rotational velocity	m/s
v_{copter}	Helicopter velocity	m/s
v_{eff}	Blade effective velocity	m/s
v_i	Blade induced velocity	m/s
$v_{i_{hover}}$	Blade induced velocity in hover	m/s
v_r	Resultant velocity	m/s
W	Weight	N
W_s	Width between drag strut and main strut	m

X	Force in x	N
x	x coordinate from the centre point	m
Y	Force in y	N
y	y coordinate from the centre point	m
Z	Force in z	N
z	z coordinate from the centre point	m
δ	Beam deflection	m
ϵ	Beam elongation	m
ζ	Inclination angle of rotor with the horizon	rad
θ	Local pitch angle	rad
θ	Aircraft pitch angle in body frame	rad
θ	Twist angle of the beam	rad
$\dot{\theta}$	Aircraft pitch rate in body frame	rad/s
$\ddot{\theta}$	Angular acceleration in pitch in body frame	rad/s ²
μ	Advance Ratio	—
ν	Poisson ratio	—
Ω	Rotational rate of the rotor	rad/s
ω	Angle velocity	rad/s
ρ	Air density	kg/m ³
ρ	Material density	kg/m ³
σ	Blade solidity	—
σ	Normal stress	N/m ²
σ_b	(yield) Bearing strength	N/m ²
σ_{cr}	Critical normal stress	N/m ²
σ_f	(yield) Tensile strength	N/m ²
σ_s	(yield) Shear strength	N/m ²
τ	Shear stress	N/m ²
τ_{rotor}	Torsion created by the rotor blade	N/m
ϕ	Aircraft roll angle in body frame	rad
$\dot{\phi}$	Aircraft roll rate in body frame	rad/s
$\ddot{\phi}$	Angular acceleration in roll in body frame	rad/s ²
ψ	Azimuth angle of rotor blade	rad
ψ	Aircraft yaw angle in body frame	rad
$\dot{\psi}$	Aircraft yaw rate in body frame	rad/s
$\ddot{\psi}$	Angular acceleration in yaw in body frame	rad/s ²
Ω_r	Angular velocity of the rotor	rad/s

1 Introduction

A military base in a foreign country needs many different kind of supplies. For example provisions, spare parts, military equipment and much more. The transportation of all these goods is a major undertaking. It is rendered even more difficult as military bases are often situated far in land (a few hundred kilometres), in possibly hostile territory and hard to reach (by road) areas.

At present, the majority of the goods to be transported are first containerised in standard ISO 20 ft containers. These containers are then shipped to a nearby transport hub, often a port. From there two options are used in general by the military. Either transport the containers further by road using military cargo convoys or transport them further by air. Transportation by road is dangerous as there is a significant chance of getting hit by Improvised Explosive Devices (IED's) or fall subject to hostile attacks. The military personnel involved could get harmed or worse even lose their lives. Furthermore, due to these safety concerns, the slow speed of the convoys trucks (relative to transportation by air) and the inhospitable terrain, it can take many days to reach the final destination. Transportation by air is the method of choice for goods that are time-critical or perishable by nature. It is both safer and faster than transportation by road. At the moment it is less efficient from both a (direct and indirect) cost and fuel perspective, because the aircraft currently used for this purpose could be better deployed to fulfil other mission objectives for which they were specifically designed.

Therefore, the Royal Netherlands Air Force (RNLAf) wants to research whether a new airborne solution is possible to overcome these shortcomings. This design problem has been given to this team, through the Aerospace Cluster. The Aerospace Cluster is a research group from the RNLAf specifically created for the sharing of knowledge and directing research for the needs of the RNLAf. The Aerospace Cluster consists among others of the Nederlands Lucht- en Ruimtevaartcentrum (NLR), Fokker Technologies, Airbus Defence and Space Netherlands and the Technical University Delft (TU Delft).

The purpose of this report is to show the path taken from conceptual design to a more detailed design and showing that a system is plausible that can comply with the following requirements. The system should be able to fly unmanned and autonomously. It should be able to carry at least 5,000 kg payload over a distance of 250 km and return without payload. This should be done without refuelling. Also, it should be faster than transportation by road and preferably cheaper. With the added challenge of being able to deliver the system for a unit cost of maximum € 500,000.

This report is the last in a series of four, but is still readable on its own. The second chapter is a short recap of the previous reports and shows how this concept came to be. The third chapter is about the power and propulsion of the rotorcraft, it describes the engines, fuel system, flight performance and the fuel calculations. After that the aerodynamics are explained in chapter four. It shows how the airfoil of the blades is chosen and how the drag of the system is calculated. Chapter five is all about how the optimum structure is chosen from the main structure to the landing gear and the container attachment system. The last chapter describing the design is about the stability, control and simulation. It shows the equations of motion and how these form the input for the control system. It shows how the rotorcraft can be controlled by only changing the collective pitch on one or more rotors. After that the navigation and avionics systems needed to operate the rotorcraft autonomous and unmanned are described. The following chapters are about risk management, sustainability, RAMS (Reliability, Availability, Maintainability and Safety) and certification, mass breakdown, cost analysis and post Design Synthesis Exercise (DSE) activities. The next chapter shows the compliance matrix, which shows a list of the requirements and if they are met. Finally, the last chapter provides the conclusions and recommendations.

2 Summary Previous Reports

Prior to this report several other reports were written during the course of this Design Synthesis Exercise: The Project Plan (PP), the Baseline Report (BR) and the Mid-term Report (MTR) [1–3]. In this chapter a short summary of the relevant parts of these previous reports is given. This is to ensure that nearly no prior knowledge is required to understand the main points of this report. The Project Plan gives an overview of the entire project. All the tasks that need to be completed are described and put in a logical order. This allows for a structured start of the project and encourages an efficient way of working. Since this report is purely about the organisation of the team and the project, it is not further mentioned in this Final Report.

The Baseline Report focused on several aspects, but the most important and relevant purpose of this report is the analysis of the requirements. The top-level and driving requirements are summarised in Section 2.1. The Mid-term Report shows the conceptual design process. The concepts and design option are described in Section 2.2 and the trade-off that decided which design is the best is given in Section 2.3.

2.1. Requirements

The main part of the Baseline Report [2] is to establish the requirements. The requirements are divided over multiple categories. These categories are the top-level-, performance-, constraints- and driving requirements. The top-level requirements, the most important requirements, were set by the RNLAf and do not depend on the different design solutions. If the top-level requirements are not met, the mission must be re-evaluated and feedback from the client must be gained. The driving requirements are a summary of the most important requirements from the other categories. These driving requirements require extra attention, especially in the design trade-off, because the design could be driven in the wrong direction when they are not met. The top-level requirements are shown in Table 2.1 and the driving requirements in Table 2.2.

Table 2.1: Top-Level Requirements

Requirement	Description
ALC-PLO-WEI-01	The aircraft shall be able to lift 5,000 kg of payload
ALC-PLO-CON-01	The aircraft shall be able to attach a 20 ft standard container
ALC-FLC-FPE-04.1	The aircraft shall be able to transport the payload over 250 km and return without this payload
ALC-FLC-FPE-04.2	The aircraft shall be able to fulfil the mission without refuelling
ALC-FLC-FCO-01	The aircraft shall be able to take off vertically
ALC-FLC-FCO-02	The aircraft shall be able to land vertically
ALC-FLC-FCO-03	The aircraft shall be autonomous
ALC-FLC-FCO-04	The aircraft shall be unmanned
ALC-ENV-WEA-05	The aircraft shall be able to withstand temperatures ranging from -50°C to 60°C
ALC-COS-01	The unit price shall be no more than € 500,000
ALC-COS-02	The operational costs shall be no more than 0.25 €/kg/100 km
ALC-COS-03	The development costs shall be within the Royal Netherlands Air Force development budget

Table 2.2: Driving Requirements

Requirement	Description
ALC-PLO-CON-02	The aircraft shall be able to attach a payload within 60 s
ALC-PLO-CON-03	The aircraft shall be able to detach a payload within 120 s
ALC-FLC-FPE-03	The aircraft shall have a minimum service ceiling of 2,000 m
ALC-FLC-FPE-05	The aircraft shall have a rate of climb of at least 8 m/s
ALC-FLC-FCO-05	The aircraft shall have a landing accuracy of 0.5 m
ALC-RAM-SAF-03	The aircraft shall have a manual override capability
ALC-SYS-NAV-02.1	The positioning system shall be accurate within 0.1 m during payload delivery
ALC-SST-04	Materials used shall be recyclable
ALC-SST-05	Materials shall be durable

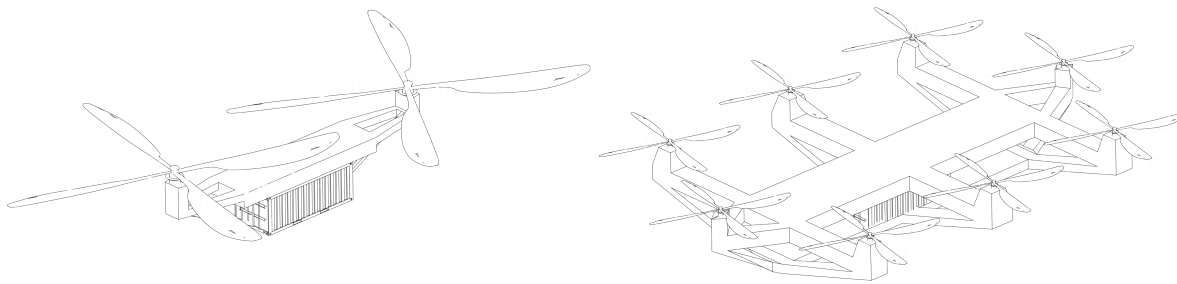
2.2. Design Options

When the requirements were set, the different design options could be determined. From all the design options, multiple concepts were established and worked out. This was done in the Mid-term Report [3]. First, different design option categories were determined, namely the lift-, propulsion-, attachment- and landing system. Then the obvious unfeasible and expensive options were eliminated and the then remaining viable options are given in Table 2.3.

Table 2.3: Viable Design Options

Lift System	Propulsion System	Attachment System	Landing System
Single Rotor	Piston Engine	Cable(s)	Wheels
Multi Rotor	Turboshaft Engine	Clamped	Skids
Tilt-Rotor with Wing	(Hybrid) Electrical Engine	Loading Bay	Legs
Airship		None	

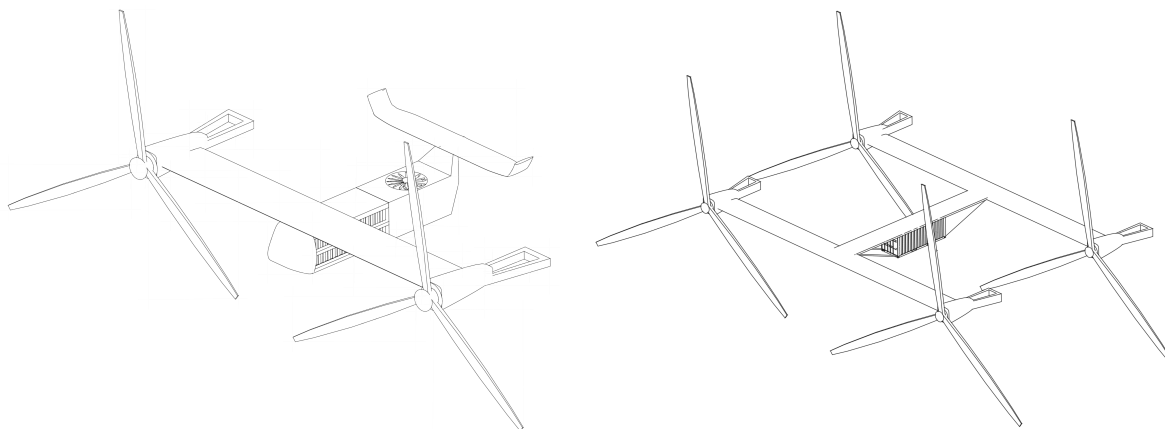
In the baseline phase it is established that the engines will be the most critical part in this design. Certified turboshaft engines which have sufficient power to lift the UAV, already cost more than the total budget set by the RNLAf. Therefore some creativity is required. Other engine options have to be explored compared to common aviation engines. Research in all types of engines resulted in two feasible options. The first option is the GM Lt4 piston engine (the engine for the Chevrolet Corvette Z06). Multiple piston engines, of which each drives a separate rotor, are able to generate sufficient thrust. If necessary these piston engines can be supported by electrical engines from Tesla during take-off and landing. The second option is to use the Honeywell T55 turboshaft engine (the engine from the Chinook). This option is more expensive, but performs better on Reliability, Availability, Maintainability and Safety (RAMS). It will also be easier and cheaper to get certification for this engine. Apart from the engine, the concepts are established based on another parameter, namely the wings. Designs with wings will have more efficient and faster cruise conditions. From these design options, five different concepts are made which are further investigated in the mid-term phase of the project. These five concepts are shown below.



(a) Tandem Concept Sketch

(b) Octocopter Concept Sketch

Figure 2.1: Two of the concept sketches



(a) Dragonfly Concept Sketch

(b) Locust Concept Sketch

Figure 2.2: Two of the concept sketches

The Tandem Rotor (Figure 2.1a) is a two rotor helicopter with a Honeywell T55 turboshaft engine. The second concept is the Octocopter (Figure 2.1b), which is an eight rotor helicopter with eight GM Lt4 piston engines, plus two Tesla S electrical engines to provide additional power during take-off and improve the controllability. The third concept is the Dragonfly (Figure 2.2a). This is an aircraft driven by one T55 engine which drives two large tilt-rotors and one electrical Tesla S engine which drives a smaller rotor (lift fan). The Dragonfly has one large main wing and one smaller tail wing. The fourth concept is the Locust (Figure 2.2b). The Locust is driven by eight GM LT4 engines and two electrical Tesla S engines. It has two large wings and four rotors that can be tilted. The last concept is the airship. The airship is beneficial because it creates "free" lift due to 'lighter-than-air gasses'. Therefore, the propulsion system is relatively cheap. However, the size of the airship is relatively large (at least 80 m long and 20 m in diameter). Because of this size the airship is an easy target for enemy gunfire. Therefore the airship concept was discarded early in the mid-term phase. Also, during the mid-term phase, the attachment- and landing system were neglected. Both systems are further examined during the final design phase in this Final Report.

2.3. Design Concept Trade-Off

To determine which is the best concept, a trade-off is set up. The main criteria of this trade-off are the technical performance, the RAMS, sustainability, costs and the feasibility. The main parameters are given a certain weight, depending on their importance. Each of these main parameters consists out of multiple sub criterion which are also given a weight relative to its main parameter. Each concept is

graded for each sub criterion and from this a final grade is computed for each concept. The concept with the highest grade will be further designed in the next phase of this project after consultation with the RNLAf. The summary of the trade-off can be seen in Table 2.4. The complete trade-off matrix can be found in the Mid-term report [3].

Table 2.4: Trade-off (main) criteria, associated weights and scores in a trade summary table. The weights and scores are calculated using the Analytical Hierarchy Process method. The weights for the sub criteria are for their relative importance in their criteria categories. The scores are given 0–3 for each sub criteria per concept. Colour codes are used for the scores: Red = 0, Yellow = 1, Green = 2 and Blue = 3.

Main criteria	Weight	Score			
		Copter		Wing	
		Tandem	Octocopter	Dragonfly	Locust
Technical performance	0.186	Poor ferry range yellow	High rate of climb yellow	High cruise speed and ferry range blue	High cruise speed and ferry range green
RAMS	0.226	Proven engine and concept blue	Hybrid engines with redundancy yellow	Proven engine and tiltrotor green	Hybrid engines with tiltrotor yellow
Sustainability	0.065	High fuel consumption green	NiCd batteries, high fuel consumption yellow	Low sound profile, low fuel consumption green	NiCd batteries, low fuel consumption green
Costs	0.386	Above budget red	On budget blue	Above budget red	Likely above budget green
Feasibility	0.138	Proven design blue	Complex engines and rotors green	Tiltrotor yellow	Complex engines and tiltrotor red
Total weighted score:		0.228 yellow	0.287 blue	0.220 red	0.265 green

The best concept from the trade-off is the Octocopter. The Octocopter fulfils all top-level requirements except unit cost, which is estimated to be € 570,000. This is only 14% more than the budget set by the RNLAf. It was later discovered that the RNLAf had set the maximum unit price this low on purpose to provoke the design team to come up with an unorthodox and original design. The engines of this concept have a relatively low reliability. However, the Octocopter has enough excess power such that it can still perform its normal operations when one engine fails. The operational costs are estimated to be 0.21 €/kg/100km and thus are well within the requirements. The Locust is a close second. The major benefits of the Locust are the relatively low operating costs and the high cruise velocity. Therefore, the trade-off suggests that the simplicity of the Octocopter and the efficiency in flight of the Locust can be combined, in order to get the best aspects out of both concepts. Thus, a design with a wing, multiple fixed rotors and assisted take-off. This conclusion is changed for the final design, after consultation with the RNLAf and our tutors. The assisted take-off is discarded, because the extra power is no longer required during take-off (especially after optimising the performance model). And because the entire assisted take-off system (including the batteries) adds significant weight and costs. A wing with fixed rotors is also discarded, because in an Octocopter design, it is estimated that the flow over such a wing will be significantly disturbed, such that its contribution to the total lift is small. Therefore, the detailed design will be made for the Octocopter, without the assisted take-off system. From this point on, the detailed design of the Octocopter is called the HELLCAT: HEavy Lifting Low Cost Autonomous Transporter.

3 Mission Analysis

The first step in designing a product is to become familiar with its purpose. In this chapter, the mission that the vehicle has to execute is analysed. This is done in several steps. First, the Functional Flow Diagram and the Functional Breakdown Structure are elaborated in Section 3.1 and Section 3.2 respectively. From that, a set-up for the operation logistics is given in Section 3.3, after which the ground operations are described in more detail in Section 3.4. In Section 3.5, a typical mission profile is outlined. The way the the vehicle is going to perform this mission is described in Section 3.6.

3.1. Functional Flow Diagram

A Functional Flow Diagram is a way to express the desired behaviour of a system, without considering a specific design. It shows the general behaviour and the functions used to achieve the mission in subsequent levels. This results in a multilevel representation of the essential functions of the system.

When airlifting containers a set of individual functions of the system can be established. These functions are based on the mission characteristics and are independent of design or concept. For this transport system, eight different mission stages can be distinguished. These mission stages are essential for the system to function properly and fulfil the mission requirements. Since the details of most systems are unknown, the exact functions associated with some steps are not defined either. The lack of a proper design concept implies that the Functional Flow Diagram (FFD) lacks a level of detail. This will be continuously updated as the detail of the system increases. A few parts of the mission, for example the *delivery-* and *return flight*, might be very similar, but could also be rather different in nature. This results in some parts that seemingly overlap, but might be different in their details. The full diagram can be seen in Figure 3.1 and Figure 3.2.

Aside from performing in normal conditions, the system should also have provisions to cope with abnormal conditions like engine failure, unexpected weather hazards, light enemy fire etc. These are defined as conditions where the UAV is still able to perform its mission without crashing. Though, some functions that are needed to cope with these can be defined. The chronological order in which these appear are not known. These are therefore described in the Functional Breakdown Structure.

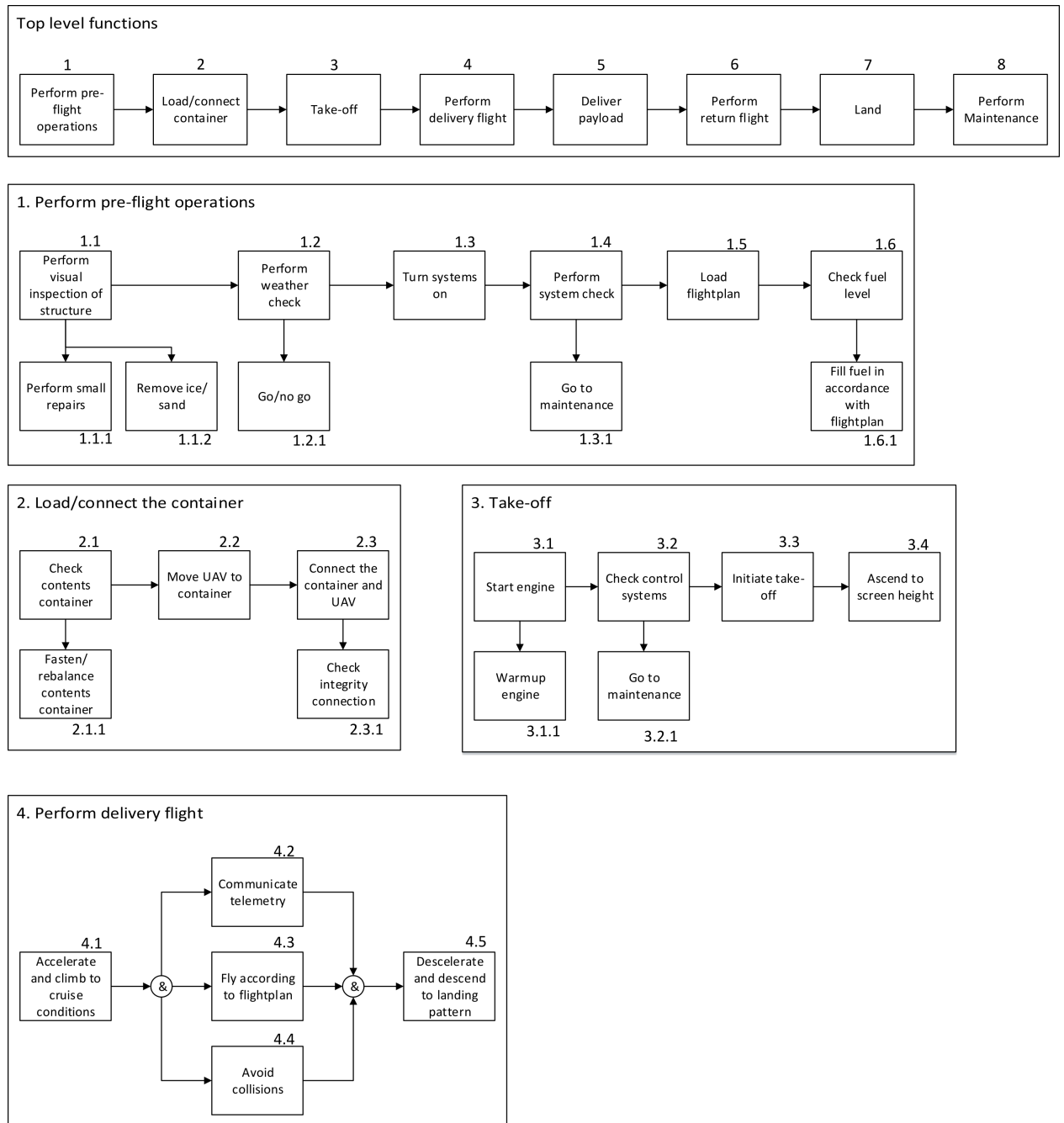


Figure 3.1: Functional Flow Diagram for airlifting containers part 1

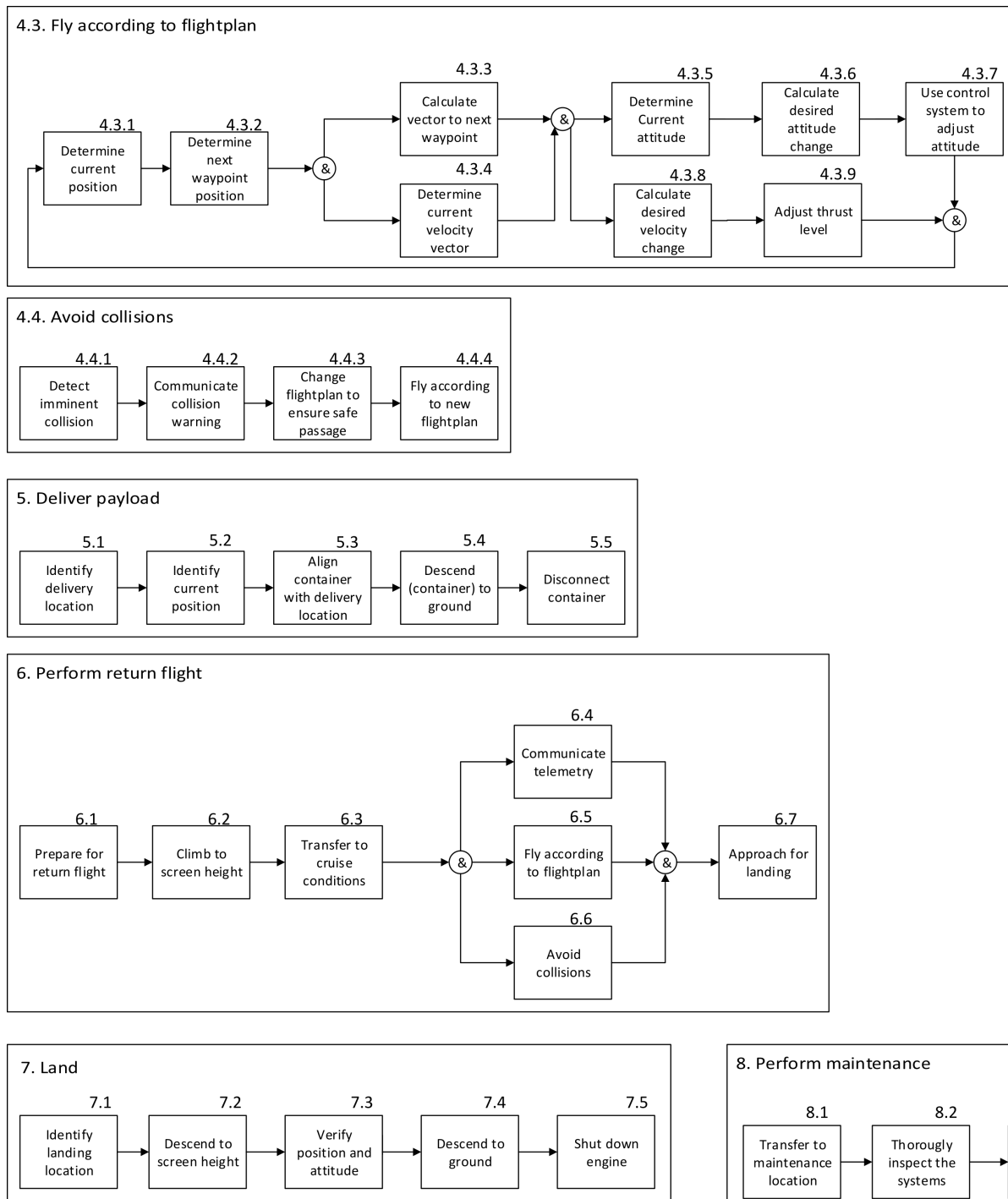


Figure 3.2: Functional Flow Diagram for airlifting containers part 2

3.2. Functional Breakdown Structure

Another tool to find the functions of the system is the functional breakdown structure (FBS). The FBS shows the elemental functions the system should provide to successfully perform its mission. These functions are closely related to Figure 3.1, the Functional Flow Diagram, from Section 3.1. However they are not sequenced, but divided by function group.

The FBS top levels are *Perform mission* and *Perform non-mission operations*. *Perform non-mission operations* includes all functions that are not considered in the *Perform Mission* branch. These functions follow from the design of the system but will not be worked out in detail as this is not the goal of the Design Synthesis Exercise (DSE). *Perform Mission* contains all mission functions including the *Abnormal* and *Emergency* operations tasks. The abnormal and emergency functions are not yet worked out in detail but provide a start for the further design phases and are included for completeness. The top level functions are shown in Figure 3.3. The *Normal Operations* branch is most complete and shows the basic functions the product should perform. It has four major branch points and covers an entire mission from pre-flight up to post-landing operations and is shown in Figure 3.4. The *Flight Operations* functions have been expanded into more detail, which is shown in Figure 3.5 and Figure 3.6. Diagrams with a 'SD'-note are scenario dependent, like extreme weather conditions or non-normal flights conditions. Diagrams in Figure 3.4 have a 'U'-note when the function is performed unmanned.

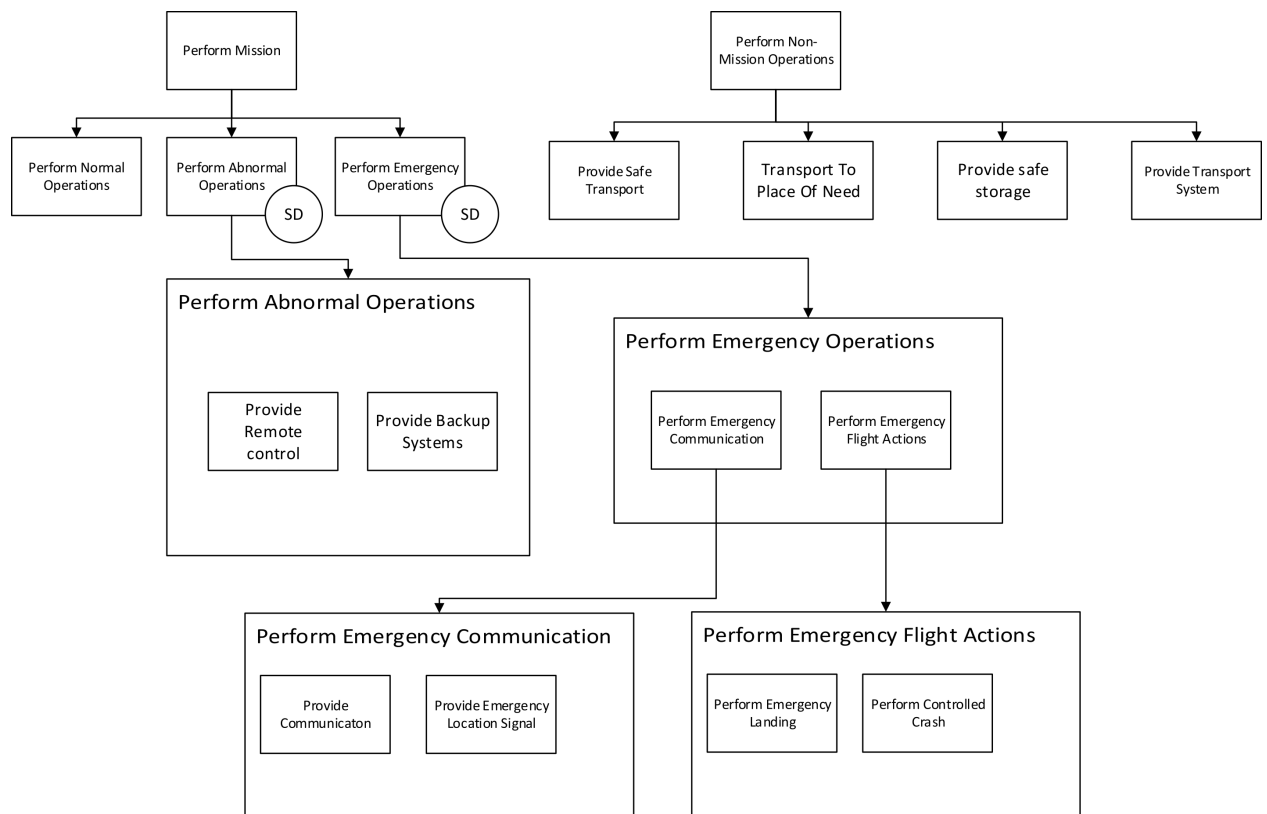


Figure 3.3: The FBS depicts the top level functions the transport system should provide

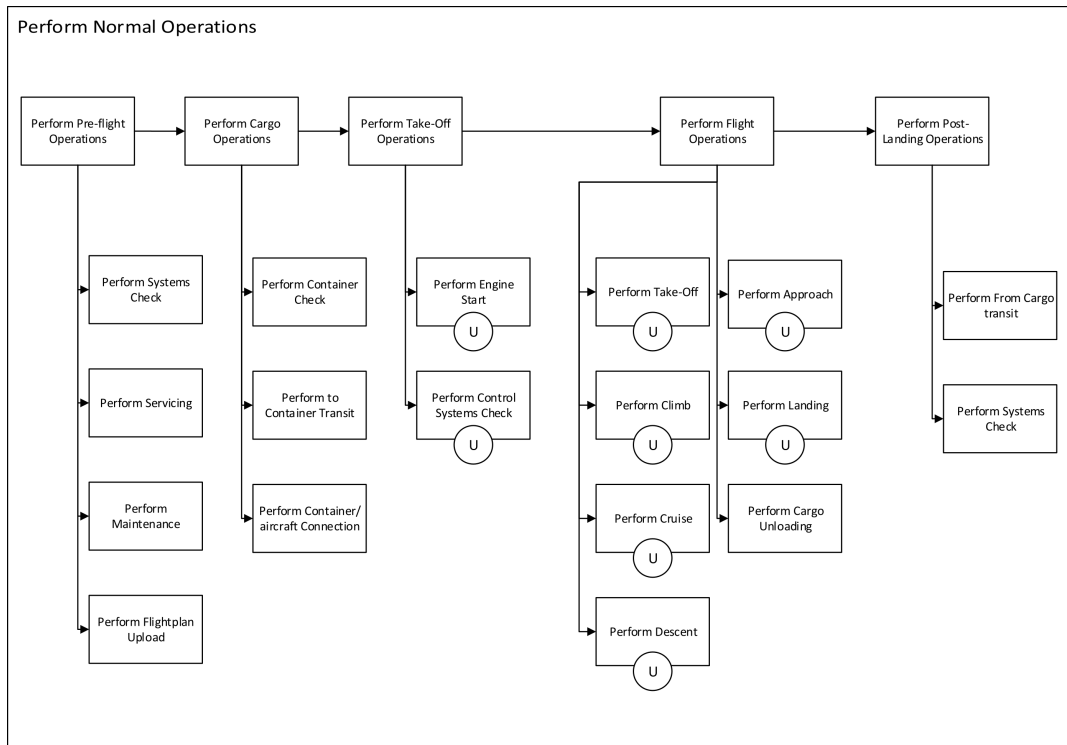


Figure 3.4: Expansion of Perform Normal Operation of Flight Operations Functions

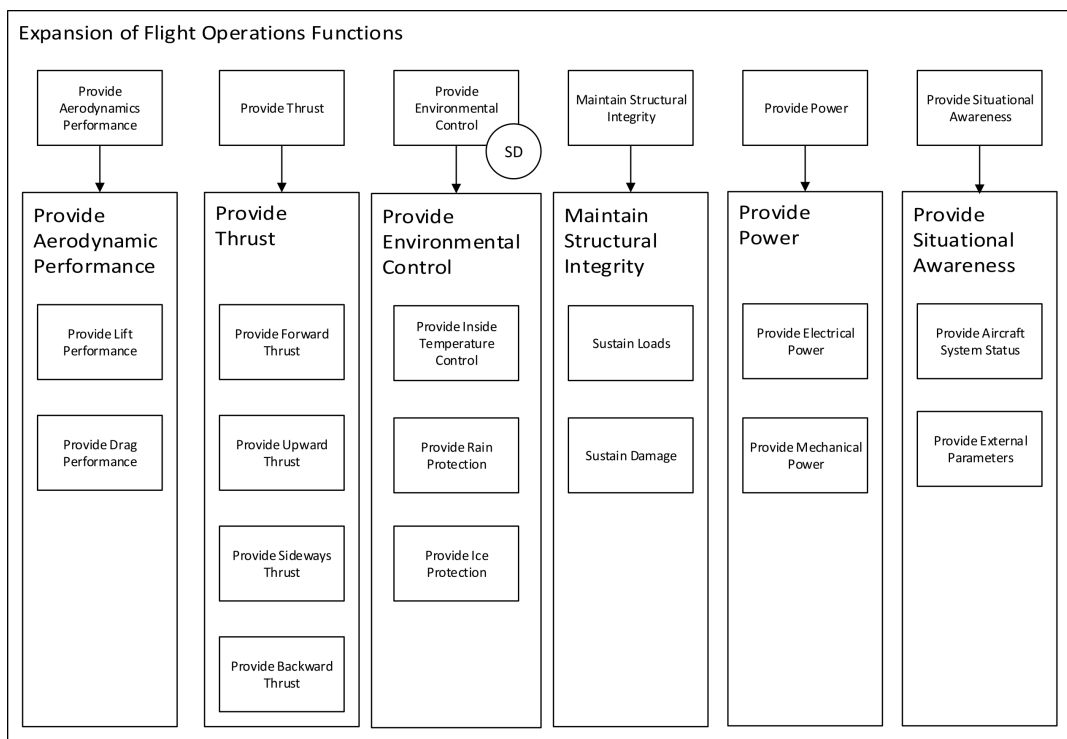


Figure 3.5: Expansion of Flight Operations Functions

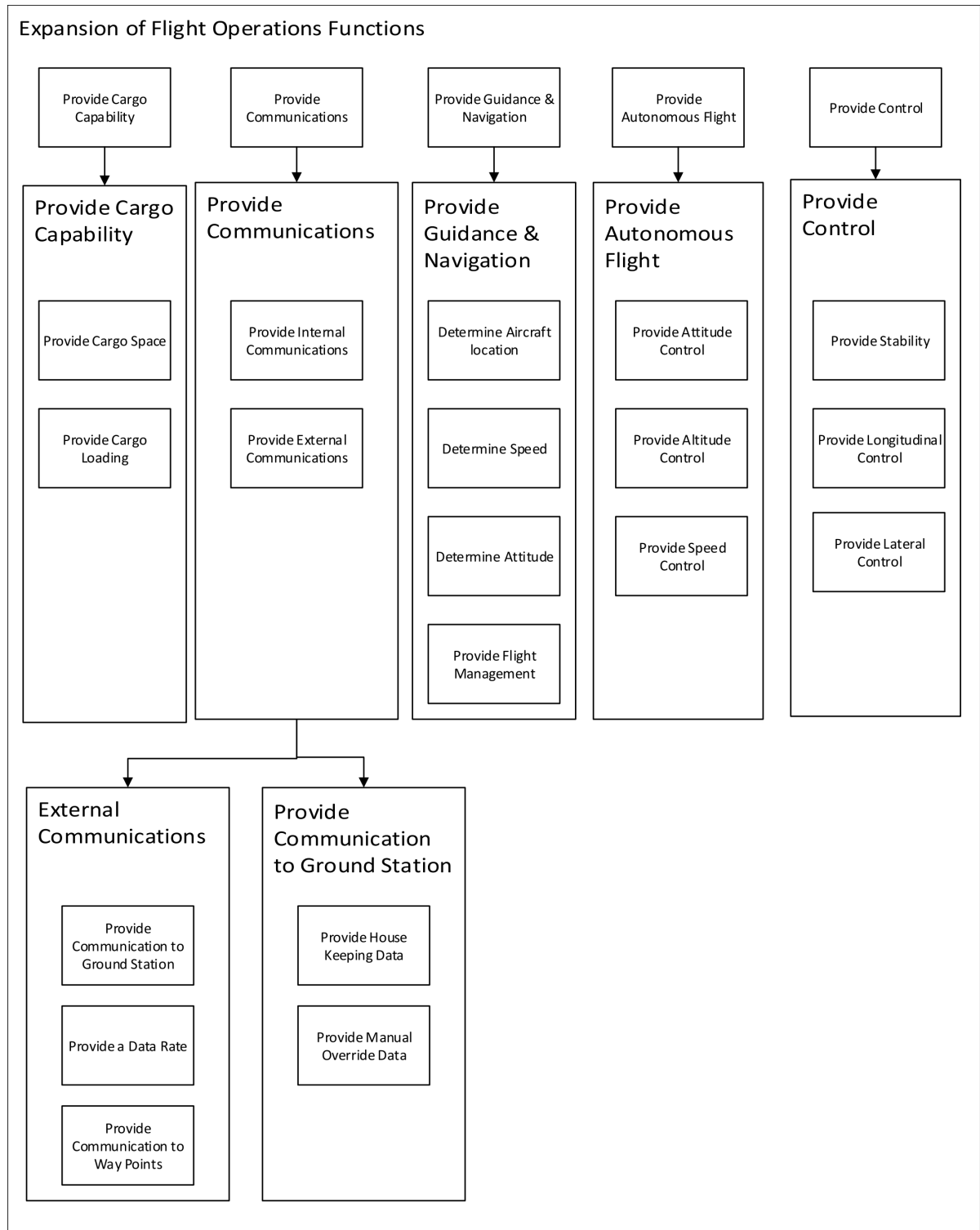


Figure 3.6: Expansion of Flight Operations Functions Continued

3.3. Operation Logistics

The operational logistics are shown step by step in a logistical order. A schematic overview of these steps is given in the Logistic and Operation Flow Diagram, which can be seen in Figure 3.7.

- 1: Once a base location is chosen, troops will have to secure and prepare a landing zone for the UAV. This area should be at least 35 m by 35 m for the UAV to land.
- 2: Container lifting equipment should be present at both the drop and pickup point. The UAV will place the container on the landing platform and take-off. The ground crew is responsible for the final location of the container.
- 3: Another landing area should be present at the harbour where the containers arrive after they have been shipped. The same size of 35 m by 35 m for this platform is required.
- 4: The UAV will land on this platform.
- 5: At the same time the containers can be loaded of the ship.
- 6: The containers are moved from the ship to the landing area where the UAV is already landed. Then the container will be place under the aircraft and lifted using jacks into the right position.
- 7: Ground personnel attaches the container to the UAV.
- 8: While the ground crew is attaching the container the UAV can be (re)fuelled, more information is given in Section 3.4
- 9: A visual inspection of the aircraft by the crew to check for any damages. Preflight operation will be carried out simultaneously.
- 10: Take-off. For further elaboration on the mission profile see Figure 3.8
- 11: Fly towards the designated area. The navigation is discussed in Section 3.6
- 12: Land. A more detailed description on the landing operations is given in Section 3.6, where the landing accuracy is discussed.
- 13: The ground crew disconnects the container and performs visual inspection of the aircraft.
- 14: Preflight procedures.
- 15: Take-off.
- 16: Fly back without payload.
- 17: Remove container from landing area so that the area is clear for the next payload delivery.

As can be seen in Figure 3.7 the steps are repeated from step 3 to 17 until all the containers are transported.

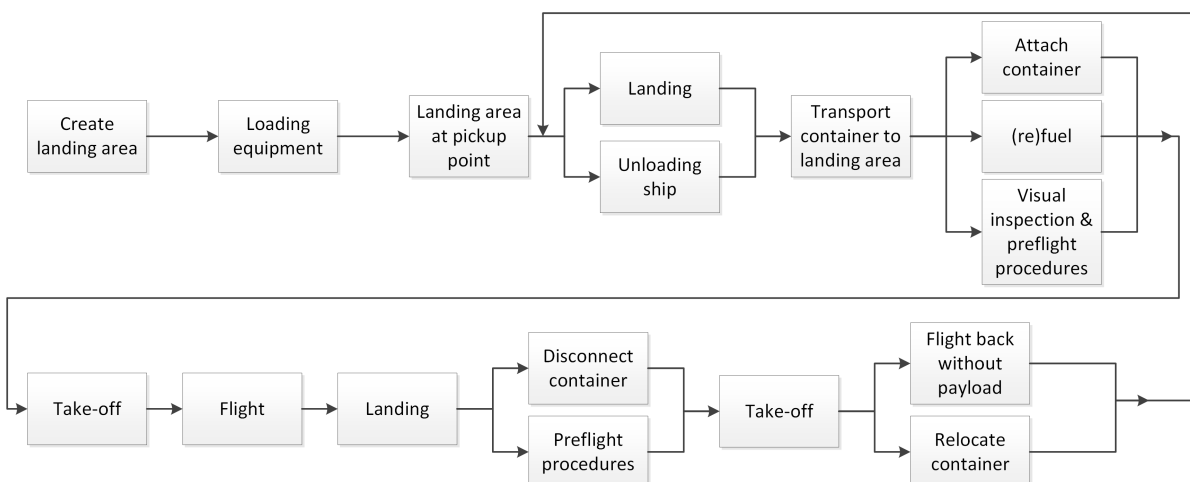


Figure 3.7: Logistics and Operations Flow Diagram

3.4. Ground Operations

Ground operations include the refuelling of the UAV, maintenance, attaching/detaching the payload and moving it from and to the UAV. The refuelling and maintenance are standard procedures compared to helicopters. The loading on the other hand differs from normal procedures. Comparable to helicopters, the payload will be suspended underneath the UAV by using cables. However, these cables are shorter than those of the helicopter and shorter than the landing gear on which the vehicle will land. This means that after landing, and when the engines are shut down, the container hangs under the UAV but still above the ground. This leaves room for a fork lift truck to drive under the container directly, without having to lift it first. Once the container is on the truck, the container can be detached by ground personnel and the truck can drive off. The unloaded cables can be attached to the frame of the UAV and once the landing/take-off spot is cleared again, the UAV can turn its engines back on and fly away safely. The same procedure but in reverse order can be performed when a vehicle arrives empty and leaves with a container. Ground personnel is accountable for positioning the container directly under the UAV and attaching the cables of the UAV to the container.

3.5. Typical Mission Profile

The typical mission profile has been defined by the client. The aircraft should be able to transport a 5,000 kg ISO 20 ft container over a distance of 250 km. At the delivery location the payload should detach and the aircraft has to be able to return to the starting point without refuelling. Furthermore, the aircraft should be able to take-off and land vertically. Due to air traffic control and safety reasons the aircraft should be able to loiter for at least 15 minutes at both the delivery and final destination. Ideally, loitering takes place at the velocity that corresponds to the minimal required power, in order to minimise the fuel usage. According to the power curve in Figure 4.8a, this velocity is approximately 26 m/s when loitering with the payload. For loitering during the return flight, this value is approximately 22 m/s, as can be derived from Figure 4.8b. Furthermore, from an efficiency point of view it is more efficient to perform VTOL as little as possible. After that, the aircraft should land or climb to cruise altitude for maximum efficiency. This mission profile can be seen in Figure 3.8.

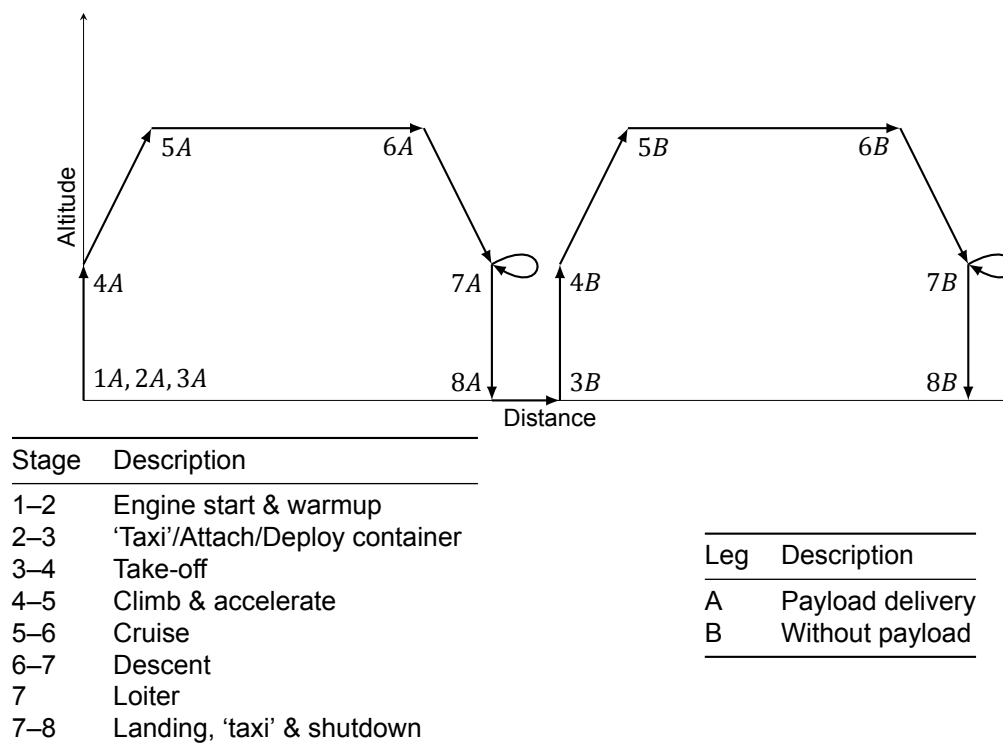


Figure 3.8: Mission profile for the default mission, which is 250 km back and forth without refuelling and in the first leg a 20 ft cargo container with 5,000 kg is transported.

3.6. Flight Operations

One of the top level requirements is that the HELLCAT shall operate autonomously. The level of autonomy however is not specified. Ideally, the coordinate of the drop-off destination would be sufficient information for the HELLCAT to autonomously plan and perform its own flight plan, including picking up and dropping off the containers without any human interaction. However, this would require some rather expensive systems. To give an indication, an off-the-shelf Terrain and Traffic Collision Avoidance System (T2CAS)¹ costs 230,000 USD. This single system already exceeds the approximately 50,000 EUR budget set for the avionics in the Mid-Term Review.

To get to an affordable autonomous solution, a trade-off between the avionic cost and the level of autonomy has been made. In this section a complete, but simplistic version of the execution of the mission is described. All systems mentioned below are described in more detail, in Section 7.4. Deviations from the flight plan as described here and suggestions to increase the autonomy level, are also given in that section.

3.6.1. Following the Flight Plan

Instead of letting the vehicle determine its own flight plan, it is chosen to pre-define the flight plan. This can be done by a GPS waypoint system, a series of coordinates that the vehicle needs to follow. The vehicle is able to do this by using its Inertial Measurement Unit (IMU) and GPS receiver. It translates the difference between its own position and the flight plan coordinate to a required yaw, pitch and roll input. The positioning accuracy required during cruise is 10 m, as defined in requirement **SYS-NAV-02.2** in Chapter 15. Assuming a clear line of sight from the antenna to the sky, and since the vehicle is flying 42 m/s during cruise, this accuracy is achievable with the vehicle's GPS receiver in combination with its IMU².

Since the vehicle is able to continue its flight if one of the engines fail, flying over cities is not necessarily off the limits. However, it is recommended to fly around cities when possible, to reduce the risk of having to make an emergency landing in a densely populated area further. In both cases, emergency landing spots can be identified along the predefined flight path. Taking into account the inaccuracy of a regular GPS system, the flight path definition turns into a safe to fly tunnel from the starting point to the drop-off zone and back. Assuming that the operation takes place in a remote area, this safe to fly tunnel is relatively easy to set up and can have a relatively large diameter as compared to a densely populated area.

Even though this concept could work by GPS and IMU alone, it cannot be assumed that other aircraft will respect and avoid the tunnel. Therefore, each vehicle is equipped with a Traffic alert and Collision Avoidance System (TCAS). This system costs approximately 21,800 USD³, less than a tenth of the 230,000 USD T2CAS previously described. To provide the vehicle with more information about its surrounding, without exceeding the avionic budget, cameras with Infrared (IR) sensors are installed. Next to enabling the use of optical flow, these cameras can also be watched directly from the ground station. This makes manually changing the flight plan from the ground segment easier, allowing to fly out of the tunnel manually.

3.6.2. Precision Landing and Take-Off

Although positioning accuracy is not required to be very high during the cruise phase, it is still of utmost importance during take-off and landing. According to requirement **SYS-NAV-02.1**, the vehicle needs to be able to position itself with an accuracy of 10 cm during landing. To provide this accuracy, a local Differential Global Positioning System (DGPS) is set at both the starting point and the drop-off zone. Furthermore, a Radio Altimeter (RADALT) is used to measure the height above the ground directly, instead of using the barometer of the IMU, resulting in a higher accuracy level. By installing a visual beacon on both locations, the cameras can be used for optical flow to identify the exact landing spot. These cameras can also be used to manually identify a landing spot, in case both beacons are unavailable. Together these systems provide the required position accuracy, safety requirements and sufficient redundancy.

¹URL: http://www.aepilotsguide.com/pdf/05-06_Archive/TCASPG05.pdf [cited 13 January 2016]

²<http://www.vectornav.com/docs/default-source/documentation/vn-300-documentation/PB-12-0004.pdf?sfvrsn=22>. [Cited 25 January 2016]

³<http://sarasotaavionics.com/avionics/gts855>[Cited 15 January 2016]

It should be noted that in order to keep the avionic system simple, the operation set-up described requires some preparation. The flight plan should be determined carefully and precisely to avoid crashes into surrounding buildings, especially for take-off and landing. Furthermore the DGPS should be set-up and a visual beacon should be prepared at both locations. This results in an affordable avionics system. Prices per subsystem are listed in the cost breakdown in Section 7.4.

4 Propulsion and Power

Now that the mission is analysed and the required functions are defined, the propulsion and power system of the Octocopter can be designed. This chapter will elaborate on the propulsion and power system by first describing the engines used and their properties, the way each engine is connected to the rotor system and the fuel system in Section 4.1. Section 4.2 shows the performance including the power calculations, the service ceiling and the fuel calculations.

4.1. Power Plant System

The engines powering the aircraft are eight LT-4 General Motor Generation V Small-Block, shown in Figure 4.1, 6.2L supercharged V8 each generating 650 hp or 485 kW and weighing 295 kg¹. An aftermarket performance tuning package manufactured by GeigerCars will be used to increase the performance. The tuned engine can provide as much as 730 hp². It is important to note that the extra power gained from overhauling the engine will only be used in an emergency setting, for example failure of one of the engines. The choice for this engine is due to the combination of high performance and low price and weight [3]. The power and torque characteristics of the stock engine can be seen in Figure 4.2.



Figure 4.1: General Motors 6.2 Liter Supercharged V8 Small Block LT4 Engine³

As one can see the maximum torque produced is 881 N m at 3,600 RPM and the maximum power of 650 hp is reached at 6,400 RPM (stock setting). The LT4 is supercharged which means the power is constant up to 3,000 m, this will be explained in Section 4.2. The engine has an advanced performance operating system that determines the optimal air to fuel ratio. The automotive industry has had much more resources and budget to improve their systems than their aircraft piston engine counterpart and although the LT4 is originally build for a high performance car, which means that the main design focus was not reliability but the engine has shown promising test results in endurance. The Engine is certified under the SAE J1349 standard⁵. This ensures that the stated power and torque are performed under standardised conditions and that the test are performed under the supervision of the SAE. The conditions are stated in Table 4.1. Temperature, humidity and pressure influences the performance of engines. The LT4 is SAE certified and a correction factor can be calculated to determine the change in power⁵. This correction factor is meant for normally aspirated internal combustion engines. The LT4 is supercharged and depending on how much the supercharger is overrated

¹URL: <http://www.chevrolet.com/performance/crate-engines/lt4.html> [cited 15 January 2016]

²URL: <http://www.autoevolution.com/news/pumped-up-chevrolet-corvette-z06-from-geiger-cars-packs-730-horsepower-ph.html> [cited 15 January 2016]

⁵URL: http://standards.sae.org/j1349_201109/ [cited 12 January 2016]

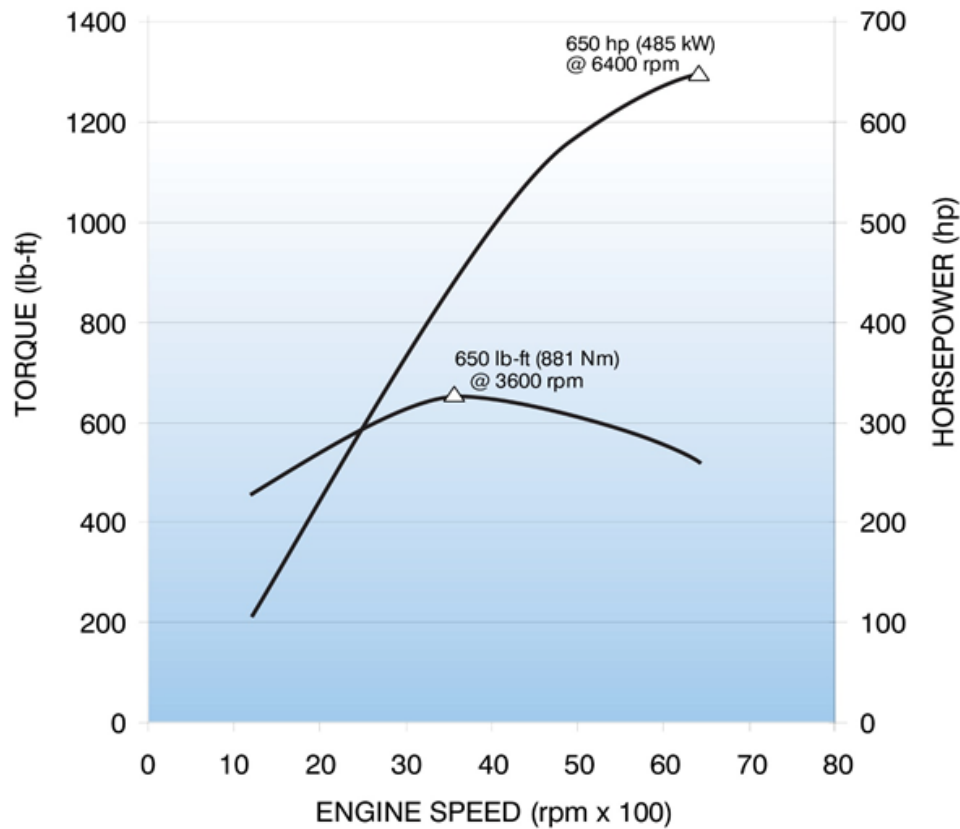


Figure 4.2: Torque and Horsepower versus RPM for the GM LT-4 V8 Small-Block⁴

Table 4.1: The standard conditions used in SAE J1349 engine tests

	Standard Condition
Inlet Air Supply Pressure (absolute)	100 kPa
Dry Air Pressure (absolute)	99 kPa
Inlet Air Supply Temperature	25 °C

the results could be better than depicted in Figure 4.3. The percentual change in power due to a change in temperature and pressure altitude with respect to the standard conditions can be found in Figure 4.3. A relative humidity of 70 % and a sea level pressure of 103,400 Pa is used in the calculations.

The design takes into account the loss of one engine during fully loaded flight while still being able to normally carry out its mission. As long as the engines are maintained properly the chance of multiple engine failure in the short mission duration is expected to be low but at this time undetermined. Car trouble happens more often than most of us like, however the failure is only in 7 percent due to the engine. Most engine failures are due to the fuel, oil pumps or fuel filters. Due to the redundancy of the fuel pumps, the use of multiple fuel filters and a far better maintenance schedule the probability of engine failure for this design will be quite lower⁶. Also note that these numbers are from all types of cars and all ages.

The engine and rotor are connected by a helical right angle, reducing, gearbox because the engine drive shaft rotates faster than the rotor. Efficiencies of such gearboxes are 94 to 98 percent, and using [8] the estimated weight is 70 kg. The rotor operates at 500 RPM which gives a gear ratio of 12.8. When the pitch of the rotor blade changes the rotor asks more torque from the engine. This will decrease the rpm of the engine. Figure 4.2 shows that as long as the engine RPM is higher than 3600 the engine is

⁶URL: https://www.adac.de/_mmm/pdf/28163_235221.pdf [cited 12 January 2016]

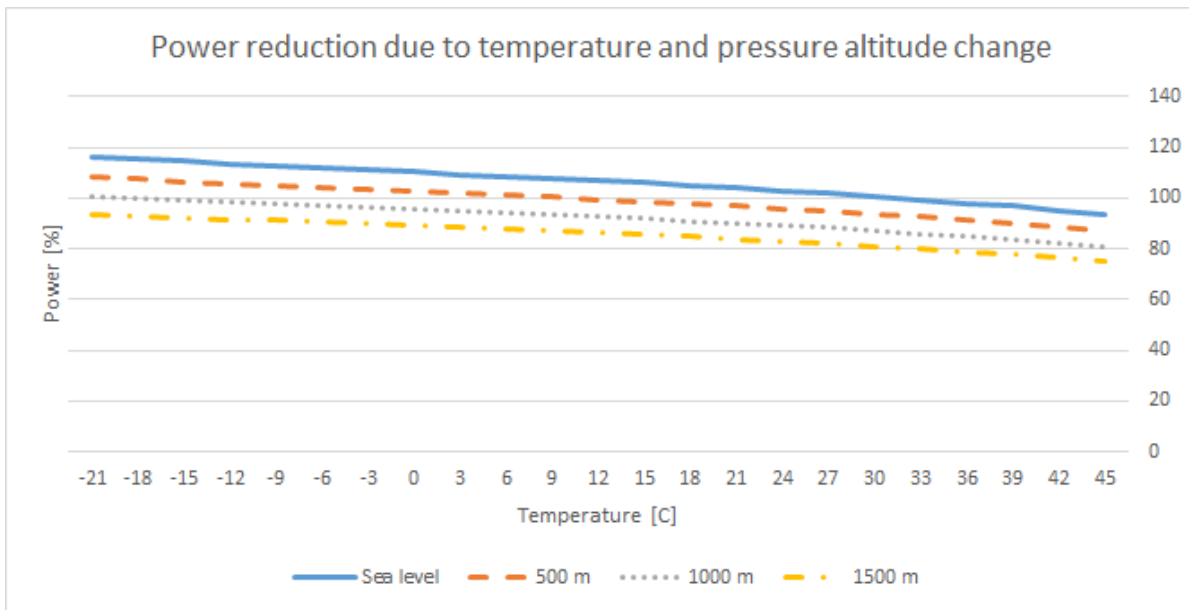


Figure 4.3: Percentual power loss due to change in temperature and pressure altitude with relative humidity of 70 % and a sea level pressure of 1,034 kPa

in the stable part and will produce enough torque to regain the previous rotational speed. To prevent motor stall due to a faster rotating rotor than engine and to release the rotor from the engine in case of an engine failure there is a sprag clutch installed between the gearbox and engine. This clutch works one way so the engine can power the rotor but the rotor cannot rotate the engine shaft. The engine is placed as close to the centre of the rotor as possible to alleviate the structural load. The hardware block diagram can be seen in Figure 4.4.

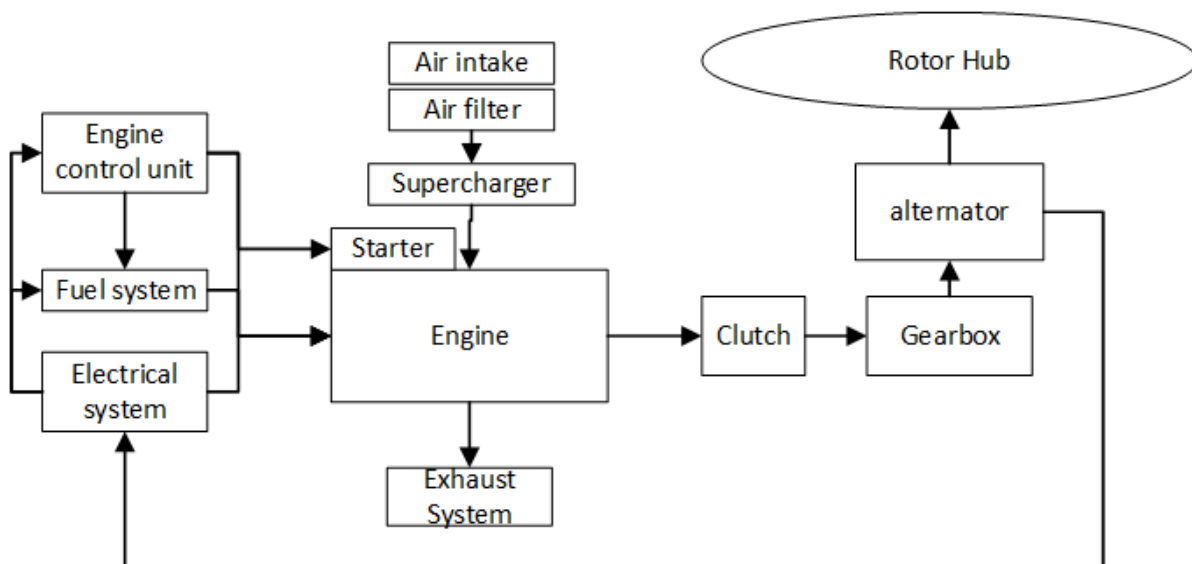


Figure 4.4: Engine system diagram

Three engines provide the electrical power by use of an alternator connected at the gearbox. Due to this there is a loss of 5 to 10 hp per engine. More about the electrical system can be found in Chapter 8.

The fuel for the engines is stored in four separate bladder fuel tanks on the cross points of the structure. The tanks store 550 litres fuel each and have a self-sealing outer shell, which is standard in aviation. There are solutions for a more protected tank, however the costs are not within the budget. Each tank

is connected with two other tanks via a dual connection, thus as one tank fails the fuel can still be distributed over the remaining tanks. Each engine has a dedicated fuel pump and each tank provides fuel for two engines (cross-feed). However when a pump fails or a line leaks the pumps can serve up to three engines. All lines have valves to close or open the lines in case of failure, and there are multiple filters between sections to ensure the purity of the fuel. The fuel diagram can be found in Figure 4.5 and shows one half of the symmetrical system. The elements used are off-the-shelf parts. The fuel used is premium gas, which has a higher octane level than regular petrol and is needed because of the high compression in the pistons. The use of lower grade petrol could result in lower performance or even blowing out the piston heads due to the premature spontaneous explosion of the air fuel mixture, this is known as knocking. The LT4 has protection against this by opening the release valves early but this will reduce the available power.

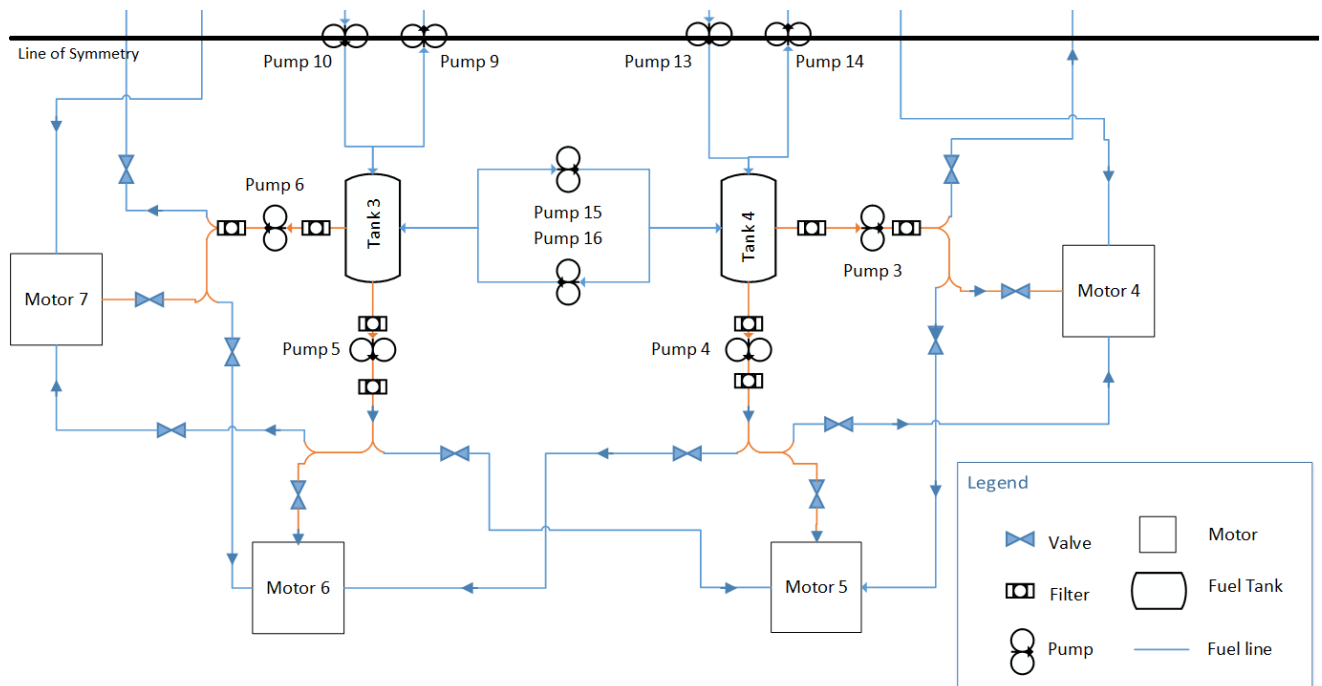


Figure 4.5: Fuel flow diagram showing tanks, filters and pumps

To reduce harmful emissions an exhaust system is connected to the engine. To prevent the exhaust system from reducing the power output of the engines a special high power exhaust is selected. The exhaust system contains an high flow catalytic converter. This exhaust minimises the back pressure and therefore increases the power output of the engine as well. A catalyst converter reduces the NO_x emissions by approximately 70% [29].

To even get a better understanding of the schematic for the combustion engines Figure 4.6 can be used. This figure gives more detail of the combustion engine control and operations than Figure 4.4. Note that a dust and sand filter is placed in the air scoop before the airfilter to deal with extra sandy environmental conditions, due to the size of the scoop there are no power losses.

To control the engines power output information can be sent to the *Engine Control Unit (ECU)*. The *ECU* then gives information to the *Air Throttle Body (ATB)* which allows for less or more air to enter. The amount of air is measured by an *air mass flow sensor* and this information is fed back to the *ECU*, which then handles the amount of fuel to be fed to the engines.

4.1.1. Recommendations

Although the automobile engine industry produces engines that are superior in most ways to aviation piston engines the focus in designing is different. Aviation piston engines are designed to have the lowest probability of failing while car engines are designed for low fuel consumption and performance. Although General Motors puts the engine through a hard test, in order to get the rotorcraft certified the engine should undergo rigorous testing. The testing is not in the scope of this design phase, but should

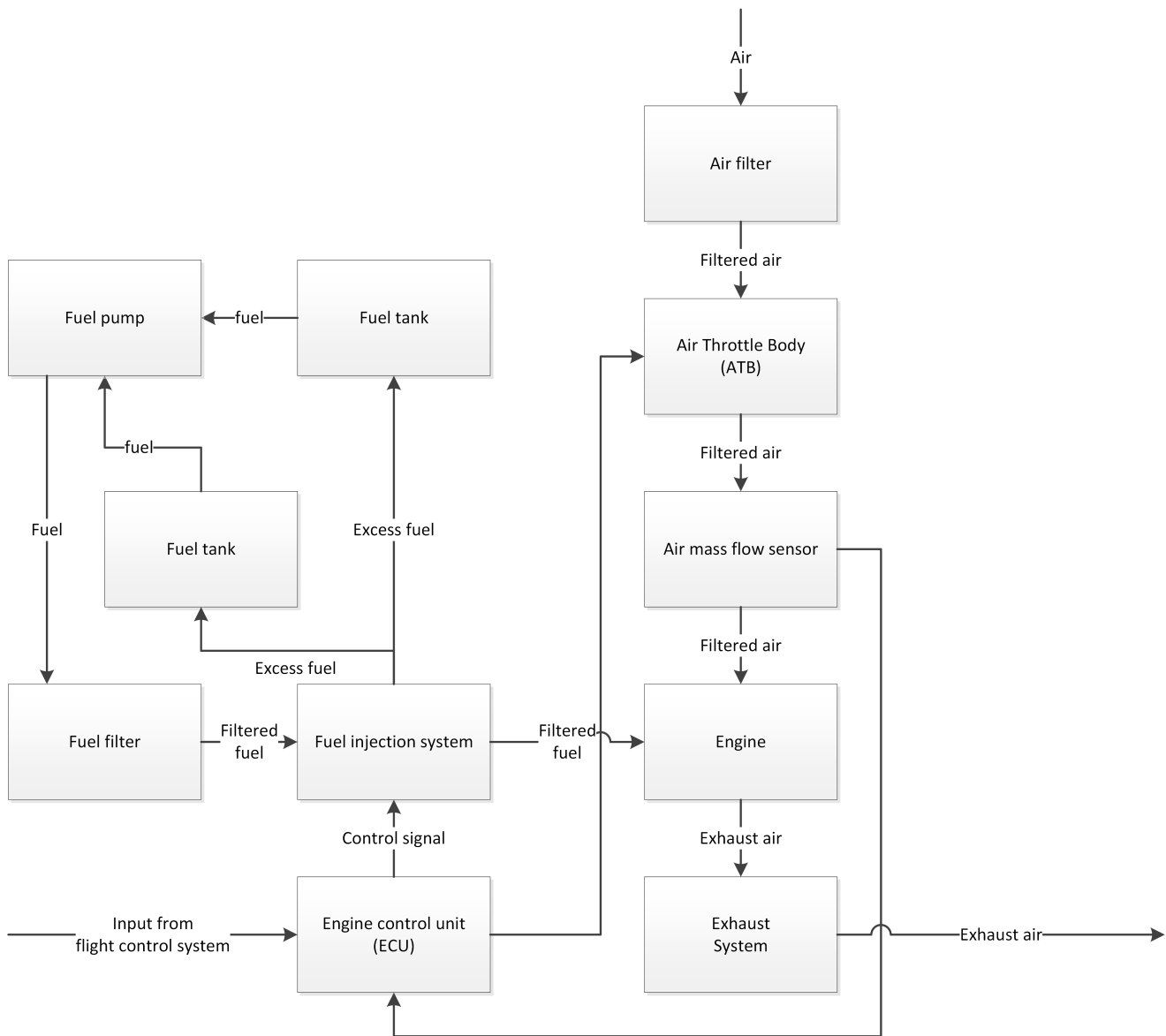


Figure 4.6: Block diagram showing the schematic of the propulsion system for the combustion engines. All system components are displayed as blocks.

have a high priority in the next phase, as this design depends on these powerful but relative cheap engines.

The fuel system depicted in the previous section is only a first conceptual design. The system should be as simple as possible due to the cost aspect. For this reason, the elements used should be off-the-shelf parts. The fuel system is redundant as one tank and several pumps may fail before an engine does not get fuel anymore. In the next design phase the system should be more detailed, for example where the sensors are placed. Other sensors that need to be added are for example the temperature, pressure and fuel gauges.

The parts used are a mix of FAA certified and automotive industry parts. FAA certified parts are the fuel tank, fuel filters, fuel lines and batteries. Parts from the automotive industry like the engines, starter, fuel pumps, air-filter etc. are not certified, but are of high quality. Using only FAA or EASA certified parts will increase the costs considerably but makes the certifying process easier and faster. Using non-certified parts will make the HELLCAT a lot cheaper but harder to certify. Also due to the higher risk of failure the craft will not be allowed to fly everywhere.

4.2. Performance

To show that the design is actually working and can perform the entire mission, a performance analysis is done. MATLAB [9] is used to perform the calculations. The assumptions made for this performance analysis are:

- A constant blade tip velocity
- A constant horizontal acceleration
- Small angles
- The In-Ground-Effect (IGE) is neglected.
- Steady, incompressible, inviscid flow.
- Instant power availability

During the mid-term phase, the air density ρ was assumed to be constant over the entire mission. For this performance analysis the air density is calculated during any point of the mission. The air density over altitude is determined from ISA-conditions. The input values for the performance calculations are given in Table 4.2. The profile drag coefficient is determined in Table 6.2 and the equivalent flat plate areas are calculated in Section 6.3.

Table 4.2: Input values for the performance constants

Symbol	Definition	Value	Unit
C_{D_p}	Profile drag coefficient	0.02	—
f	Equivalent flat plate area	19	m ²
k	Induced power factor	1.2	—
M	Figure of Merit	0.7	—
N_{rot}	Number of rotors	8	—
OEW	Operational Empty Weight	7,500	kg
P_{engine}	Total power available per engine	485,000	W
PW	Payload Weight	5,000	kg
r	Rotor disk radius	4	m
R	Range	500,000	m
$t_{mission}$	Total mission time	13,500	s
SFC	Specific Fuel Consumption	0.2	kg hr/hp
V_{tip}	Blade tip velocity	210	m/s
σ	Blade solidity	0.048	—

4.2.1. Power Calculations

The MATLAB program must be able to calculate the power that is required at any point during the mission. The method to perform these calculations is found in the book *Helicopter Theory* by *W. Johnson* [5]. The required power P_{req} consists out of three parts: The induced power, the profile drag power and the parasite drag power. First the induced power $P_{induced}$, this is the power that is required to achieve a certain thrust level. For the induced power the induced velocity is needed. The induced velocity $v_{i_{hover}}$ for each rotor is calculated by:

$$v_{i_{hover}} = \sqrt{\frac{W}{2 \cdot \rho \cdot \pi \cdot r^2 \cdot N_{rot}}} \quad (4.1)$$

Where W is the total weight of the UAV. The induced velocity is closely linked to the hover efficiency. This can be seen in Figure 4.7. As the total disk area gets larger less power is needed to hover. Therefore a larger area is preferred. However using very large rotors limits the forward speed capabilities, so the area is divided onto eight rotors to still be able to fly at 42 m/s.

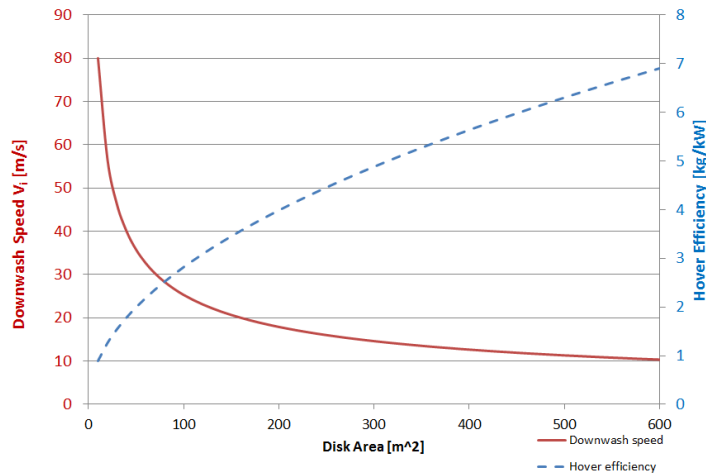


Figure 4.7: Disk loading and hover efficiency as a function of rotor area

When the induced velocity is known the required thrust T can be determined. v_r in Equation (4.2) is the resultant velocity between the forward and the induced velocity.

$$T = N_{rot} \cdot 2 \cdot \rho \cdot r^2 \cdot \frac{v_i^3}{v_r} \quad (4.2)$$

$$P_{induced} = k \cdot T \cdot v_i \quad (4.3)$$

$$P_{profile} = \sigma \cdot C_{Dp} \cdot \rho \cdot V_{tip}^3 \cdot \pi \cdot r^2 \cdot (1 + 4.65 \cdot \mu^2) \quad (4.4)$$

Where μ is the advance ratio, the ratio between the flight velocity and the blade tip velocity. $P_{profile}$ is the power that is required to overcome the profile drag of the rotor blades. Then the parasite power is determined. P_{par} is the required power to overcome the parasite drag, the air resistance of the entire body.

$$P_{parasite} = 0.5 \cdot \rho \cdot f \cdot V^3 \quad (4.5)$$

$$P_{req} = P_{induced} + P_{profile} + P_{parasite} \quad (4.6)$$

From these calculations, the power curve is plotted for a flight with payload in Figure 4.8a and for the way back without payload in Figure 4.8b. This shows the required engine power to fly at a certain speed. Also the contribution from the different powers are shown. The lowest point in the total power curve shows the flight velocity with the maximum endurance. For this design however the velocity with maximum range is more interesting. This is the value to the right of the maximum endurance velocity (to the right of the point for the minimal required power). This is because there is a minimal power increase necessary, but with a relatively high velocity increase. Therefore the ideal cruise velocity is determined at 42 m/s. When flying faster than the ideal cruise velocity, the parasite drag gets significantly larger compared to the other power contributions. The equivalent flat plate area is reduced to 13 m² when the UAV flies without container. It can be seen in the graph that this effects the parasite drag. The maximum velocity of the UAV is 60 m/s, when flying without payload this velocity is 70 m/s. This is where the total required power is equal to the available engine power, therefore this estimation is only based on the excess power. Section 6.2.3 also addresses aerodynamic limitations to the maximum velocity. The mechanical losses from the engine and its components are only considered in the available power. This mechanical efficiency is estimated to be 0.90. All the velocities and powers are determined at an altitude of 1,000 m.

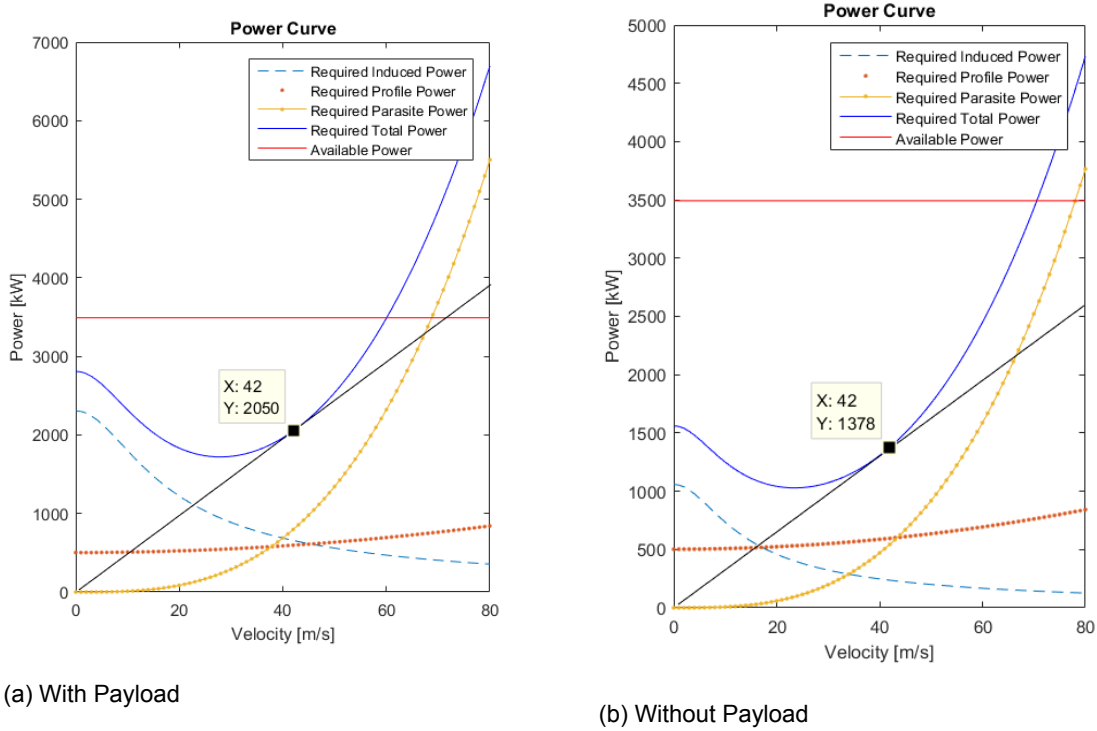


Figure 4.8: Power Curve

The with payload, the engine uses 60% of its power and without payload that value is 40%. The excess power, the difference between the required power and the available power, can be used to gain altitude. The maximum rate of climb is set at 8 m/s. The required engine power decreases significantly with an increasing forward velocity. Therefore the engines only have to run at full power for a short amount of time, approximately four minutes. After those four minutes the required power decreases sufficiently to still achieve a rate of climb of 8 m/s, as can be seen in Figure 4.9b. This value is based on the initial requirements. A deficiency in the model is that the UAV can instantly achieve a certain rate of climb due to the excess power. At higher altitudes, there is less excess power. Therefore it takes longer to climb to a certain altitude (with respect to the ground) as can be seen in Figure 4.9b. This is mainly because the required lift-off power is higher due to the lower air density.

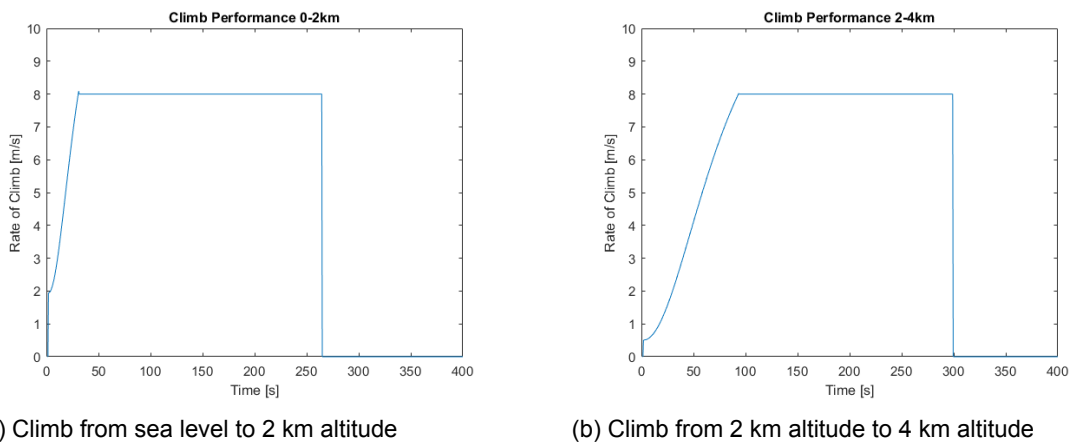


Figure 4.9: Climb performance

4.2.2. Service Ceiling

The theoretical service ceiling for a helicopter is defined as the maximum altitude, where it can lift off with a climbing speed of 0.5 m/s. The service ceiling is determined graphically by plotting the required hover power as a function of pressure altitude, against the available engine power. Both powers are dependent on the density of the air and this density depends on the pressure (ISA) altitude. The hover power is calculated by dividing the induced power from Equation (4.3), by the figure of Merit M . From the book written by *E. Torenbeek* [4], it is known that a supercharged piston engine does not lose any of its power up to 3,048 m (10,000 ft) pressure altitude. Above that a loss of 3% per 304.8 m (1,000 ft) is assumed.

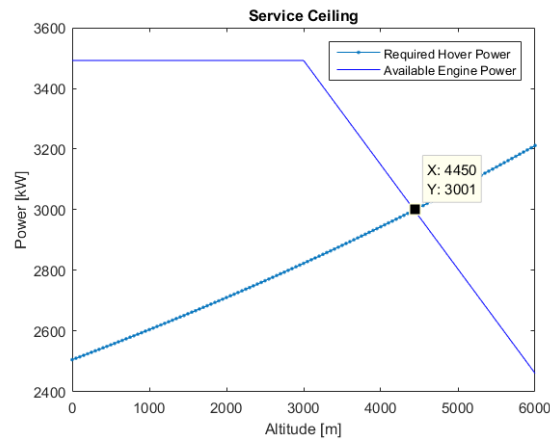


Figure 4.10: Service Ceiling

Figure 4.10 plots the required hover power, plus the minimal rate of climb against the available engine power. It can be seen that the service ceiling is 4,450 m. Thus the UAV will still be able to lift off the ground at an altitude of 4,450 m. When a higher forward velocity is gained, the aircraft will be able to fly higher. This is because the forward velocity gives extra mass flow through the rotor disk. This extra mass flow causes the required (induced) power to be lower. The extra fuel for loiter time is 250 kg. The SFC for maximum endurance (with payload) is 0.12 kg/s. Therefore, the loiter time is calculated to be 32 min. This is the loiter time for the entire mission, so for transporting the payload and for returning without.

4.2.3. Fuel Calculations

This fuel weight FW is calculated separately for 250 km with and without payload. The factor of 1.25 accounts for the extra fuel usage during take-off and landing plus the loiter time. The mission time in this equation is approximated by dividing the range by the cruise velocity, so the extra take-off and landing time are neglected. The cruise power for a flight with payload is 2,050 kW and for the way back it is 1,378 kW. The total fuel weight is then calculated, using Equation (4.7), as 2,000 kg.

$$FW = \frac{SFC \cdot P_{cruise}}{60 \cdot 60} \cdot t_{mission} \cdot 1.3 \quad (4.7)$$

The price of gasoline is assumed to be €0.47 ⁷. The total fuel that is used during one mission is determined by using Equation (4.7), however the 1.3 factor is reduced to 1.15 because only the extra fuel for the take-off and landing has to be taken into account. This makes the fuel contribution to the operational costs 0.09 €/kg/100 km. The ferry range is determined by calculating the fuel consumption without payload and then compute the distance it can cover when its fully fuelled. The fuel consumption without payload, at the optimal cruise velocity of 42 m/s, is 0.103 kg/s. Again the factor of 1.15 is applied to account for the extra necessary fuel for take-off and landing.

$$R_{ferry} = \frac{2000}{1.15 \cdot 1000} \cdot 42 = 700 \text{ km} \quad (4.8)$$

⁷URL: <http://www.brandstofprijzen.info/brandstof-zonder-belasting.php> [cited 25-01-2016]

4.2.4. Verification and Validation of the Performance Model

All the power calculations must be verified and validated against data from actual existing helicopters. Verification of the MATLAB code is done in a simple way. All the separate equations in the programme are calculated by hand (and a graphical calculator). The outcomes are then compared to the MATLAB outcomes. The programme is then adjusted and corrected until both values are a perfect match. Then it is checked if the boundaries of the programme are correct. The simulation is performed and plots of the height, velocity, rate of climb and power against (mission-)time are made. It is checked if the height does not exceed the set cruise altitude, if the velocity does not exceed the cruise velocity, if the rate of climb does not exceed the set maximum rate of climb and if the used power does not exceed the available power. The conclusion is that if sufficient iterations are made, the model is valid. Sufficient iterations are at least one iteration per (mission-)second.

Then, to validate the method, the data (dimensions, power output and weight) from the Chinook⁸ and from the K-Max⁹ is used as an input file for the created MATLAB program. The output is then compared to known data (maximum velocity, cruise velocity and climb performance) in Table 4.3. All the properties are calculated at standard sea level conditions.

Table 4.3: Validation Performance Model

Vehicle Property	K-Max Data	K-Max Calculations	Chinook Data	Chinook Calculations
V_{max}	51 m/s	58 m/s	88 m/s	92 m/s
V_{cruise}	41 m/s	44 m/s	65 m/s	68 m/s
C_{max}	12 m/s	9 m/s	8 m/s	10 m/s

From Table 4.3 it can be concluded that the used method is valid for at least velocities up to cruise velocity. The errors remain within 10% for the cruise velocity. For the maximum velocity the differences are growing more significant. This is due to the fact that the assumptions for this model become less valid for higher velocities. The calculated climbing performance is in the same order of magnitude of the actual values. The differences are due to additional power losses that occur in actual flight. Since the drag coefficients are unknown for the K-Max and the Chinook, the equivalent flat plate areas are estimated to be 3 m² for the K-Max and 4 m² for the Chinook. These values are an estimation from the reader of the course AE4213 [10], based on the MTOW.

⁸URL: <http://www.globalsecurity.org/military/systems/aircraft/h-47.htm> [cited 12-1-2016]

⁹URL: <http://www.lockheedmartin.com/content/dam/lockheed/data/ms2/documents/K-MAX-brochure.pdf> [cited 12-01-2016]

5 Structures

After carefully considering all the components of the mission analysis and the propulsion and power system, this chapter presents the structure of the design. A structure serves multiple purposes, such as providing strength and stiffness, carrying loads, serving as attachment for other components and as storage for fuel and systems. The structure has to be designed in such a way that it fulfils the set constraints and requirements with a minimal mass for the structure. This means the structure should be optimised for, often conflicting, multiple criteria. The design of the structure consists of three highly linked parts: structural design, material selection and production selection. Changing one of these will have major influence on the other parts, since a continuous interaction exists between them. However, in this report, only the final results will be discussed.

First the main layout of the structure and rotor configuration is determined in Section 5.1. The method by which the container is attached to the main structure is defined in Section 5.2. In Section 5.3 the material selection process is described and the material for all main parts is selected. With the main layout known and the material selected finally the main structure can be designed and analysed, which is done in Section 5.4. Finally, the production is discussed. Apart from the three important aspects of structural design mentioned above, the structure is also dependent on the other groups such as aerodynamics, stability and control and performance and propulsion. For example, depending on the shape, the drag changes and hence the overall performance of the aircraft. Alternatively, certain decisions could negatively change the control and stability of the aircraft.

5.1. Overall Rotor and Structure Configuration

An important aspect is the layout of the entire structure. The design of the main structure is crucial for the success of the entire system. It has to be strong, lightweight and low cost. Therefore different options were considered. The four main layouts that were considered are shown in Figure 5.2. The names of the configurations are the Tic-tac-toe (Figure 5.2b), Spiderweb (Figure 5.2a), Cross (Figure 5.2c) and the original (Figure 5.1).

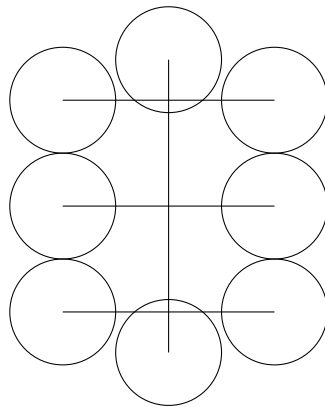


Figure 5.1: Old 'oval' configuration of the Octocopter [3]

Original Layout This layout was the initial design, when the eight rotor concept was proposed. This layout aims for the rotor blades to be the maximum size in the allowed design space of (35 m x 35 m). This means that the rotors have optimal disc-loading and that the engines need less power to create the same amount of lift. The structure consists of four straight beams, which means assembly is relatively straight forward. However, the fact that car engines are used instead of licensed aircraft engines means that engine failure has to be taken into account, as the probability of an engine failure is higher compared to a licensed aviation engine. In case of an engine failure from one of the engines at the sides, the loss of lift and the compensation of that loss by the engine on the opposite side, will create a torque in

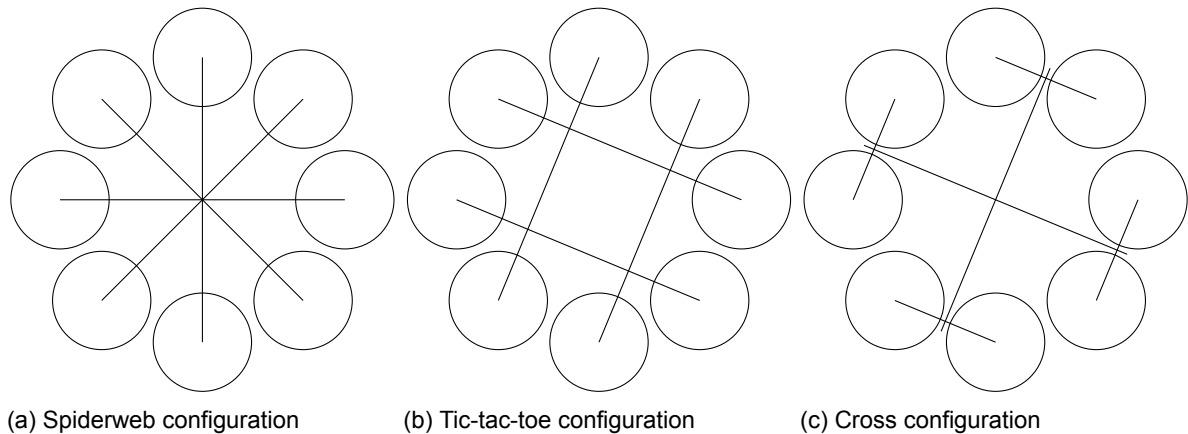


Figure 5.2: Different configurations concept for the rotor and structure layout.

the middle beam. The structure must be designed in such a way that it can cope with this increase of torque. From a stability and control point of view, if one of the longitudinal engines fails, it is harder to keep the UAV stable.

Spiderweb Layout The cross set up features the engine at an equal distance from each other. The engines are placed at the end of each beam. This is to make sure that each beam almost endures the same loads and thus four equal beams can be used. All the beams connect to one single point in the middle. This implies that in case of an engine failure there is a moment created at that point and this point has to cope with the stresses created by this force together with the forces of the other beams make this an complex problem. From the control perspective, with the engines equally spaced, an engine failure can be easily adjusted for by its neighbouring and opposing engines.

Tic-tac-toe Layout This design's driving force is its simplicity. Four beams in a well known tic-tac-toe layout with an engine placed at the end of each beam. All engines are equally spaced and thus this lay-out has the same advantages for controllability. However, because a single beam is intersected twice with at least 2 rotor radii of length in between them, a single engine failure will not lead to a large torque created in the intersecting beams.

Cross Layout For the cross layout the same problem occurs as for the spiderweb. In case of an engine failure, the beam attached will create a torque on the intersecting beam. In this setup it also creates a torque in the beam that is attached to the engine itself. This would make the design of the structure more complex in comparison to the other set ups.

The tic-tac-toe configuration is chosen because of its simplicity, four main beams with an engine at each end. The simplicity of the design means that beams can be used that are easily and cheaply produced (or even bought off the shelf). Therefore lowering the cost of the structure. Another advantage of its simplicity is that it will be easy to assemble which also lowers the (unit) cost. The layout of the design is also advantageous in the fact that torsion does not play a significant role, as for example opposed to in the cross configuration. In the case of a one engine failure the torque in the beams would increase significantly. This is not the case in the 'tic-tac-toe' setup and thus the total structure can be designed to be more lightweight.

5.2. Attachment System

Another important aspect of the design is the attachment system of the container to the UAV itself. A lot of options have been studied for different configurations. In the end a cable connection system was chosen because this system has a couple of advantages over the other options (for example: rigid attachment system in the middle square). Cables are easy to use by ground personnel and can be quickly replaced. Furthermore, the cables are lightweight and low-cost.

Even with the choice made that the cable design will be in the final product, there was still the plan to see which configuration was the best. Two configurations were studied. The first configuration attaches four cables to the four upper corners of the container and to the four intersection of the beams. For the second configuration, ropes are attached to the end of each beam. Two cables are attached to each upper corner of the container. This configuration includes 8 cables. Each of the options mentioned have their own advantages. For each of the configurations, the container is placed 1.5 m below the main structure. A load factor of 2 is used, together with a safety factor of 3, in order to assure the container can be attached to two cables and to take gusts into account.

Attached at the Intersections When the cables are connected at the beam intersections, the cables are shorter than when attached to the end of the beams. Also, since only four cables are used, the cables will be lighter and less expensive. Another advantage is that the ropes will be more vertical from the UAV down to the container resulting in a lower tensile force in the cables. This tensile force is calculated to be 167.75 kN. This means thinner cables can be used lowering the price further. After some calculations the total length of all four cables¹ was determined to be 13.68 m and with a unit cost of 76.63 €/m. The cost would be turned out to be € 1,048.35. The weight of four cables is 21.17 kg. Lugs attach the container to the cables, for this four Camlok Container Lifting Lugs² are used, with a total cost of € 503.25 and weight of 112 kg. However, the lugs that connect the rope to the container work either in vertical direction or in a maximum of 50° in the longitudinal direction of the container. This means that these lugs are not designed to cope with the angles at which the ropes are attached. They are not designed to bear the loads in this direction. Therefore the ropes are also connected right above the container with the other ropes. This will make sure that the lugs will only carry vertical loads which they are designed for. It means that some extra cable and four connection pieces are required. The extra cable length for this is 16.99 m, resulting in an extra cost of € 1,302.10 and extra weight of 26.29 kg. The four connection pieces, Gunnebo Anja 858 Super Shackles³ will cost € 291.08 and weigh 19.2 kg. The final weight of this cable attachment system configuration is computed to be 178.66 kg, costing € 3,145

Attached at the Beam Ends This option was considered because it lowers the bending caused by the lifting forces by counteracting the vertical force at the end of the beam. It decreases the vertical force acting on the end of beam by 6.13 kN. The maximum tensile force in the cables is 217.61 kN. This might have a positive effect on the beam structure with respect to bending, resulting in lower stresses and thus a lighter beam might be created. Therefore, the cost is lower and the total weight of the UAV as well. Since the maximum tensile forces are roughly the same as the four cable configuration, the same cables can be used. The cost for this system are as follows. The total cable length of eight cables is 65.88 m, resulting in a cable weight of 101.97 kg and a cost of € 5,048.84. As in the other configuration the connection of the cables above the container is the same. This results in a total price of € 7,145.27 and a final weight of 259.46 kg.

It was decided that the attachment system would be attached at the intersections. The resulting normal forces and bending forces the cables caused on the end of the beams made it worse than was originally thought. It was predicted that the bending moment created by the thrust would be minimised, this was not the case. Due to control, stability and operational purposes, it is better for the container to be as close as possible to the structure. The container must be high enough of the ground in order for a lift cart to drive underneath the container. This leads to high angles of the ropes connected to the end of the beam generating huge normal forces and bending moment around the z-axis. These are higher than the ones without the connections at the end of the beam. Thus the structure would end up with a higher weight than when attached at the intersections. So the four cable option has a lower weight and is cheaper.

¹URL: http://unionrope.com/Resource_/PageResource/Aircraft%20Cable-AC-313.pdf [cited 15 January 2016]

²URL: <http://www.dlhonline.co.uk/camlok-container-lifting-lugs-32t-to-56t-w11-1319-p.asp> [cited 15 January 2016]

³URL: <http://www.liftingsafety.co.uk/product/gunnebo-anja-858-super-shackle-bow-shackle-range-3-300kg-150-000kg-4.html> [cited 15 January 2016]

5.3. Material Selection

As already mentioned, material selection is one of the three major aspects of structural design. As such it is extremely important for the overall performance of the final resulting structure. First the method by which the materials are selected is established in Section 5.3.1, then the materials will be selected for multiple cases at Section 5.3.2 and Section 5.3.3.

5.3.1. Material Selection Process

During the material selection within set constraints and requirements the most optimal material has to be chosen. Herein a trade-off has to be made between often conflicting objectives (for example minimising both weight and cost at the same time). To be able to do this in a structured way and make full use of the complete number of materials available in the world a material selection method is needed. Once the method is known the materials can be selected using this approach. The material selection method as dictated by *Ashby* [11] has been chosen. This method consist of four steps for the material selection approach. These four steps are:

Translation Identifying the requirements, constraints, functions and desired objective parameters the material should comply to.

Screening From all available materials those that do not comply to the parameters set by the translation stage are eliminated as possible candidates.

Ranking The remaining candidates are ranked based on the objective parameters (optimisation criteria) using a performance index to order the material from best to worst.

Supporting information From the highest ranking materials more information is collected. This includes secondary information about for example sustainability, producibility, local conditions, etc. From the material indices and supporting information the best suitable material can then be chosen.

To make full use of many of the materials available a computer software tool for the screening (ranking and supporting information) stage will be used. Using this tool many materials can be explored and the screening of these materials can be done quickly. Furthermore, the materials can be easily ranked based on the optimisation criteria (the performance index). Finally, supporting information for each material will be readily available, which will make this process more quick and reliable. In this chapter the *CES EduPack (2015) by Granta* [12] will be used for this purpose. Its main feature is that it follows the principles as defined by Ashby. Furthermore, the sustainability aspects (such as primary and secondary use of energy, CO₂ emissions, toxicology, recyclability, the complete life cycle and End of Life (EOL) solution, and much more) of materials and their associated production processes can be easily explored. Unless otherwise stated the Aerospace database of the CES EduPack will be used during the material selection process.

The properties of the chosen material will be determined using this program for the structural analysis calculations. The (yield) shear strength is missing from the properties. As such a rule of thumb is used to calculate an approximation using: $\sigma_s = 0.55\sigma_f^4$. In this equation σ_s is the (yield) shear strength and σ_f the tensile (yield) strength. Finally, it has been decided to only look at metals for the design. Several reasons should be mentioned. First, the structural analysis of metals and composites are quite different in nature. It would require more time to both investigate composite and metal designs, which was determined not to be sufficient for this stage of development. Furthermore, composites are in general harder and thus more expensive to produce. Therefore, to keep unit costs down, the decision has been made for simple, easy to produce structures. Metals (especially aluminium) are, compared to composites, often used in aerospace applications and less of a liability, which should be accounted for in the development risk.

The materials will be selected using the Ashby material charts approach using the CES program. An objective parameter for example maximising $\frac{\sigma_f}{\rho}$ can be visualised on a chart. All materials with an equal ratio (so $\frac{\sigma_f}{\rho} = C$ for which C is a certain constant) are equally good on this criteria. As such a line can be drawn on a σ_f vs ρ chart with a slope of 1 and undefined C. By increasing this C, more and more materials disqualify, since they score too low on these criteria. For multiple objective parameters a

⁴URL: https://en.wikipedia.org/wiki/Shear_strength [cited 13 January 2016]

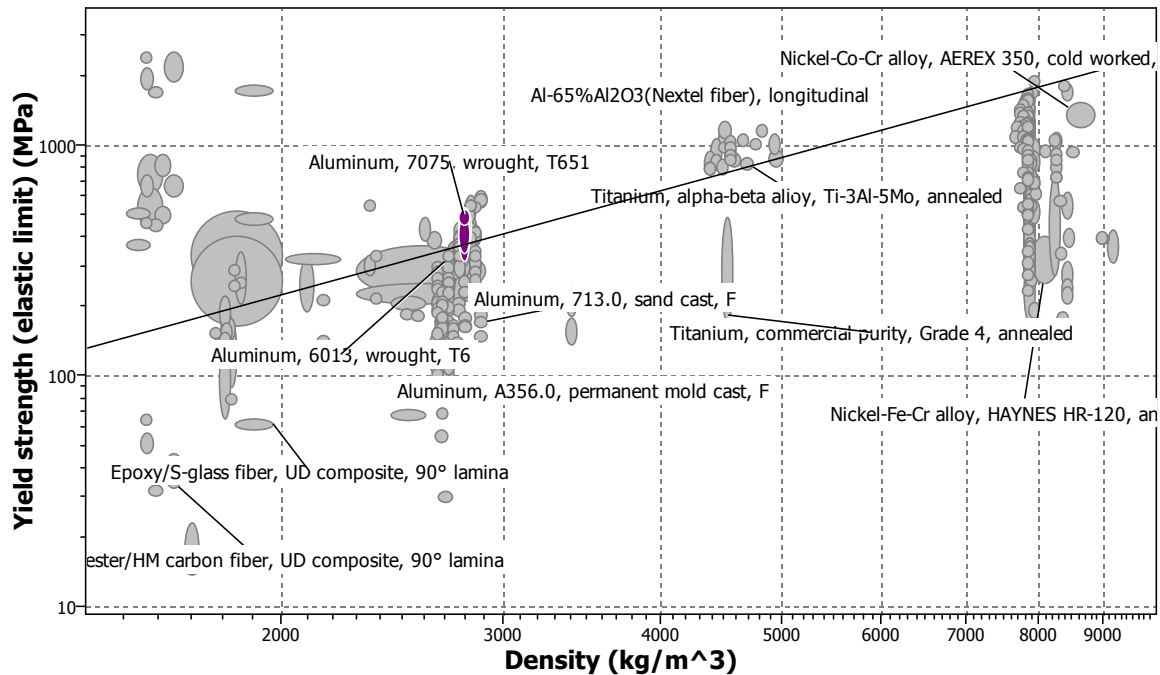


Figure 5.3: Example of a material selection chart for the selection of the main beam parameter for the objective parameter specific yield strength ($\frac{\sigma_f}{\rho}$). The greyed out materials have failed the screening process (all stages combined). The line shows the objective parameter for a constant ratio C . The parameter is maximised. Therefore only materials above this line passes this screening stage.

performance index can be created as a measure on how good each material is in total (all objective parameters taken into account) The performance index is a joint value to be able to rank the materials with multiple objective parameters. This is done by using the constants as trade-off factors. This process is done automatically by the CES material selection program. One material selection chart for the material selection for the main beam structure is given in Figure 5.3.

5.3.2. Beam Material Selection

The material of the main beam structure (to which the engines, rotor, container, fuel and all other components are attached) will be chosen using the method explained above. First the translation stage is done. Then the results of the combined screening, ranking and documenting stage.

Translation The function of the material is extremely important in determining the material shape and production process. Therefore, first the primary function of the structure should be established. The main beam structure should be able to transmit the loads. For this beam it will primarily be loaded in a bending moment. This due to the thrust of the rotors at the end of the beam and the weight in opposite direction near the centre. The top of the structure will primarily be loaded in compression and the bottom in tension during (normal) flight conditions. As such preferably two materials could be chosen—one for the tension and one for the compression case—however this will be harder to produce. Furthermore, in reversed load cases (for example on the ground when the thrust force is absent) the structure should still be able to handle the loads. From a cost and simplicity standpoint of view it is decided that only one material will be used for the complete beam. The structure should also be sufficiently stiff from a control and stability and aerodynamics point of view. Furthermore, the option to be able to store fuel and other components directly inside the structure is preferred. The structure/material should also behave appropriately over the complete operational range. The final structure should also have minimal environmental impact and be relatively cheap to produce. The main objective of the design of the structure is to make it as lightweight as possible within reasonable costs, so no hard to produce or

expensive materials will be used.

From the above mentioned functions that are required for the structure the main requirements, constraints and objective parameters can be deduced. For this the focus lies on the material selection. These constraints, requirements and objective parameters are directly inserted in the CES program.

Several requirements have been set for the design, which translate in constraints for the choice of material. One of these is: "The aircraft shall be able to withstand temperatures ranging from $-50\text{ }^{\circ}\text{C}$ to $60\text{ }^{\circ}\text{C}$." (see Table 2.1 in Chapter 2). To ensure this the minimum maximum service temperature is set to $60\text{ }^{\circ}\text{C}$ and the maximum minimum service temperature to $-50\text{ }^{\circ}\text{C}$. The aircraft will be primarily be operated in warm and humid environments. Furthermore, the cargo containers are delivered at a port from which the aircraft will transport them to the military base. As such also a salty corrosive environment should be taken into account for the operational life of the aircraft. Therefore, the resistance to (salt) water is set to limited use to excellent in the program.

As mentioned in the explanation of the material selection process (Section 5.3.1) the choice has been made to go for a cheap and easy to produce product. Also the focus lies purely on metals. Therefore, a requirement for metal (hot or cold) forming has been set for the material selection. To ensure the material will not be disproportionally expensive a maximum of 20 €/kg is set for the material cost. Also the UV radiation capability of the material has been set to good to excellent and the flammability to slow-burning to non-flammable. The last due to the risk of engine failure and risk of being hit by foreign projectiles. Finally, sustainability should be taken into account. The choice has been made to make it at least completely recyclable for the EOL.

For the translation step of the material selection method, first the requirements have to be set. The first requirement is recyclability of the material for the EOL solution. Further Requirement: End-of-life (recyclability), Metal hot forming (acceptable to excellent), metal cold forming (acceptable to excellent),

As previously mentioned the beam is primarily loaded in bending and needs to be strong and stiff. Additionally it should be designed to be damage tolerant and have appropriate fatigue strength, while being lightweight. Furthermore, the shape is pre-specified. The objective parameters are given in terms of specific values (as a ratio of the objective parameter and the density of the material). For the strength

criterion the ratio $\frac{\sigma_f^2}{\rho}$, for the stiffness $\frac{E}{\rho}$ and for the damage-tolerant (fatigue) σ_f should be maximised. σ_f is again the tensile (yield) strength, the E is the Young's modulus and finally ρ is the density of the material. [11]

Screening, ranking & documentation Using the constraint, requirements and objective parameters for the material as identified in the translation stage the screening process can begin. The importance of each individual objective parameter is cranked up as much as possible. This to reduce the number of materials left for the ranking and documenting stage. Especially a lot of weight is put in the fatigue requirement as this is of primary importance for aerospace applications. The results of the screening and ranking phase can be seen in Table 5.1. The materials left from the screening process include multiple Aluminium 7075 alloys with different treatments and one Aluminium 7175. All materials are widely used in aerospace applications and do not seem to have any negative drawback with respect to each other. Furthermore, the material properties lie close together. As such the choice is made to use Aluminium 7075 T6510/1 for the main beam structure. Aluminium 7175 is better in quite a few areas (particularly strength). However, it is slightly worse in Young's modulus. Since the main beam structure is also primary vibration limited this property is invaluable (see Section 5.4.3). Though, the 7175 material is perfect for other applications such as a landing gear (see Section 5.3.3).

Table 5.1: Result of the screening and ranking stage for the material for the main beam structure.

Material name	Performance index (—)
Aluminium 7075 T6510/1	0.00307
Aluminium 7075 T62	0.00305
Aluminium 7075 T651	0.00305
Aluminium 7075 T6	0.00304
Aluminium 7175 T66	0.00303

5.3.3. Landing Gear Material Selection

In this section, the material selection method is applied at the landing gear. A translation, screening, ranking and documentation is performed.

Translation There are many similarities between the main beam structure and the landing gear. As such the differences are stretched in this subsection. The requirements and constraints for the material selection are identical for the main beam structure. The difference is primarily in intended purpose of the structure and the associated objective parameters to fulfil these functions. The main strut for the landing gear primarily has to have a high bearing strength. It should also be stiff enough to not fail in column buckling. The drag struts can be seen as simple trusses (only loaded in either tension or compression). Therefore, these need to have high tensile and bearing strength and has to be stiff enough to not fail in column buckling. The stiffness can also be achieved with a high moment of inertia of the structure. As such there is not much weight given to this objective parameter. In comparison to the main structure there is also no need to store anything. It is advantageous from a manufacturing point of view to limit the number of materials used. As such the choice has been made to use just one material for the landing gear. From these function described above the objective parameters can be deduced, which are maximising stiffness $\left(\frac{E}{\rho}\right)$, bearing strength $\left(\frac{\sigma_b}{\rho}\right)$, fatigue σ_f . The symbols are the same as before. Additionally σ_b means the (yield) bearing strength of the material.

Screening, ranking & documentation Similarly to before the materials can be screened and ranked using the constraints, requirements and objective parameters. The results of this process can be seen in Table 5.2. As can be seen from the table similar materials as for the main beam structure are the result. Aluminium 7175 T66 is the best one and as earlier mentioned has far better material strength in comparison to the 7075. As such this material will be chosen for the landing gear as this will result in the most lightweight design.

Table 5.2: Result of the screening and ranking stage for the material for the landing gear structure.

Material name	Performance index (—)
Aluminium 7175 T66	0.169
Aluminium 7075 T6510/1	0.164
Aluminium 7075 T6	0.163
Aluminium 7075 T652	0.160
Aluminium 7075 T76510/1	0.158
Aluminium 7175 T73511	0.153

With the materials selected the structure can be designed and the shape can be optimised for the applied loading case and the material selected in this section.

5.3.4. Aerodynamic Fairing Material Selection

The main structure of the UAV due to the relatively large size and rectangular shape is very undesirable from an aerodynamic drag point of view. This has adverse effects on the performance and control characteristics of the aircraft. To reduce these effects the drag should be lowered. This should be done preferably in a cheap, lightweight way without changing the main structure. This is done by applying aerodynamic fairings around the structure. By giving the main beams a more streamlined shape the aerodynamic drag is reduced. The material for the aerodynamic fairings is selected in this subsection.

Translation The main function of the aerodynamic fairings is to alter the shape of the main structure and as such reduce the drag and enhance the performance characteristics. For this a material is required that is able to keep its shape in the airflow under all conditions. As it only has to alter the shape it can be made of a very lightweight and cheap material. As the fairings are outside the structure it can also protect the main structure a bit from its environment. As such at minimum the fairings perform well in the environment the aircraft is in operated. This means the operating temperature range of -50°C to 60°C , resistance to (sea) water (limited use to excellent), UV radiation (good to excellent) and be

resistive to fire (slow-burning to non-flammable) (or slow burning). These are the constraints set for this material. The requirements are again that it should be a recyclable material and it should be able to be manufactured in a simple way. For example the fairings should be able to be produced by simple cutting of a foam like material. The objective parameters for the material selection are density and cost. With most priority going to mass as the material cost will relatively be less important as long its easy(/cheap) to manufacture. For this material selection the foam material database is used. This due to the very limited (and virtually non-existent) number of foam and other really low density materials that are suited for fairings.

Table 5.3: Result of the screening and ranking stage for the material for the aerodynamic fairings. In order of the material density.

Material name	Recyclable (—)
Aluminum-SiC Foam (0.07)	YES
PVC coss-linked foam	Only downcycle
Phenoloic foam (0.035)	Downcycle & biodegradable

Screening, ranking & documentation Aluminum fulfils all requirements and constraints. It's lightweight and it has the added benefit that the aerodynamic fairings could also be used for energy absorption, crash protection, thermal insulation and much more. This makes the fairings multi-functional. Smartening the design by giving things multiple purposes. However, the material is a poor fit as aerodynamic fairings. The material is too coarse, which will cause too much drag and defeat the purpose of fairing in the first place. Furthermore, the density for a foam is still too high. With approximately 3 m³ of foam material required it would mean it would weight about 204 kg, which would add considerably a lot of structural weight. Therefore, the requirement for the EOL of the material is made less strict. The result is two more materials that could be chosen from.

The Phenoloic material has several benefits over the PVC foam material (and as such is chosen as the foam material). It is bio degradable by the white fungus *Phanerochaete chrysosporium*⁵ and could be used for other purposes (thermal insulation and energy absorption). This material has bad durability against alkalis as such there is a need for coating/painting to protect the fairings against this and/or care during maintenance (cleaning products used on the aircraft).

5.4. Structural Analysis and Design

The material selection for the structures has already been conducted in Section 5.3. The important aspect from this section is that the focus is on a metal structure, which has an uniform material. Similarly to the material selection section is to start with some basic assumptions and describe the overall method and tools used. This is done in Sections 5.4.1 and 5.4.2.

5.4.1. Assumptions, Notes and Failure Modes

In this subsection the main assumptions for the structural analysis are summarised. These assumptions will be applicable to all structural analysis calculations. Furthermore some additional notes will be mentioned along with the failure modes each structure is test for.

Assumptions An important aspect of structural analysis is the assumptions made. The assumptions made are itemised down below.

General

- Thin-walled structure (constant shear flow over thickness, neglect thickness to the power two and higher order terms)
- Cross-section has two planes of symmetry (shear centre in the centre of the cross-section)
- Linear material/structure (small displacements and deflections, thus tensile and compression Young's modulus are equal)

⁵URL: https://en.wikipedia.org/wiki/Phenol_formaldehyde_resin [cited 22 January 2016]

- Material is isotropic
- Constant/uniform material in the beam
- Beam is long with respect to its depth (beam theory applicable)
- Beam is perfectly straight
- No imperfections in the structure (notches, holes, manufacturing imperfections, rivets, attachments, etc)
- 3D structure can be modelled as individual beams
- Vertical displacement of the beam due to shear is negligible (only due to bending)
- All loads are applied to the centre of the cross-section
- Neglected thermal stresses
- Neglected dynamic loads (in static analysis)
- Gust induced load factors neglected
- No extreme manoeuvres
- Linear fatigue assumption
- Mass of the beam neglected
- Distributed load from fuel weight neglected (modelled as a point load)
- For buckling, eccentricities are neglected
- For buckling, initial bending of the beam is neglected
- For buckling, imperfections in the beam manufacturing is neglected

Discretization in cross-sectional elements

- Beam can be discretized in N_x elements with small length dx
- Constant internal normal and shear forces and moment and torsion
- Constant cross-sectional shape

Discretization of cross-sectional element in plates

- Cross-section can be discretized in N_p elements and stress determined for each point
- Plane stress applicable (thickness really small)
- Stresses constant over plate
- Principal stress along the circumference of the cross-section is zero⁶

⁶URL: http://icozct.tudelft.nl/TUD_CT/CT3109/collegestof/elasticiteitsleer/files/CT4145Lecture_Notes-version7.pdf [cited 25 January 2016]

Additional Notes There are several notes that need to be taken into account for the structural analysis. A safety factor of 1.5 is applied to all failure conditions (unless otherwise mentioned). This safety factor is the minimum required value as dictated by the certifications (EMACC) [15]. The safety factor is intended to ensure the structure will not fail and that there is appropriate margin built in. It also accounts for the assumptions and small calculation errors (computer discretization errors). The main beam structure is designed for the maximum load factor. As mentioned in the assumptions gust loading has not been taken into account. As such the maximum (limit) load factor for a rotorcraft⁷ is given in Equation (5.1).

$$n_{max} = \frac{T_{max}}{W} \quad (5.1)$$

In the n_{max} is the maximum (limit) load factor, T_{max} the maximum thrust output of the rotorcraft and finally W the (design) weight of the aircraft. The maximum thrust output of the rotorcraft is 240 kN. The weight is set to 14.5 metric tonnes. As such the maximum load factor is approximately 1.69. The ultimate load factor (limit load times the safety factor of 1.5) is thus 2.54, which is used as the load factor for the structural calculations. The minimum load factor is assumed to be zero for the main structure, which is reasonable for any normal operations for a rotorcraft.

The aircraft is designed for approximately 10,000 cycles or equivalently 5,000 missions. This gives the structure of the rotorcraft a low operational lifetime in return for a low operational empty weight (and thus low costs).

Failure Modes The structure has to be designed in such a way that it will not fail when the loads are applied. A structure can fail in a multitude of ways. Not all these failure criteria are applicable to all structures. In case of a truss structure, one that will only carry axial loads (tension or compression), only the yield, column buckling, fatigue and minimum thicknesses are applied.

- Yield tensile strength (σ_f)
- Yield bearing strength (σ_b)
- Yield Von Mises stress (σ_f)
- Yield Shear strength (σ_s)
- Maximum beam deflection (in two direction) (δ)
- Maximum beam elongation due to axial loads (ϵ)
- Maximum twist angle (ϕ)
- Minimum fuel capacity for fuel storage within the structure
- Euler column buckling
- Local buckling of the plates
- No signs of fatigue under the set design number of load cycles (approximately 10,000)
- Minimum thickness for manufacturing purposes

5.4.2. Structural Analysis Tool

The main assumptions, failure modes and equations determined in Section 5.4.1 are used in the structural analysis calculations. A structural analysis tool has been created for multiple purposes. Among others it allows for faster calculations, change small things when necessary (extend the programme) and to optimise the structure for mass. This is more advantageous over a purely analytical approach, which would mean redoing everything for each individual problem. With a good designed numerical programme a lot of code can be reused. This means less verification steps, less development time and more complex problems can be solved.

⁷URL: <http://soliton.ae.gatech.edu/people/dschrage/AE8804/RDII%20Struc%20Design.ppt> [cited 25 January 2016]

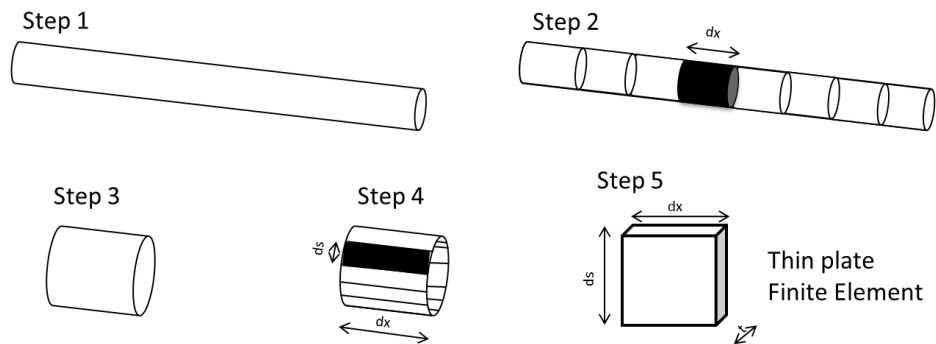


Figure 5.4: Visualisation of the discretization method used in the structural calculations.

General Information Structural Optimisation Tool The tool has been created using Python [13] and follows the Object Oriented (OO) programming paradigm. In its essence it is a python module consisting of multiple files. Several files contain a lot of functions to be used in multiple locations to allow as much code reuse as possible. Examples of this are the function for calculating stresses or plot functions. The remaining files are used for the actual structural analysis problems. For example there is one that defines an object, which is the main beam structure. One can instantiate this beam with some dimensions (such as the total length of the beam), a cross-section type (with dimensions) and a material to apply to the beam. After instantiation loads can be applied to the beam, the stresses can be calculated and finally it can be checked whether the beam fails according to the pre-specified failure modes for the structure. The cross-sections are objects themselves. The programme has been created in such a way that cross-sections are not fixed to a specific structure, but can be easily swapped.

As described above the main work flow of the programme is to instantiate (in the programme) a structure with some dimensions, material and cross-section, then apply loads and calculate stresses and finally to check whether the structure fails. This has been done specifically to make the programme as flexible as possible. Due to the concurrent engineering approach used in this project it can not be fully known in advance on which dimensions a restriction is placed on or which parameters to optimise for. Using the above mentioned approach this can be changed rather easily without changing how computations are done. This makes the programme more useful in multitude of cases and more robust (as changes can be made rather easily when design requirements change).

The programme uses discretization of the beam in small elements to be able to calculate the stresses in a numerical way. The beam is first discretized in N_x elements along the span of the beam. For each small beam element the cross-section and internal loads and moments are held constant. The length of such a small beam is dx for which $dx = \frac{N_x}{L}$, with L being the total length of the beam. Each small beam element is again further discretized along the outer edge in N_p points. Each element being a thin plate with dimensions $ds \cdot dx \cdot t$. With ds small length across the circumference of the cross-section and t the thickness of the cross-section. This way the shear flow can be calculated along the cross-section without having to rely on analytical solution, which would violate keeping cross-section and stress calculations separate. An added benefit is that each finite element can be thought of as a small thin plate. On these plates the plane stress assumption is applicable. As such the stresses on the beam can be calculated using 2D stress tensors rather than the full 3D calculations, which simplifies the stress analysis, calculations and computation times. The discretization method used can be seen in Figure 5.4.

Optimisation In aerospace engineering minimising mass of the aircraft is one of the most important objectives, which should always be aimed for. To accomplish this within the set (dimensional) constraints the design of the structure should be optimised. One can optimise for shape (type of cross-section), topology (overall design of the structure) or size (dimensions). The programme is able to optimise both for shape (between the implemented types of cross-sections) and size. Topology is not possible as that is fixed for the type of structure implemented (for example the main beam structure or the landing gear strut).

For the structures designed in this chapter shape optimisation is used. Each free variable (that is not fixed and can be freely changed within a pre-specified range) is simultaneously optimised for using

one of the methods described above. An example of a free variable might be (for example) the radius of a cross-section. During optimisation each beam is instantiated with the given fixed and free variables, loads determined, stresses calculated and then each the beam is tested on each failure mode. If the beam fails on any failure mode the beam is failed. As optimisation requires an objective function to be minimised the mass of the beam is returned when it does not fail and set to infinity when it fails. For the brute grid method (described below) this can easily mean that during the optimisation process of one beam 160,000 (20^4) total instances of beams are evaluated (with four free variables: width, height, top thickness and web thickness and 20 points per free variable).

As optimisation is a computational expensive activity several methods are used with different pros and cons. Gradient approaches are not possible, due to the design of the programme and the necessity of being able to bound the free variables in the optimiser. The methods that are used fall into two categories; brute grid and differential evolution.

Differential evolution is a method of optimising an function. A generation of (semi)-random structures (candidate solutions) is generated. Each structure in a generation is analysed and the best are crossed and mutated, which forms the new generation. This continues until some parameter is met. The advantage over the brute grid approach is that it is fast and can quickly produce results, but the solution can easily overshoot. As such it is great to get a fast and good initial guess to use as starting point in the brute grid approach, which can further refine the result. During calculations in general about at most 50 generations were needed.

The brute grid approach discretize each free variable (n total) in a pre-specified possible range in equal N points. For each point (total of N^n points) in the n dimensional cube a structure is created and the objective function can be evaluated. The disadvantage of this approach is that, depending on the number of variables n and the resolution N , it scales bad and computation times are long.

In an attempt to speed things up an alternative version of the brute grid approach was created. This method does the brute grid approach several times with a low resolution N . Each time it searches the solution in a narrower domain around an initial guess x_0 . The solution of each iteration is used as a new guess x_0 for the next iteration. If the solution lies on the boundary of the domain the iteration is done again, but now with the domain translated. The advantage of this approach over the pure brute grid approach is that it can be reasonably faster (as long as the initial guess x_0 is chosen correctly and not many times an iteration has to be redone). Parallel versions of the above mentioned algorithms were tried. However, due to Python's limitation (GIL;Global Interpreter Lock) this did not gave a significant increase in computation speed.

The advantage of all above mentioned optimisation techniques is that they are more likely to find global optimums over local optimums than traditional gradient approaches. This results in a more optimised and thus more lightweight structure.

For all these methods an objective function is optimised (minimised). In each case a structure with certain parameters is instantiated, loads applied and the stresses calculated. If the structure fails on any of the specified failure conditions the objective function returns an infinite mass for the beam. This to ensure it will always be higher than any structure that succeeds. If the structure does not fail the mass of the structure is returned. This way the structure can be optimised for the mass.

Visualising the results One important aspect is properly interpreting the results and using them in a meaningful way. This can be done using visualisation. Several things are possible with the programme. The first is to simply plot loading diagrams and/or Von Mises stress in a simple graph. However two other things have been done. The first is to automatically generate the CATIA [14] Computer Aided Design (CAD) model to see how the resulting structure looks like. Secondly, the structure can be visualised in 3D using OpenGL (see Figure 5.5). This shows the Von Mises stress (or some other parameter) plotted using a colormap over the structure for each discretized point. This has many advantages to interpret and verify the results. For example it can be verified whether there are no anomalous discontinuities in the stresses and if it looks as expected.

Verification & Validation Each function and equation used in the programme has been independently verified using an analytical approach for a simple case in so called unit testing. In addition to the unit testing several other methods were used. The loading diagrams were verified by comparing them with



Figure 5.5: An example of the OpenGL output for the main structure beam in flight direction.

a free beam calculator⁸. As explained earlier the 3D visualisation was used to see if the Von Mises stress distribution looked as intended and if there were not any discontinuities. Furthermore CATIA was used to verify the mass calculations for the structures. Also many units were tested analytically by hand calculations. These unit tests (where applicable) were implemented as automatic unit tests in the Python program. This to ensure continuous verification of the solution. Finally, it was also verified whenever the solution converges (discretization error to zero) when the number of discretizations increased (N_x and N_p). It is determined that already 1000 beam elements with 32 points along the cross-section is more than enough for these structures. These values also will be used in the design of the structures below.

Since this concept is a novelty, very little validation data is possible to obtain. Therefore, it is recommended to validate this concept in a further design stage. This can be done using Finite Element Method and/or experimental testing. However a simple sensibility test can be done. All results in this section are reasonably and as such can be assumed to be correct.

5.4.3. Design of the Main Structure

In order to determine the dimensions of the main structure beams, a model has to be set up. Then, the loading diagrams can be plotted and the design results can be shown.

Model In order to determine the exact dimensions and weights of the main structure, a structural analysis has to be performed. This is done using a model of one single beam. In reality, all four beams are clamped to each other. However, a tic-tac-toe structure in which all beams are clamped to each other is statically indeterminate. In order to simplify calculations, only individual beams are analysed. These individual beams are modelled to be hinged to the other beams, as can be seen in Figure 5.7a. Also, these beams are assumed to be loaded symmetrically. The analysis of each individual beam is done twice. First, in the xy-plane, then in the xz-plane. For each beam, this axis system is the same. In other words, the beams that are placed parallel to flight direction and the beams that are placed perpendicular to flight direction both have the x-axis in the direction of the length of the beam. This can be seen in Figure 5.6. This figure also depicts all major loads acting on the main frame like thrust of the rotors, weight of weight of the craft and forces of the cables. A lot of moments are not included in this figure, but they are explained in Table 5.4. Loads are applied at the outer sides of the beam, at points A and D. Six loads can be applied per point: forces in x, y and z-direction (F_x , F_y and F_z), moments around the y and z-axes (M_y and M_z and a torque around the x-axis (T). The forces in y-direction are assumed to be equal and in the same direction (symmetry assumption). However, the forces in z-direction are placed in opposite direction. Each beam is attached to the other beams at points B and C. As said, these points are modelled as hinges, simply supporting the beam. In these points reaction forces act in order to keep the beam in static equilibrium. These reaction forces can be calculated using the following equations:

$$F_{C_y} = -\frac{M_{A_z} + M_{D_z} + F_{D_y} \left(\frac{L}{2} + R\right) - F_{A_y} \left(\frac{L}{2} - R\right)}{2R} \quad (5.2)$$

$$F_{B_y} = \frac{M_{A_z} + M_{D_z} - F_{A_y} \left(\frac{L}{2} + R\right) + F_{D_y} \left(\frac{L}{2} - R\right)}{2R} \quad (5.3)$$

$$F_{C_z} = \frac{M_{A_y} + M_{D_y} - F_{D_z} \left(\frac{L}{2} + R\right) + F_{A_z} \left(\frac{L}{2} - R\right)}{2R} \quad (5.4)$$

⁸URL: <http://bendingmomentdiagram.com/> [cited 10 January 2016]

$$F_{B_z} = -\frac{M_{A_y} + M_{D_y} + F_{A_z}\left(\frac{L}{2} + R\right) - F_{D_z}\left(\frac{L}{2} - R\right)}{2R} \quad (5.5)$$

Since these points are hinged, no reaction moments act here. It can be seen that no forces are applied at A and D in x-direction. As a result, no reaction forces at B and C in x-direction are included. However, there are forces acting in B and C, which are external forces induced by the cables. These forces apply a compressive force over the length of the beam from B to C.

$$F_{B_x} = -F_{C_x} \quad (5.6)$$

With these reaction forces known, loading diagrams can be made. Using these loading diagrams, internal loads can be determined: the internal normal force (N) (axially into the beam in the x-direction in the beam coordinate system), the internal shear forces (V_y, V_z), internal bending moments (M_y, M_z) and the internal torsion (T). These internal loads determine the final cross section of the beam. The internal stresses these loads will induce, are never allowed to exceed the maximum stresses. The equations used and explained in this section are all derived from Megson [17]. In order to calculate the stresses in the beam, a few equations are needed. First the equation for normal stress:

$$\sigma = \frac{N}{A} - \frac{M_y z}{I_{yy}} - \frac{M_z y}{I_{zz}} \quad (5.7)$$

Here, σ is the normal stress and A is the cross sectional area. Since the normal stress also depends on the internal bending moments around the y and z axis see Figure 5.7b, these are included too. A rectangular cross section is chosen, since this cross section is relatively efficient in bending (the major load acting on the main structure) and subsystems can be stored inside. The normal stress due to bending moment is dependent on the location in the cross section, y and z , and also on the moments of inertia around these two axis I_{yy} and I_{zz} . The shear stresses are computed from the shear flow q .

$$\tau = \frac{q_s}{t} \quad (5.8)$$

Here, τ is the shear stress and t is the thickness of the plate in which the shear is acting. This equations uses the thin-walled cross section assumption. The shear flow can be calculated as:

$$q_s = q_b + \frac{T - \oint p q_b ds}{2A} \quad (5.9)$$

Here, p is the distance from a web to the shear centre and s is the length at which the shear flow acts Figure 5.7b. In this equation, q_b can be calculated using the following:

$$q_b = -\left(\frac{V_y}{I_{zz}}\right) \int_0^s t y ds - \left(\frac{V_z}{I_{yy}}\right) \int_0^s t z ds \quad (5.10)$$

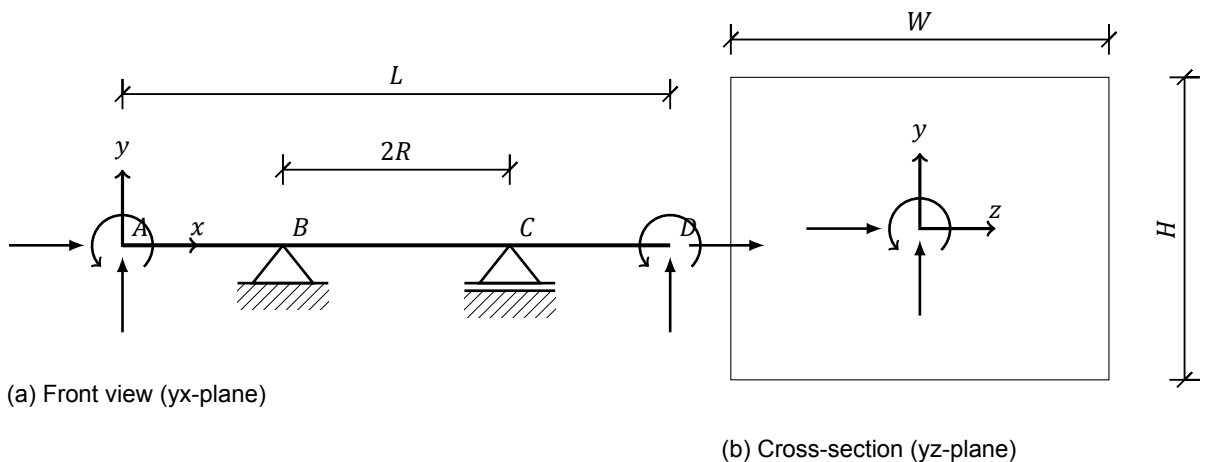


Figure 5.7: Beam forces and dimensions. Forces are indicated by straight arrows and moments with the curved arrows applied at a point.

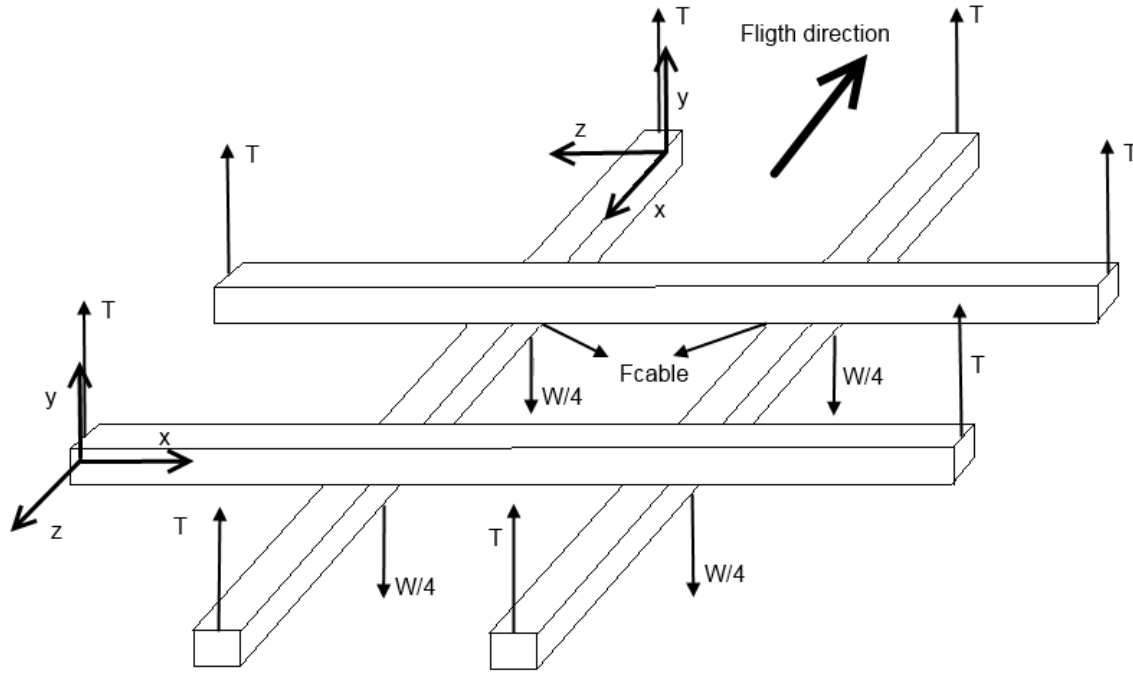


Figure 5.6: Free Body Diagram showing all major forces acting on the main frame. The axis system of the beams perpendicular to flight differ from those parallel to flight direction.

As stated in the Section 5.4.1, the beams may not yield in Von Mises, fail in column and plate buckling, no failure due to loads above the fatigue limit over time and may not deflect too much. Since the rotors can not clash into each other, the deflection criterion is needed. First, the Von Mises yield criterion is shown. The Von Mises yield criterion is as follows:

$$\sigma_y = \sqrt{\sigma_x^2 + 3\tau^2} \tag{5.11}$$

Where σ_y is defined as the Von Mises yield criterion, σ_x is the normal stress and τ is the shear stress. The column buckling equation is:

$$P_{cr} = \frac{n^2\pi^2EI}{(k \cdot L)^2} \tag{5.12}$$

P_{cr} is the critical compressive force at which the beam will buckle. The factor k accounts for what support both ends of the beam have. thus changing the effective length of the beam. This beam (modelled as a two hinged beam) therefore has a k of 1. n determines in which mode the beam buckles. However, the first mode is only determined so n is 1, E is the materials Young's modulus and I the lowest moment of inertia. The plate buckling equation is shown below:

$$\sigma_{cr} = \frac{4\pi^2E}{12(1-\nu^2)} \left(\frac{t_{sk}}{b_{sk}} \right)^2 \tag{5.13}$$

σ_{cr} is defined to be the critical stress at which the plate buckles, ν is the Poisson's ratio and t_{sk} and b_{sk} are the skin thickness and width. The fatigue criterion is:

$$S_a = S_{a,0} \left(1 - \frac{S_m}{S_u} \right) \tag{5.14}$$

Here, S_a is the allowable stress amplitude, $S_{a,0}$ is the stress amplitude required to produce fatigue failure at N cycles with zero mean stress, S_m is the mean stress and S_u is the ultimate tensile stress. Since the rotors are not allowed to clash into each other, the beams may not deflect too much. Therefore, the rotor may not move $0.10 \text{ m} \left(\frac{8.2-8}{2} \right)$ in the direction of the other rotor. So, the beam on which the

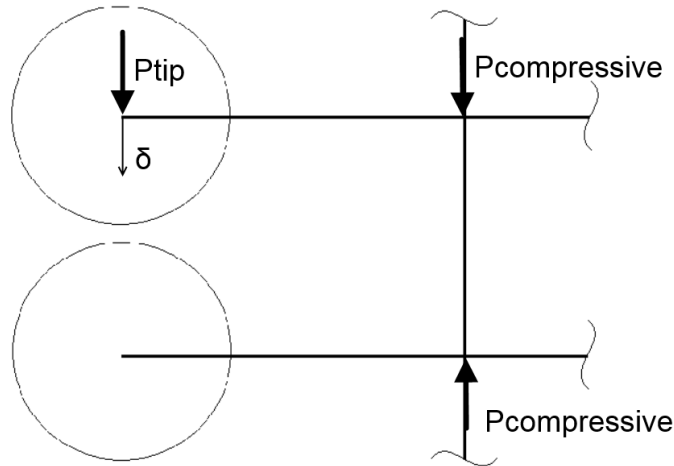


Figure 5.8: Schematic top view of two rotors. The deflection of one cantilever beam depends on the total tip force (at the rotor) and the compressive force of the beam perpendicular to it.

rotor is placed, may not deflect more than 0.10 m at the tip. This deflection can occur due to deflection of this beam itself, but also due to compressive deflection of the beam perpendicular to this beam, see Figure 5.8.

$$\delta = \frac{P_{tip} L_{rotorbeam}^3}{3EI} + \frac{P_{compressive} L_{perpendicularbeam}}{EA} < \frac{0.10}{SF} \quad (5.15)$$

P_{tip} is the load applied at the tip of the rotor beam, $L_{rotorbeam}$ is the length of this beam, $P_{compressive}$ is the compressive load applied at the perpendicular beam and $L_{perpendicularbeam}$ is the length of this perpendicular beam. The safety factor is called SF.

Loading diagrams Using Equation (5.2), Equation (5.3), Equation (5.4) and Equation (5.5), loading diagrams can be determined, see Figures 5.9 to 5.12. These loading diagrams are plotted for both the beams perpendicular and the beams parallel to the flight direction. For both of the beams diagrams are plotted in the xy-plane and the xz-plane.

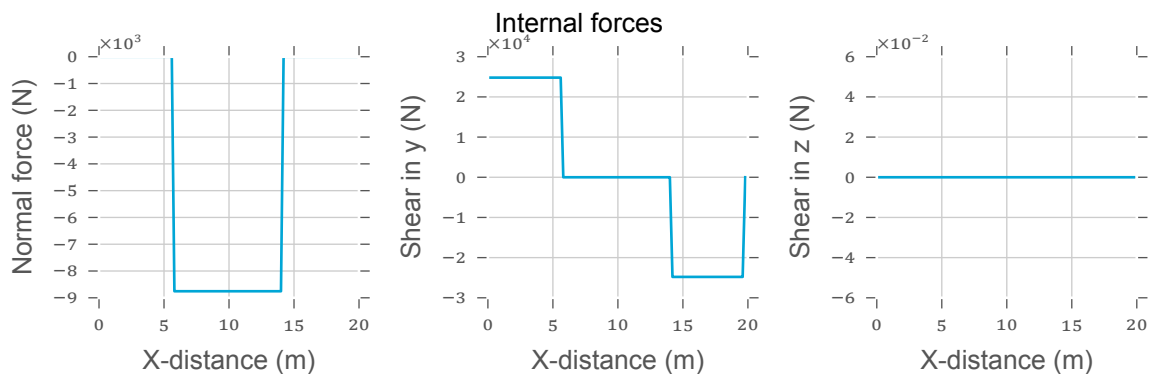


Figure 5.9: Force loading diagrams in x, y & z direction for the main beam structure in flight direction

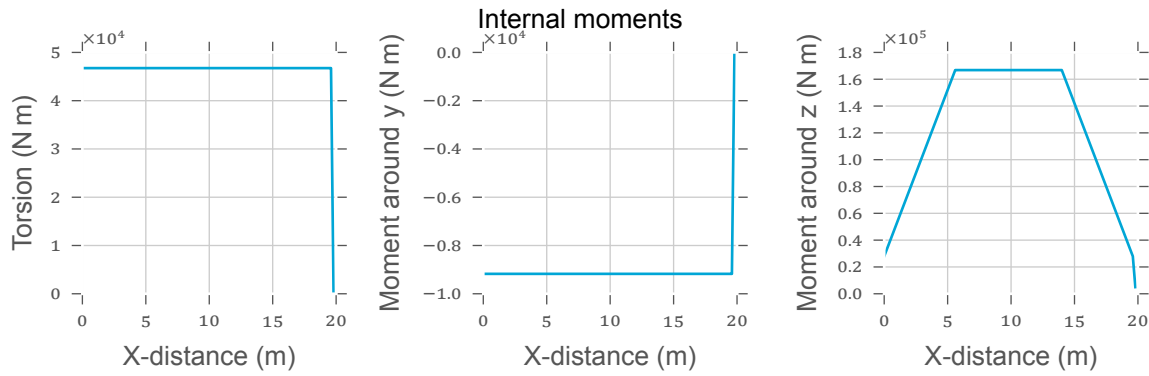


Figure 5.10: Moment loading diagrams in x, y & z direction for the main beam structure in flight direction

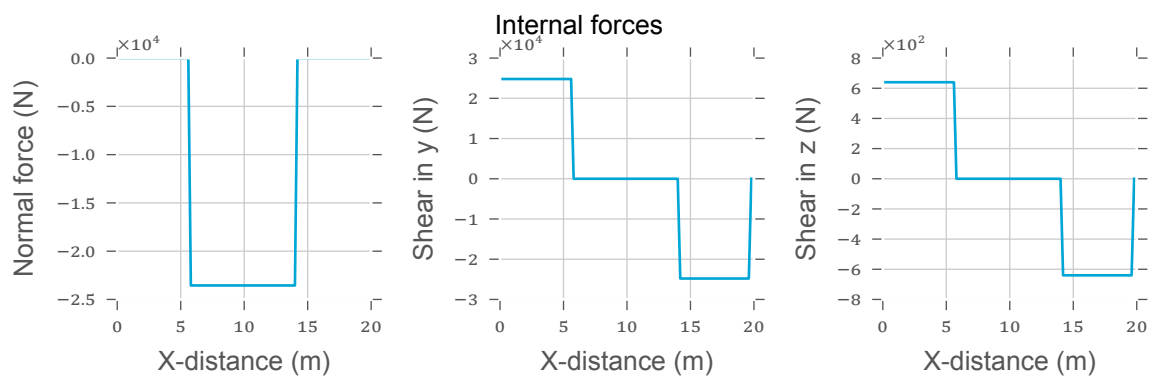


Figure 5.11: Force loading diagrams in x, y & z direction for the main beam structure perpendicular on flight direction

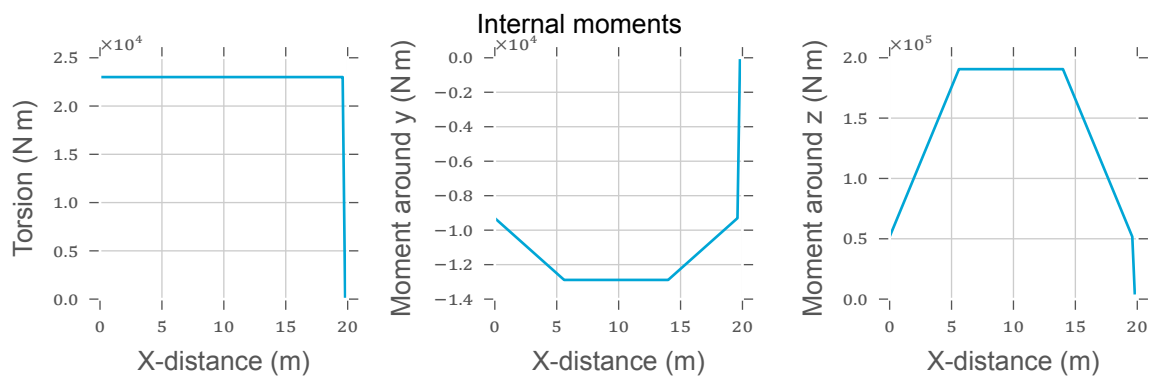


Figure 5.12: Moment loading diagrams in x, y & z direction for the main beam structure perpendicular on flight direction

Results Using the structural analysis tool Section 5.4.2 and the applied load case (see Table 5.4) a beam can be optimised. The results of this process can be seen in Table 5.5. The applied loading is determined by the Aerodynamics and Flight Propulsion and Performance group for cruise conditions. The aforementioned load factor is used to design the aircraft for all load conditions. As stated before, each beam is optimised for weight. In other words, a lot of different beams have been analysed, varying the height, width, top plate thickness and side web thickness of the cross section. In the end, the beam with the lowest weight that still did not fail in any of the failure modes was chosen.

Table 5.4: Load case for which the main structure is designed. Only point A is given. Point D is symmetrically loaded with respect to point A. Descriptions are given on the source of the loads.

Description	Flight direction	Perpendicular	Unit	Description
F_{Ax}	0	0	kN	Axial loads at rotor location
F_{Ay}	23.25	23.25	kN	Thrust loads
F_{Az}	0	0.64	kN	Rotor drag
M_{Ax}	46.747	23	kN m	Uneven thrust distribution (see Figure 6.10h)
M_{Ay}	9.175	9.175	kN m	Rotor torsion
M_{Az}	23	46.747	kN m	Uneven thrust distribution (see Figure 6.10h)
F_{Bx}	0.8755	23.552	kN	Cable compressive force

Table 5.5: Summarisation of the main structure. Values are per beam.

Description	Flight direction	Perpendicular	Unit
Length	19.8	19.8	m
Width	0.6	0.77	m
Height	0.7	0.4	m
t_{top}	0.0018	0.0035	m
t_{web}	0.0016	0.0015	m
Material	Aluminium 7075-T6501/1		
Mass	243.46	364.63	kg

Vibrational Analysis In order to guarantee structural integrity during its operating life vibrations have to be studied, the natural frequency has to be known. The first step to compute the natural frequency (ω) is to model the beam into a structure that is close enough to reality to be reliable and still simple enough to be computable with the help of simple methods. The situation for half a beam is shown in Figure 5.13 and the simplified FBD is also shown in Figure 5.14. First the beam perpendicular to the flight direction is shown. m_1 and m_2 are the masses (will be discussed later). Stiffness of the springs (k) drawn in the FBD is the bending stiffness of the original beam given in equation Equation (5.16). With $L_1 = 4.1$ m, $L_2 = 5.7983$ m, $E = 82 \cdot 10^9$ and $I_y = 2.5652 \times 10^{-4}$ m⁴. However, k_1 also has the beam in flight direction attached, so this stiffness of that beam also has to be added to k_1 in order to create the equivalent stiffness. The stiffness of the intersecting beam is also equal to Equation (5.16). This is for the up and down oscillation. In order to know the side to side oscillation the moment of inertia around the z-axis has to be computed which leads to $I_z = 4.5332 \times 10^{-4}$ m⁴. In this case the Equivalent stiffness of the beams intersecting is also different because now this beam is being compressed instead of bent. Thus that stiffness is different and is as shown in Equation (5.17) The same has to be done for the beam in flight direction which has a different cross section and thus a different moment of inertia and stiffness in both directions ($I_x = 7.9850 \times 10^{-4}$ m⁴ and $I_z = 6.0763 \times 10^{-4}$ m⁴). Once these are known the next step can be taken.

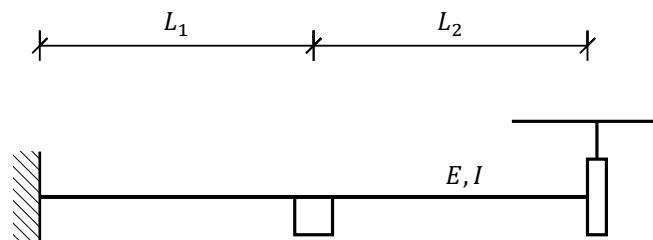


Figure 5.13: front view of half the structure cut at the middle

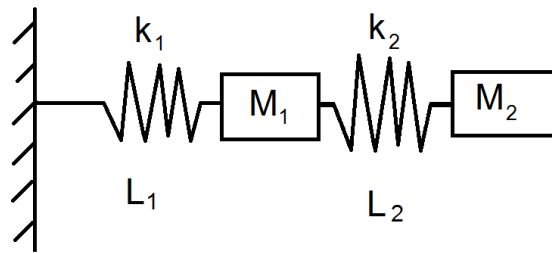


Figure 5.14: FBD of the problem

$$k = \frac{3EI}{L^3} \tag{5.16}$$

$$k_{compression} = \frac{EA_{compressedbeam}}{L_1} \tag{5.17}$$

First the constitutive equations and equations of motions are set up and combined creating the following equations in matrix form Equation (5.18):

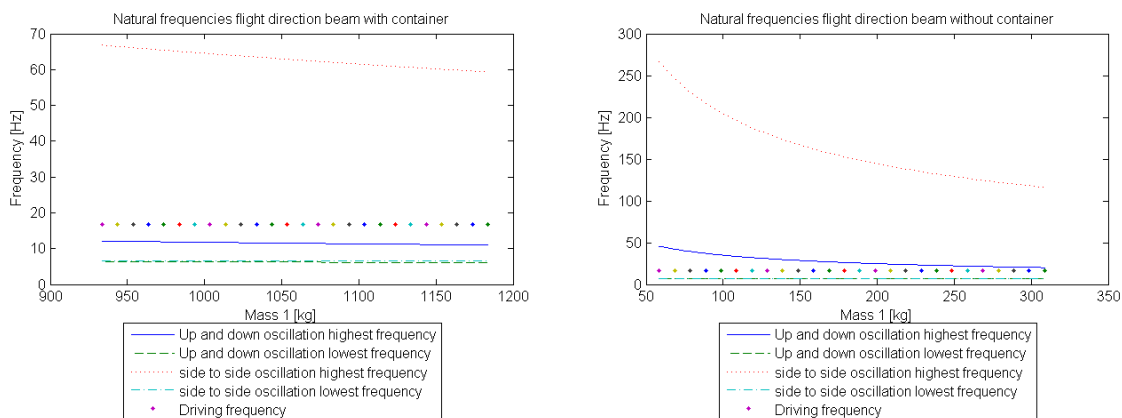
$$\begin{bmatrix} m_1 & 0 \\ 0 & m_2 \end{bmatrix} \begin{bmatrix} x_1 \\ x_2 \end{bmatrix} + \begin{bmatrix} k_1 + k_2 & -k_2 \\ -k_2 & k_2 \end{bmatrix} \begin{bmatrix} x_1 \\ x_2 \end{bmatrix} = \begin{bmatrix} 0 \\ 0 \end{bmatrix} \tag{5.18}$$

Assuming the harmonic displacement (Equation (5.19)) and entering that into the matrix Equation (5.18) leads to Equation (5.20)

$$\underline{x} = \hat{x}e^{i\omega t} \tag{5.19}$$

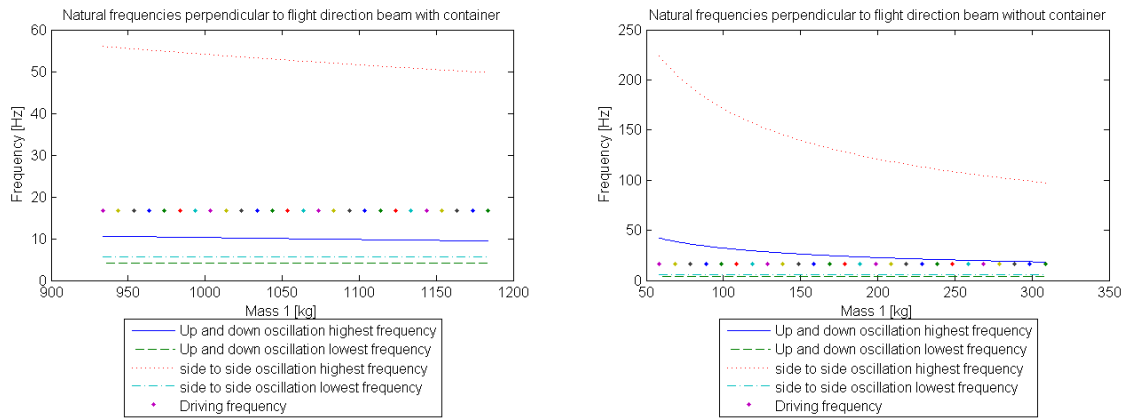
$$\det \begin{bmatrix} -\omega^2 m_1 + k_1 + k_2 & -k_2 \\ -k_2 & -\omega^2 m_2 + k_2 \end{bmatrix} = 0 \tag{5.20}$$

The trivial solution is when the displacement is 0. The other solution is the one that is important and gives the natural frequencies. This is done by setting the determinant of matrix Equation (5.20) equal to 0 and solving for ω and then dividing by 2π to get the frequency in Hz. This is done in MATLAB. The mass m_1 is not a constant, this mass takes account for the fuel and the landing gear (58.63 kg), this means that the mass during the mission decreases and drops significantly when the container is detached. This is shown in the plots below where Figure 5.15a and Figure 5.16a are the frequencies with container, Figure 5.15b and Figure 5.16b without. Mass m_2 is a constant, consisting of the engine and rotor hub and is equal to 450 kg.



(a) Natural frequencies of the beam in flight direction with container (b) Natural frequencies of the beam in flight direction without container

Figure 5.15: Natural frequencies for the beams in flight direction



(a) Natural frequencies of the beam perpendicular to flight direction with container (b) Natural frequencies of the beam perpendicular to flight direction without container

Figure 5.16: Natural frequencies for the beams perpendicular to flight direction

These frequencies are essential for the design because an external force with the same frequency can create resonance. If this is the case and nothing is done about it it might lead to catastrophic failure. Such a driving frequency acting on the structure can come from e.g. aerodynamic forces or forces from the rotors. In this case the rotor frequency is considered as the critical driving frequency. The rotors spin at 500 RPM. This means that per rotation there is twice a lift maximum and minimum. It results in a driving force frequency of 16.67 Hz. As can be seen in Figure 5.15a, Figure 5.15b, Figure 5.16a and Figure 5.16b none of the natural frequency lines cross the driving frequency. Although, the natural frequencies of the up and down oscillation in both beams with out the container come close to the driving frequency. The natural frequency that comes closest to the driving frequency can be read from Figure 5.15b and is 20.13 Hz and from the beam perpendicular flight direction is 18.36 Hz. This is right after the container has been detached. As the fuel decreases the natural frequency goes up and the difference between them grows. The difference between the driving frequency and the natural frequency might still be too small and further investigation should be done to see if this will turn out to be a problem. Shifting with the masses is an option or making the beam stiffer to get a higher natural frequency.

The situation on the ground is also examined. Here m_2 stays the same and m_1 has a lower mass because the mass of the landing is now resting on the ground. Thus the stiffness of k_1 increases, again using Equation (5.16) and Equation (5.17) with the area of the landing gear 0.0013 m^2 and the moment of inertia being $6.2832 \times 10^{-6} \text{ m}^4$ and then adding the compressive stiffness as well as the bending stiffness to k_1 in the case for up and down oscillation and side to side oscillation, respectively for the beams in both directions. For the beam perpendicular to the flight direction the closest natural frequency to the driving frequency is when the container is attached and has all the fuel remaining (take-off conditions) is 5.66 Hz all the other situations have been studied and have a smaller difference between the two frequencies. For the beam in flight direction, the critical situation is the up and down oscillation when the container is being dropped of so half the fuel and on the landing pad. This gives a natural frequency of 12.45 Hz. However these situations are on the ground and last for a short time. This is because of the ground operations that require the engines to be turned of when landed and thus the driving frequency will only be present for a short time. More rigorous testing should be done to see if this gives any problems. This MATLAB model has been tested with easier values and calculating them analytically. These values were the same and thus this method was verified.

5.4.4. Design of the Landing Gear

The landing gear design is similar to that of the main structure. First a model is established, after which loading diagrams can be plotted. Also, the shock absorbers are discussed. Finally, the results are stated.

Model The landing gear is designed using the same method as the main structure. The landing gear consists of a main strut, making a 90° angle with the beam above. This strut is modelled as a beam. The

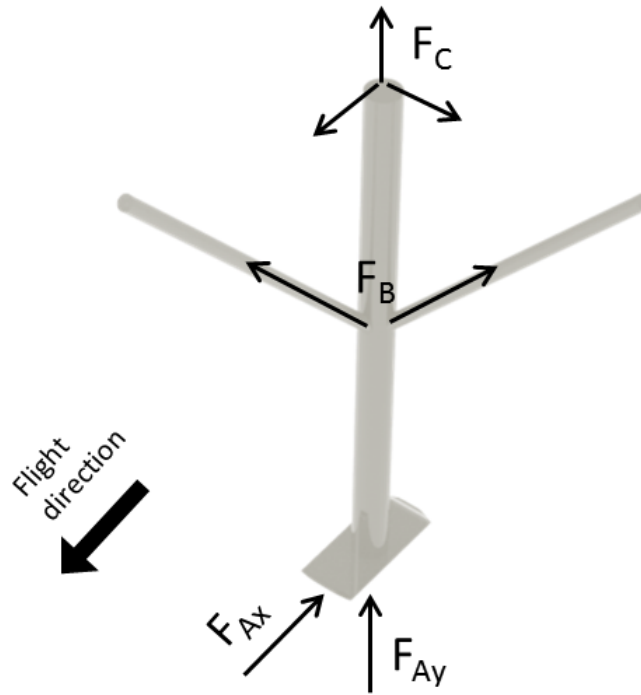


Figure 5.17: Landing gear 3D view showing the forces.

main strut is connected to two drag struts, which can transfer perpendicular loads to the beam above. These struts only transfer axial loads. The landing gear layout can be seen in picture Figures 5.17 and 5.18. Reaction forces are calculated in C and B. The drag struts can transfer loads at point B, using a hinge as connection. The beam transfers loads at point C, where it is modelled to be hinged to the main strut. The main strut has a length L , the drag strut has a height H_s and width W_s . All external loads are applied at point A. These loads are defined to be F_{Ax} and F_{Ay} . First, only the main strut is analysed. In order to compute the reaction forces in B and C, the relation between F_{Bx} and F_{By} has to be established:

$$\frac{F_{Bx}}{F_{By}} = \frac{H_s}{W_s} \quad (5.21)$$

This equation holds, since the drag strut can only take up axial loads. Now:

$$F_{Bx} = -\frac{L}{W_s} F_{Ay} \quad (5.22)$$

$$F_{By} = -\frac{L}{H_s} F_{Ay} \quad (5.23)$$

$$F_{Cx} = -F_{Ax} + \frac{L}{W_s} F_{Ay} \quad (5.24)$$

$$F_{Cy} = \left(\frac{L}{H_s} - 1 \right) F_{Ay} \quad (5.25)$$

Using the reaction forces, the internal loads can be computed. Like for the main structure, the internal stresses may never exceed the maximum stresses plus safety factor. Using equations Equation (5.7), Equation (5.9), Equation (5.8), Equation (5.11), Equation (5.12), Equation (5.14) the sizing of the beams can be done in order to comply with this.

Using the reaction forces at point B (Figure 5.18), it can be determined what loads the drag struts will encounter. As said, these drag struts can only be loaded in compression and tension. So, for these struts there will be looked only at normal stresses. So, for this analysis, only Equation (5.7),

Equation (5.12) and Equation (5.14) are used. F_{A_y} is set to be equal to half of the weight of the aircraft plus safety factor and landing load factor. Since during landing, the aircraft might also move parallel to the ground, a force F_{A_x} will be induced. This force is defined as:

$$F_{A_x} = F_{A_y} \cdot \mu \quad (5.26)$$

Here, μ is the friction coefficient, which is defined to be equal to 0.45⁹ (the friction between concrete and steel to design for the worst case scenario). F_{A_z} is defined to be equal to F_{A_x} . Now, the 3-dimensional problem can be analysed by analysing two of the same 2-dimensional problems. The landing gear cross section is chosen to be circular, since the main load acting on it will be a compressive axial force. Circular cross sections are highly effective in withstanding these kind of loads.

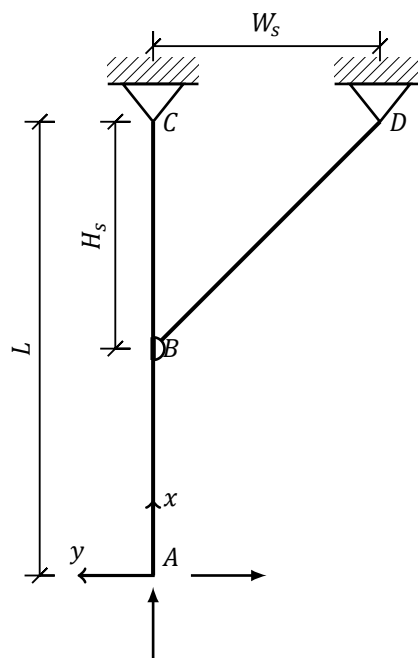


Figure 5.18: Landing gear model. Forces are indicated by straight arrows applied at a point.

Loading diagrams The shear force diagram of the main landing strut is shown in Figure 5.19 and the bending moment diagram in Figure 5.20. It has to be noted that these diagrams are computed for the pure 2-dimensional problem. In the yz -plane, the loading diagrams will be the same, but the x can be replaced by z . For the drag strut, the normal force is shown in Figure 5.21.

⁹URL: www.mae.ncsu.edu/silverberg/statics%20and%20dynamics%20web/Table%202.doc [cited 13 January 2016]

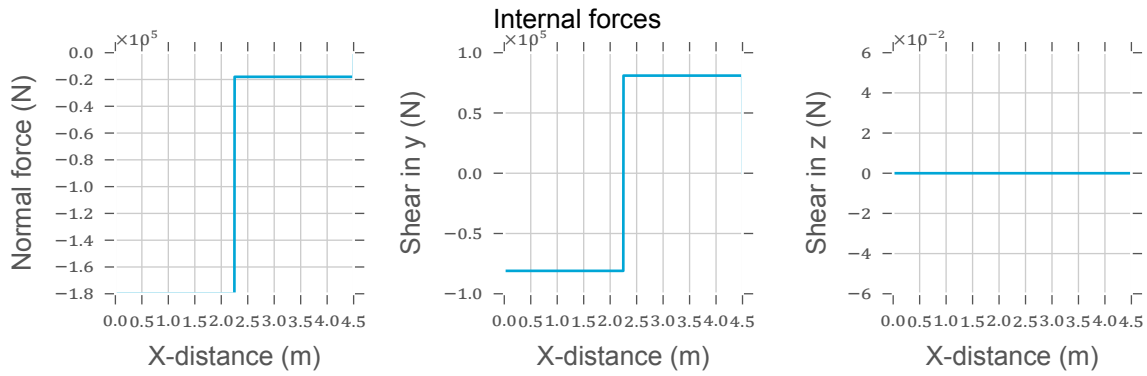


Figure 5.19: Force loading diagrams in x, y & z direction for the landing gear strut

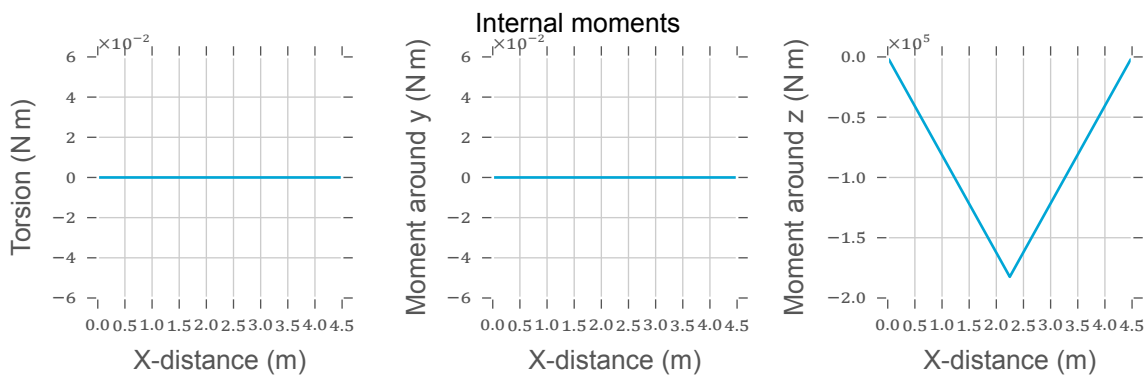


Figure 5.20: Moment loading diagrams in x, y & z direction for the landing gear strut

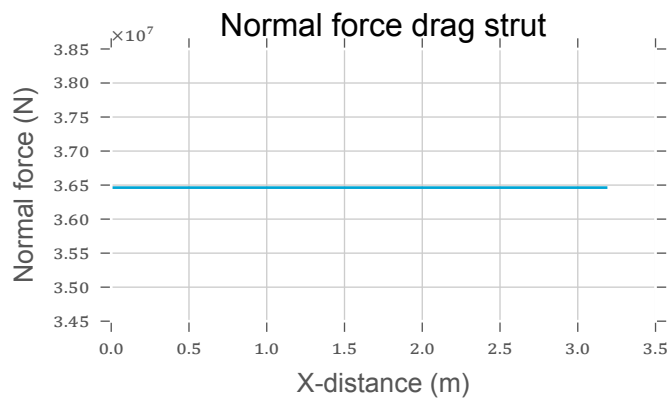


Figure 5.21: Normal force in the drag strut for the landing gear

Results With the safety factor of 1.5 and landing load factor of 1.3 and the weight perfectly distributed on all 4 gears, the landing gear struts can be sized using the structural analysis tool. The free variables have been defined as radius (which is restricted to be less than 0.15 m due to aerodynamic performance) and thickness of the circular cross section. The results can be found in Table 5.6.

Table 5.6: Summary of the landing gear struts. Values or per beam/strut.

Description	Main strut	Drag strut (short)	Drag strut (long)	Unit
Length	4.59	3.25	3.39	m
Radius	0.1	0.055	0.062	m
Thickness	0.002	0.001	0.001	m
Material	Aluminium 7175-T66			
Mass	24.18	3.09	3.69	kg

5.4.5. Design of Landing Pads

In order to prevent sinking away in soft soils, such as loose sand in desert environments, the ground contact surface area should be increased to keep the ground surface contact pressure under the bearing capacity of the underlying soil. For this several designs were considered. Skids, skis and pads are in general lighter than wheeled landing gears, require less maintenance, are more reliable and with a large contact area you can land on almost any soft surface. They are the ideal choice for a VTOL aircraft. Due to the requirements of being able to operate in extreme temperatures (from -50 to 60 °C) the choice has been made to design one of these for the HELLCAT. Landing ski's were found to be too heavy and bulky, but would allow the rotorcraft to land on snow and other very soft soil types. After that landing skids were considered, but would become too heavy due to bending moments. As such landing pads are considered, which are designed in this subsection.

Model The landing gear pads are designed for a contact pressure of 3.5 psi (24 kPa), which ensures it does not sink away in nearly any soft surface (loose sand <100 kPa, soft clays and silt <75 kPa¹⁰). However, landing on very soft surfaces like some kinds of soft snow is not achievable. The landing gear encounters the same forces as previously described in the design of the landing gear (see Section 5.4.4). A normal force and the accompanied surface drag force. For the landing gear these forces are modelled as distributed forces over the ground contact surface. The resulting model can be seen in Figure 5.22.

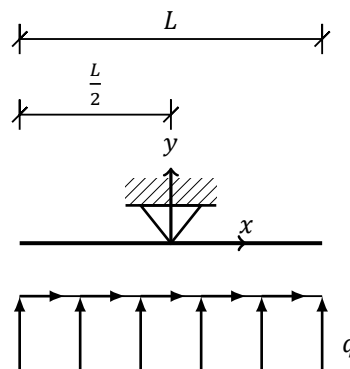


Figure 5.22: Model for the design of landing pads

$$A_{min} = \frac{F}{P_{max}} \quad (5.27)$$

$$q_y = P \cdot W \quad (5.28)$$

$$q_x = q_y \cdot \mu \quad (5.29)$$

$$R_y = q_y \cdot L \quad (5.30)$$

$$R_x = q_x \cdot L \quad (5.31)$$

¹⁰URL: <http://environment.uwe.ac.uk/geocal/foundations/founbear.htm> [cited 15 January 2016]

Results Maximum length inwards (from main strut to the direction of the container) set by operations is 0.95 m for easy and fast ground operations to give the forklift enough ground clearance. To have some margin the maximum total length for a landing pad is set to 1.2 m. The advantage of a longer landing pad is better drag performance and a lower structural weight. As such the trade-off is made between aerodynamics, operations and structures. The results of this can be seen in Table 5.7. The pads are optimised for length, width and thickness. A solid rectangular cross-section is used.

Table 5.7: Pad dimensions and characteristics for under the landing gear to ensure the aircraft will not sink away in sand or other types of soils

Description	Value	Unit
Length	1	m
Width	0.45	m
Thickness	0.022	m
Material	Aluminium 7175-T66	
Mass	27.67	kg

5.4.6. Shock Dampers

For the shock dampers it was also chosen to buy off the shelf. Thus it had to be investigated which shock dampers are big and stiff enough to withstand the force of the weight of the aircraft when it touches down. Even in rough landing conditions. After some research it was discovered that the shock dampers from Ace-Ace were able to fulfil the job. Especially the *MC64150EUM – 2*¹¹. This shock damper is capable of 0.15 m/s to 5 m/s, on request under 0.15 m/s and up to 20 m/s. This means that the spring is able to withstand much more than what the UAV will encounter during normal operations, it is determined that the landing gear is able to withstand an impact of 1.5g this relates to deceleration of the UAV on the dampers when it lands with 2.12 m/s. This is well within the range of the dampers. The price of the damper is € 371.63 with a weight of only 5.10 kg. This brings the total cost and weight of 4 dampers to € 1,486.52 and 20.4 kg. It was determined that for a crash landing the UAV would have a speed towards 12 m/s.

5.5. Production Plan

The production of the aircraft consists of manufacturing, assembly and integration. The main steps which have to be followed are displayed in Figure 5.23. First, all the necessary components must be bought. This includes sheet material, attachment materials like rivets, adhesives and bolts, but also whole subsystems like engines, fuel pumps, rotor blades, wires and cables. Also, products that contribute to the manufacturing and assembly of the aircraft like tools and jigs have to be bought or produced.

The sheet material has to be formed into the right shape. Due to the size of the main structure beams, first the sheet metal has to be cut in the right shape. For this, straight, constant width sheets have to be cut which are not very complex to produce. These sheets will have to be attached to one another using attachment material. Due to the size, shape and material choice of the landing gear components, the main struts and drag struts are suitable to be produced using sheet metal curving. This is done because custom dimensions are used. As such, no tubes can be directly purchased of the shelf. The landing gear pads will be made from partly curved sheet metal.

Now, the beams of main structure can be attached and the individual components of the landing gear can be attached. All components of the engine group (engine, engine parts and rotor hubs and blades) will be assembled. In the meanwhile, the main structure and the energy supply (fuel systems and batteries) are be assembled. Then, the main structure and engine group are put together, after which the landing gear is assembled to this. Now, the avionics and cables can be installed.

After a painting, the quality check can be performed. If the products pass the check, they will be delivered to the customer. During all manufacturing and assembly processes, quality control will have to assure that all parts of the manufacturing and assembly have met the quality requirements, ensuring ownership satisfaction.

¹¹ http://ace-ace.com/wEnglisch/pages/Produkte/index.php?IdTreeGroup=281&IdProduct=2070&navid=1&mid=10435#hk_6 [Cited20-01-2016]

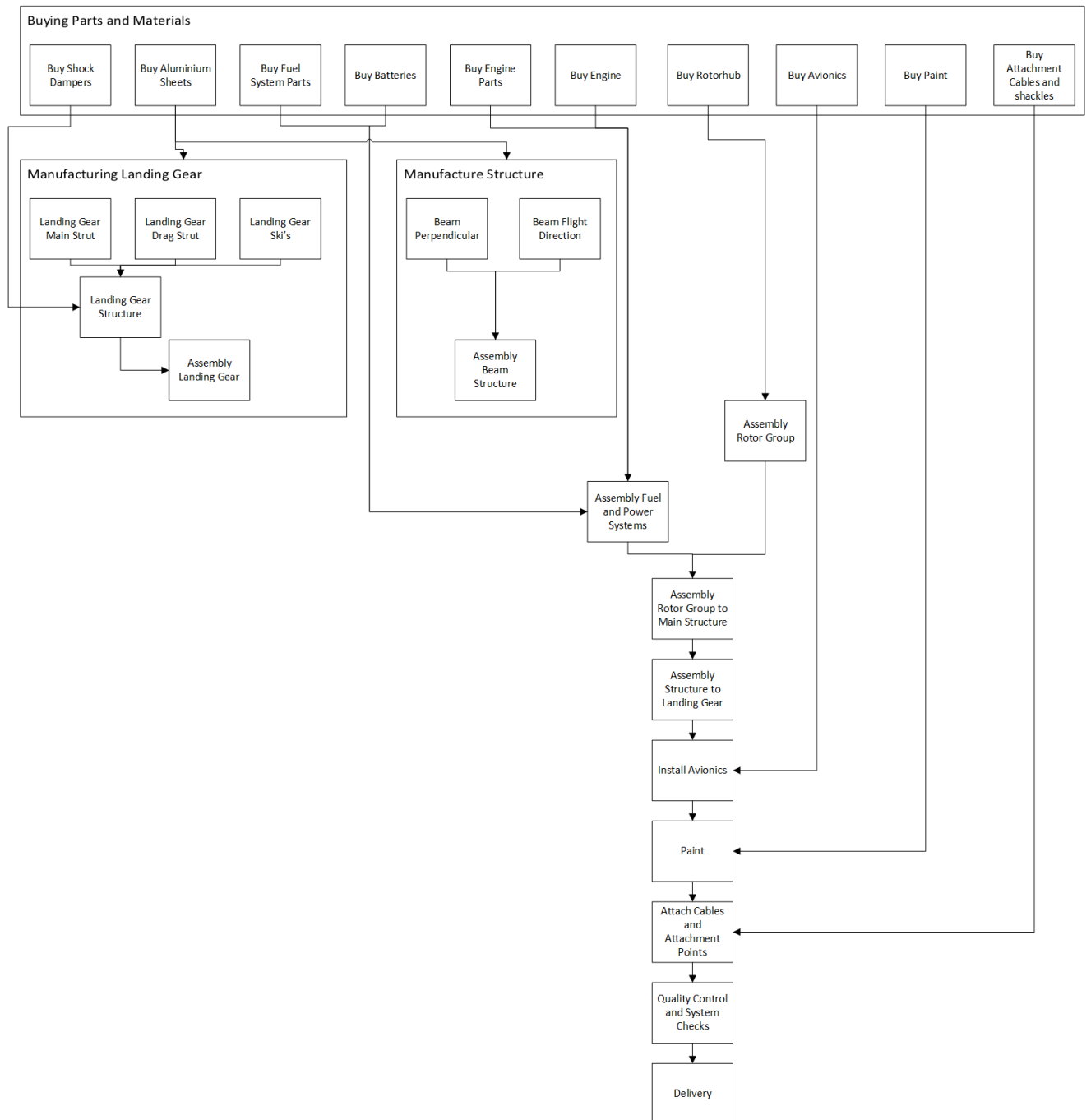
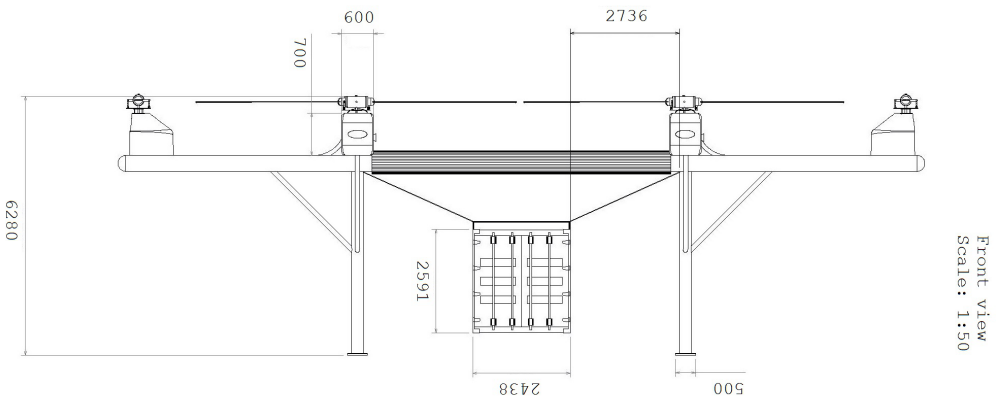


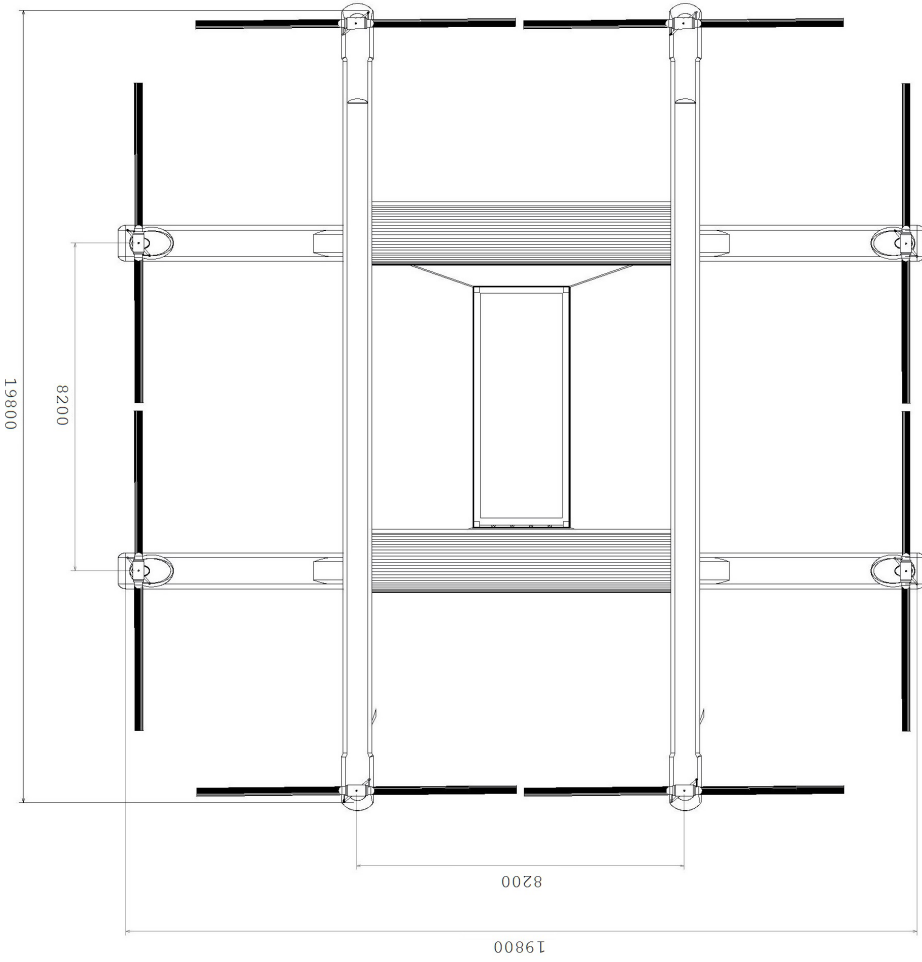
Figure 5.23: All steps needed for the manufacturing, assembly and integration of the aircraft

5.6. Results

Combining the results from Sections 5.4.3 to 5.4.6 a technical drawing in three views can be made, see Figure 5.24. This gives an overview of the main structural dimensions.



Top view
Scale: 1:50



Left view
Scale: 1:50

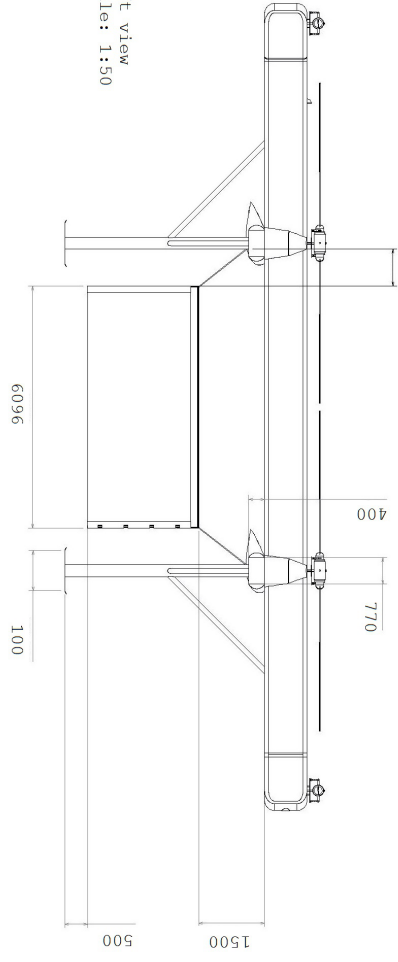


Figure 5.24: Three view technical drawing of the resulting structure

5.7. Recommendations

The structural analysis performed in the chapter uses a simplified model of reality. In other words, assumptions have been made in order stay within the time limitations of this project.

For example, no local stresses are calculated in the current analysis. If local stresses would be included, local stiffeners and ribs would be necessary. This is also the case for other assumption, like not including holes, damage, maintenance cutouts. Also, thermal stresses and gusts have not been taken into account in this analysis. All of these additions would make the structure heavier than it is now. However, the design can be further improved by using stiffeners, multiple materials per beam, taper and variable thicknesses. Including local stresses would imply that the current method is no longer applicable. Finite Element Method has to be used as an addition in order to improve on this. With FEM, more complex indeterminate structures can be modelled, too. This would also improve the accuracy of the results.

The purpose of this structural analysis is to get an estimate of the dimensions and weights needed in order to provide strength and stiffness, serve as attachment system and store subsystems. Making less assumptions in the future would, generally speaking, make the structure heavier, but a smarter structure could make it more lightweight.

6 Aerodynamics

The aerodynamic performance is of extreme importance given the size of the HELLCAT. This chapter provides the aerodynamic performance. First, the rotor characteristics are shown in Section 6.1. Then, in Section 6.2 Blade Element Theory (BET) is used to obtain the forces acting on the rotor blades. Section 6.3 elaborates on the drag forces acting on the UAV. All these forces cause an aerodynamic moment, which is shown in Section 6.4.

6.1. Rotor Characteristics

This section illustrates the process of selecting and optimising the rotor blade. First, an airfoil is selected in Section 6.1.1. To achieve a better lift distribution the blades are twisted, which is discussed in Section 6.1.2. Third, the costs of the rotor blades are estimated in Section 6.1.3. Last, the rotor system design is shown in Section 6.1.4.

6.1.1. Airfoil Selection

It has been decided to design the rotor blades, instead of buying standard blades used in other helicopter designs. This is because high performance of the blades is required, since car engines are used. Newly designed airfoils as the VR-12 and VR14 have a higher lift coefficient and an approximately equal drag coefficient compared to standard blades, as can be seen in Table 6.1. The NACA 63-015 and NACA 0012 are commonly used in rotorcraft.¹

The development of specifically designed airfoils for rotorcraft comes with many difficulties originating from large variation of the flow conditions along the blade. The flow velocity distribution is highly asymmetric, the rotating blade on the advancing side, besides the rotational speed, also has the forward speed to account for. The resulting velocity can reach the speed of sound at the blade tips. On the contrary, the retreating blade moves away from the relative airflow, causing a decrease in the velocity vector.

Another important aspect when designing or selecting an airfoil for lifting rotors is the pitching moment coefficient, as the pitching moment determines the forces acting on the control mechanism. It should have a near-zero value. A high value pitching moment also causes the blade to twist resulting in undesirable aerodynamic effects and lowering the rotor performance. It also introduces vibrations into the system which lowers the life expectancy of the rotor hub components.

From the point of view of conditions appearing on the advancing blade, the airfoils are designed to delay drag divergence to higher Mach numbers. This is done by using thin airfoils with limited camber. The retreating blade is sought to have high values for maximum lift coefficient at small and medium subsonic Mach numbers. [18] This can be achieved by using thicker airfoils with greater camber. The solution to this problem is to use thinner airfoils near the tip and thicker, cambered airfoils inboard. Based on the requirements mentioned above Kania et al. stated that the best existing airfoils are VR-12, VR-13, VR-14, OA-3XX and the DM-H3&4 families. The VR-12 airfoil will be used at the inboard part of the rotor blade, while the VR-14 airfoil will be used near the tip. These airfoils are selected based on their

¹URL: <http://m-selig.ae.illinois.edu/ads/aircraft.html#helicopters> [cited 25 January 2016]

Table 6.1: Lift and drag characteristics of different airfoils for $Re=1 \times 10^6$

	VR-12	VR-14	NACA 63-015	NACA 0012
C_l for 0°	0.13	0.08	0	0
C_l for 5°	0.79	0.7	0.55	0.56
C_l for 10°	1.26	1.18	1.02	1.08
C_d for 0°	0.006	0.005	0.006	0.005
C_d for 5°	0.009	0.008	0.008	0.008
C_d for 10°	0.013	0.015	0.016	0.015

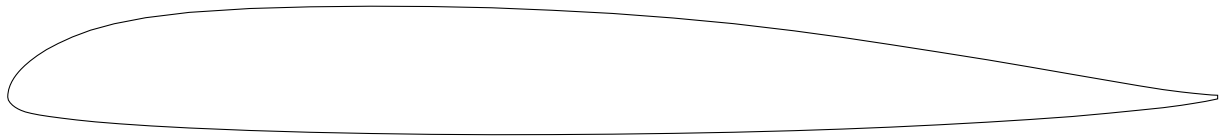


Figure 6.1: Boeing-Vertol VR-12 airfoil

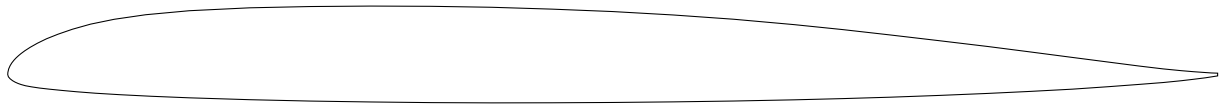


Figure 6.2: Boeing-Vertol VR-14 airfoil

better performance in maximum lift coefficient at $M=0.4$ and drag divergence at $C_l = 0$. Also, more data is available for these airfoils. The VR-12 airfoil can be seen in Figure 6.1 and the VR-14 airfoil can be seen in Figure 6.2. These figures are obtained using the link that is mentioned in the footnote on this page.²

Table 6.2 shows the drag divergence Mach number, the maximum lift coefficient for a Mach number of 0.4, the zero lift angle α_{L0} , the $C_{l\alpha}$ slope, the drag coefficient C_d and the lift to drag ratio of the VR-12 and VR-14 airfoils.

Table 6.2: Characteristics of the VR-12 and VR-14 airfoils

	VR-12	VR-14
M_{dd}	0.8	0.84
α_{L0}	-0.85°	-1.20°
$C_{l\alpha}$ between -5° and 14°	5.7	5.7
C_d for α_{eff} between -5° and 14°	0.02	0.02
C_{lmax} for $M = 0.4$	1.45	1.26
$\frac{C_l}{C_d}$	60	64

The lift coefficient as a function of angle of attack is plotted in Figure 6.3 and Figure 6.4 for the VR-12 and VR-14 airfoil respectively. These figures are obtained using XFLR5 for different of Reynold's numbers.

6.1.2. Optimum Twist

Each point on a rotating blade travels at a different velocity. The velocity decreases from the tip to root. The distance travelled by a blade element increases further away from the root as the circumference increases for each element. The variation in velocity on the disk is visualised in Figure 6.5 where the highest velocity is present at the blade tip on the advancing side perpendicular to the free-stream velocity.

²URL: <http://airfoiltools.com/> [cited 18 January 2016]

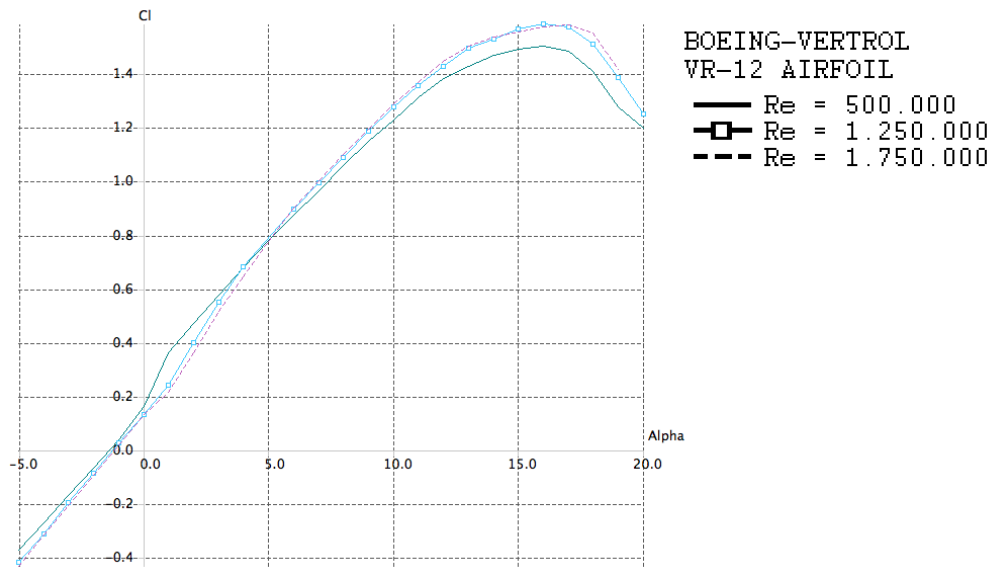


Figure 6.3: Lift coefficient versus angle of attack for the VR-12 airfoil

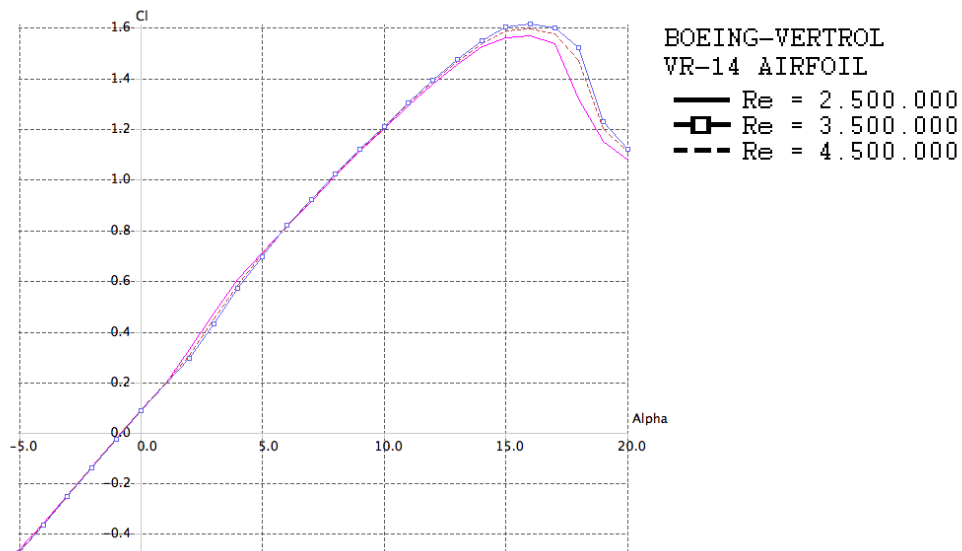


Figure 6.4: Lift coefficient versus angle of attack for the VR-14 airfoil

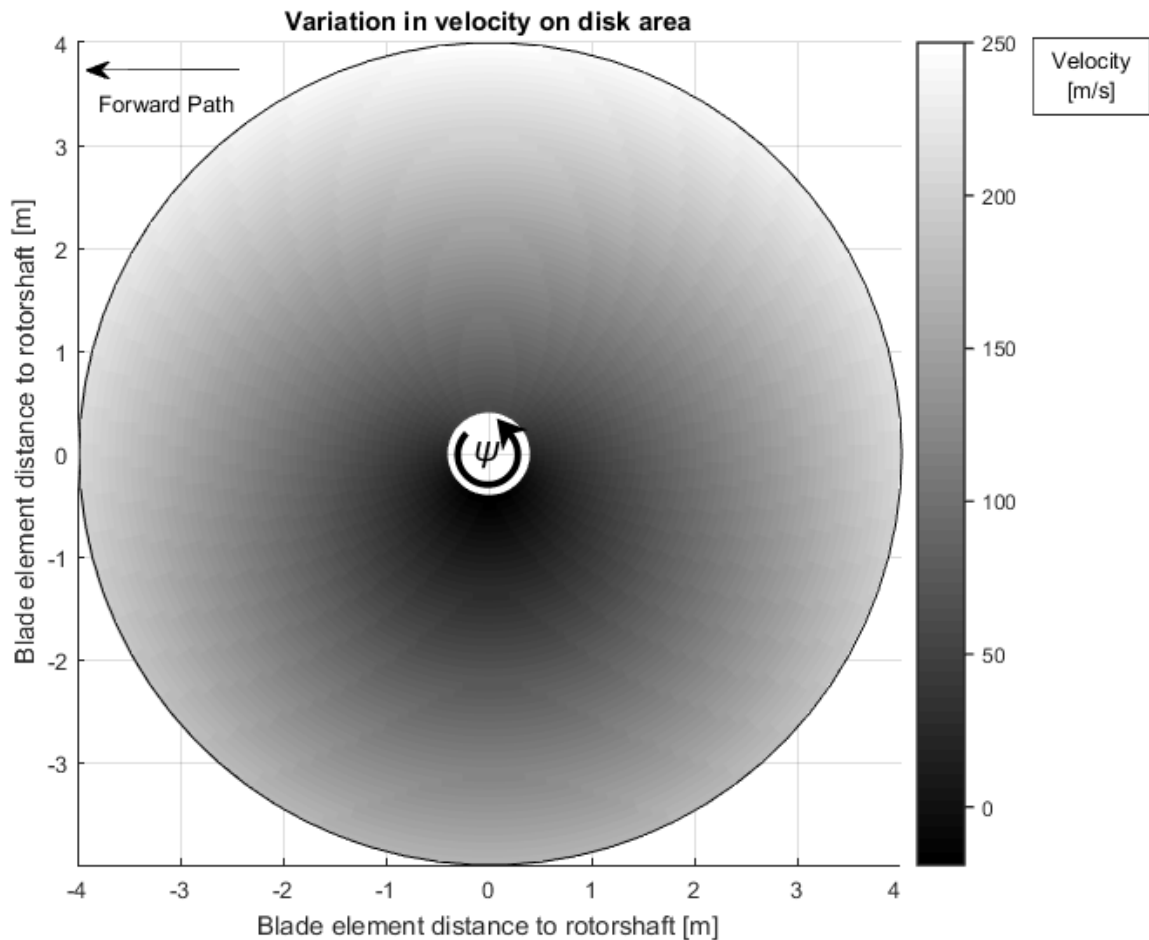


Figure 6.5: Velocity variation on disk area

There is also a velocity component normal to the rotating blade v_i . This changes the effective angle of attack α_{eff} for each blade element. This results in a difference in the contribution to drag and lift in every distinct element on the blade, both getting larger when shifting closer and closer to the blade tip. As a consequence, a non-linear lift distribution over the blade is present. To avoid this effect of a rotating lift-device the blades are twisted to achieve a linear lift distribution. Figure 6.6 shows the lift distribution for an ideal twisted blade compared to an untwisted blade.

To improve the lift distribution, a twist angle is introduced in the blades such that the effective angle of attack α_{eff} is more constant over the blade span. To find the optimal twist, the C_l , in function of the angle of attack, can be varied to achieve a higher lift capacity, as the density, velocity and blade area are somewhat constant. Figure 6.5 shows the variation in velocity in function of the span location and azimuth angle ψ is present, which also gives a different Reynold's number affecting the C_l . This can be seen in Figure 6.3 and Figure 6.4. Two different airfoils are used in the blades, the VR-12 for the root half and the VR-14 for the tip half as shown in Section 6.1.1.

Figure 6.7a and Figure 6.7b show the lift and α_{eff} over the span for the untwisted and twisted blades, respectively. A blade with linear twist of 6° already greatly improves the lift distribution compared to a non twisted blade.

6.1.3. Cost Estimation

The blades as designed need to be manufactured. The costs per rotor blade are estimated using [19]. The manufacturing cost are the sum of the material, labour and equipment costs. The cost can be seen in Table 6.3.

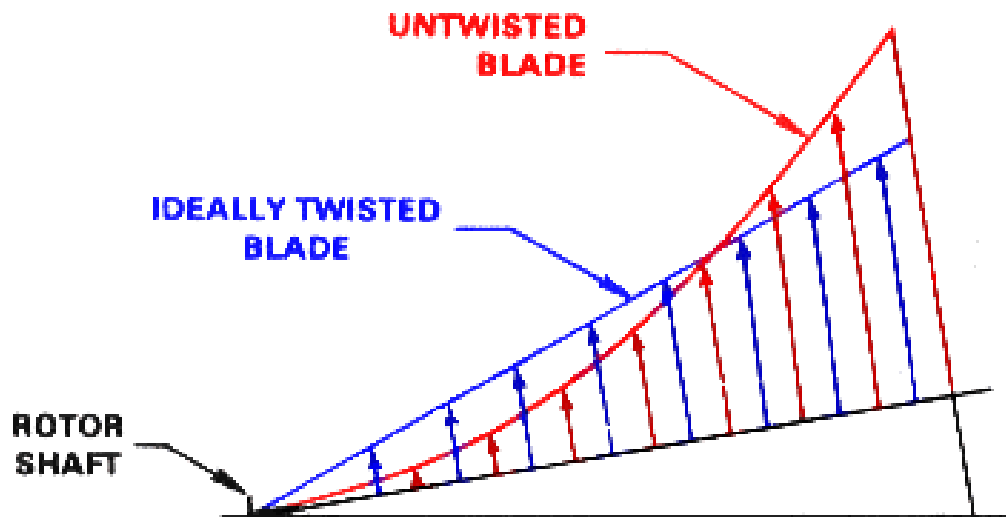
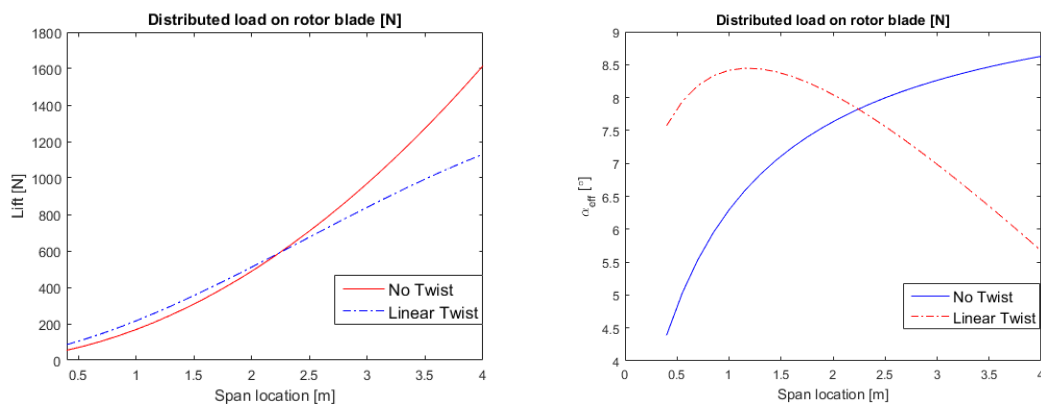


Figure 6.6: Lift distribution along the blade for a twisted and untwisted blade



(a) Lift distribution of the twisted and untwisted blade (b) α_{eff} of the twisted and untwisted blade

Figure 6.7: The figures show the lift and α_{eff} of the advancing blade for a twisted and untwisted blade at a velocity of 41 m/s

Table 6.3: Manufacturing cost for one composite blade

	Material	Labour	Equipment	Production
Sheath	57	322	219	598
Pocket	131	276	191	598
Spar	76	260	202	538
Honey comb core	140	125	120	385
Total cost for one blade (US\$)				2,119

The amount of material that is needed is determined from the size specifications. This is then multiplied with the unit cost of that material to obtain the material cost for each activity. The cost of the material is found in the inventory database. Separate components are then added together to obtain the total material cost of the product.

In order to calculate the labour cost involved, the labour cost are retrieved out of the employee code database and then multiplied by the total time a certain amount of employees are working on the component.

To determine the equipment cost the machine cost rate has to be known. "The machine cost rate for each production machine is calculated based on maintenance costs, operating cost, equipment asset and the number of operation hours." [19] Now, the operating hours for the particular products should be multiplied with the machine cost rate to find the total cost.

6.1.4. Rotor System Design

The rotor system is the rotating component of a rotorcraft which generates lift. Figure 6.8 shows a two bladed rotor system design, which consists of the following parts:

- **Jesus nut:** Singular bolt that holds the mast onto the hub, failure of this part is catastrophic.
- **Hub:** Sits on top of the mast and hooks up the control tubes to the rotor blades.
- **Blade grips:** Attaching points that link the rotor blades to the hub.
- **Pitch change horn:** The vertical movement from the rotating pitch control tubes is converted to blade pitch with the pitch change horn.
- **Rotating pitch control tubes:** Tubes that are connected to the swashplate and blade grips via the pitch change horn, they change the pitch of the blades.
- **Swashplate:** Translates inputs into motion of the rotor blades.
- **Non rotating control tubes:** Moves up and down together with the swash plate to change pitch.
- **Mast:** Rotating shaft going to the transmission, which connects the rotor to the rotorcraft.

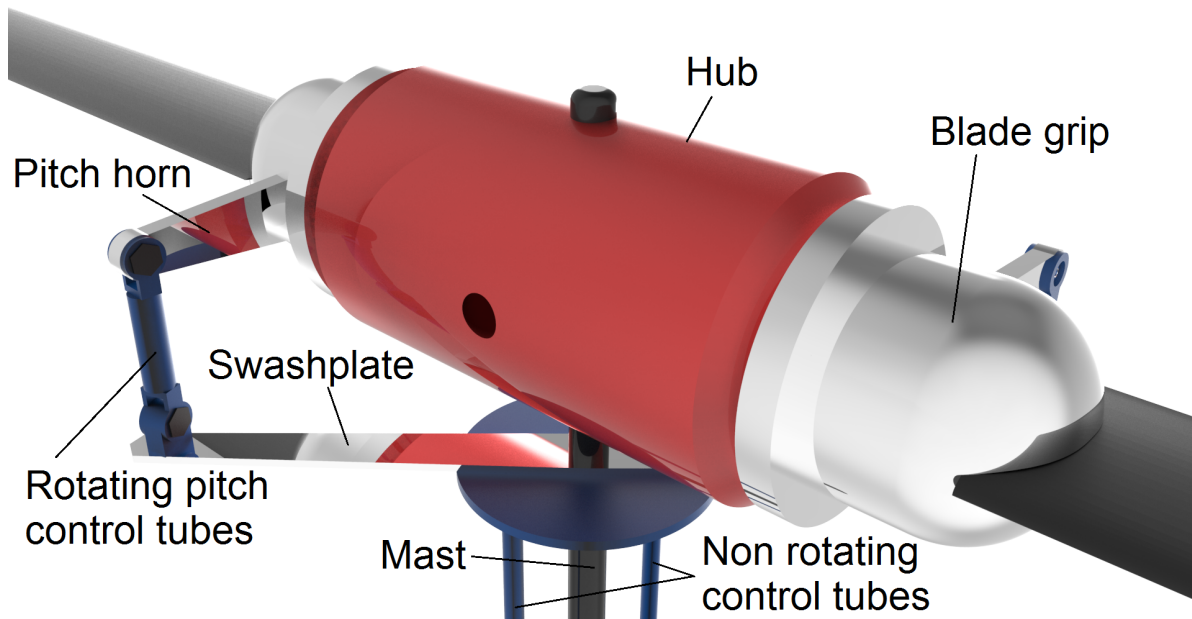


Figure 6.8: Schematic 3D view of the rotor system design

There are three types of rotor design when it comes to the connection between the hub and blades. The fully articulated system, the semi-rigid and the rigid system. The fully articulated system allows the blades to move independently from each other through a series of hinges. The semi-rigid system has a teetering hinge, which allows the blades to flap in opposite motions like a seesaw. A rigid system is hingeless. All three have their advantages and disadvantages which are shown in Table 6.4. Lead-lag hinges are used together with a teetering hinge. This is not worked out in detail, due to time constraints.

Table 6.4: Differences between the types of rotor designs [24]

System Type	Advantages	Disadvantages
Fully articulated	Good control response	More complex, greater cost
Semi-rigid	Simple, low stresses in blades	Slower control response, higher vibrations than multi-bladed systems
Rigid	Simple design, crisp response	Higher vibrations than articulated rotors, higher bending loads on shaft that cause fatigue

6.2. Blade Element Theory

The Blade Element Theory (BET) looks upon small sections of the rotor individually. For this model the computation software tool MATLAB was used. The individual elements are then added to get the total forces acting on the rotor blade. In this model the rotor blade is split into 50 pieces and calculations are made for 200 different azimuth angles for 50 different flight speeds. The model that is used takes the following assumptions into account:

- the vertical down wash velocity v_i over the rotor disc is constant over the disc area
- γ : local inflow angle of the free stream air C_d is considered to be constant at 0.02 for α_{eff}
- C_{l_α} is constant at 5.7
- The blades have no interference with each other

In order to use this model the following parameters, for each element, have to be calculated:

- v_{eff} : local speed of the free stream air
- γ : local inflow angle of the free stream air
- α_{eff} : local effective angle of attack

It is also good to note that the model has an iterative nature. The vertical induced velocity has to be calculated numerically [5] and this iteration process goes as follows:

1. Make an estimation for the induced velocity v_i
2. Calculate v_i for forward velocity
3. Recalculate v_i and go to step 2 until the values converge

This calculation for the v_i is shown in Equation (6.1). For each result six iterations are performed. The error after five iterations is smaller than 0.01%. Therefore the number of iterations is considered to be sufficient.

$$v_{i_{j+1}} = \frac{v_{i_{hover}}}{\sqrt{(v_{copter})^2 + (v_{copter} + v_i)^2}} \quad (6.1)$$

The value of $v_{i_{hover}}$ can be calculated using Equation (4.1) from Section 4.2.1.

6.2.1. Calculating the Blade and Free Stream Air Angles and Velocities

First the local speed that each blade element experiences has to be calculated. This can be done by using Equation (6.2).

$$v_{blade} = \sqrt{v_{rot}^2 + v_i^2} = \sqrt{(R_{blade}\Omega)^2 + v_i^2} \quad (6.2)$$

In this formula v_{rot} is computed by multiplying the rotational rate of the rotor, Ω , times the radius of the blade element, R_{blade} , and v_i is the vertical down wash speed of the air. Then the angle at which each blade element encounters the free stream air, γ , has to be calculated. Equation (6.3) shows the formula that can be used.

$$\gamma = \tan\left(\frac{v_i}{v_{blade}}\right)^{-1} \quad (6.3)$$

However this angle is only valid for the UAV in hover. When introducing forward velocity an adjustment for the blade velocity has to be done. In this adjustment it is assumed that the angle of inclination, ζ , is small. The angle of inclination is the angle the rotor disc makes with the flight path angle. The adjustment can be done by adding the air speed of the UAV, v_{copter} , to the rotational speed of each

blade. This can be done for all possible azimuth angles ψ , as shown in Equation (6.4). The azimuth angle is further described in Section 6.2.4.

$$v_{blade} = \sqrt{v_{rot}^2 + v_i^2} = \sqrt{(R_{blade}\Omega + v_{copter} \sin(\psi))^2 + v_i^2} \quad (6.4)$$

The result of this formula has to be used in Equation (6.3) to get the correct angle for the free stream air γ . The effective angle of attack for each blade element can then be computed by using Equation (6.5).

$$\alpha_{eff} = \theta - \gamma \quad (6.5)$$

6.2.2. Lift, power and drag determination at varying pitch angles

The thrust and drag produced by the blade sections can now be computed, since the basic parameters are known. The vertical lift component for each section can be calculated by using Equation (6.6). In this formula the lift coefficient is calculated first

$$T = (C_{l_\alpha}(\alpha_{eff} + \alpha_{L0}) \cos(\gamma) - \sin(\gamma)C_d)0.5v_{eff}^2S_{blade}\rho \quad (6.6)$$

The next step is to calculate the drag. This drag is comprised of two parts: the profile drag, D_p , and lift induced drag, D_i . The profile drag is the force associated with the blade movement through the air whilst the lift induced drag is caused by the horizontal component of the lift force. Equation (6.7) and Equation (6.8) give the equations to calculate the profile and induced drag respectively.

$$D_p = v_{eff}^2C_dS_{blade} \cos(\gamma)0.5\rho \quad (6.7)$$

$$D_i = (C_{l_\alpha}(\alpha_{eff} + \alpha_{L0}) \sin(\gamma) - \cos(\gamma)C_d)0.5v_{eff}^2S_{blade}\rho \quad (6.8)$$

Because the drag has an opposite direction on each rotor blade they produce a torque on the driveshaft. By using a matrix multiplication of the elements with the distance to the drive shaft the torque and thus engine power required can be calculated. This is shown in Equation (6.9) and Equation (6.10) respectively.

$$\tau_{rotor} = ([D_p] + [D_i]) [R_{blade}] \quad (6.9)$$

$$P_{required} = \frac{RPM_{rotor}\tau_{rotor}}{9,548.8} \quad (6.10)$$

Figure 6.9 depicts the induced and profile power curve for a lift of 17,500 N.

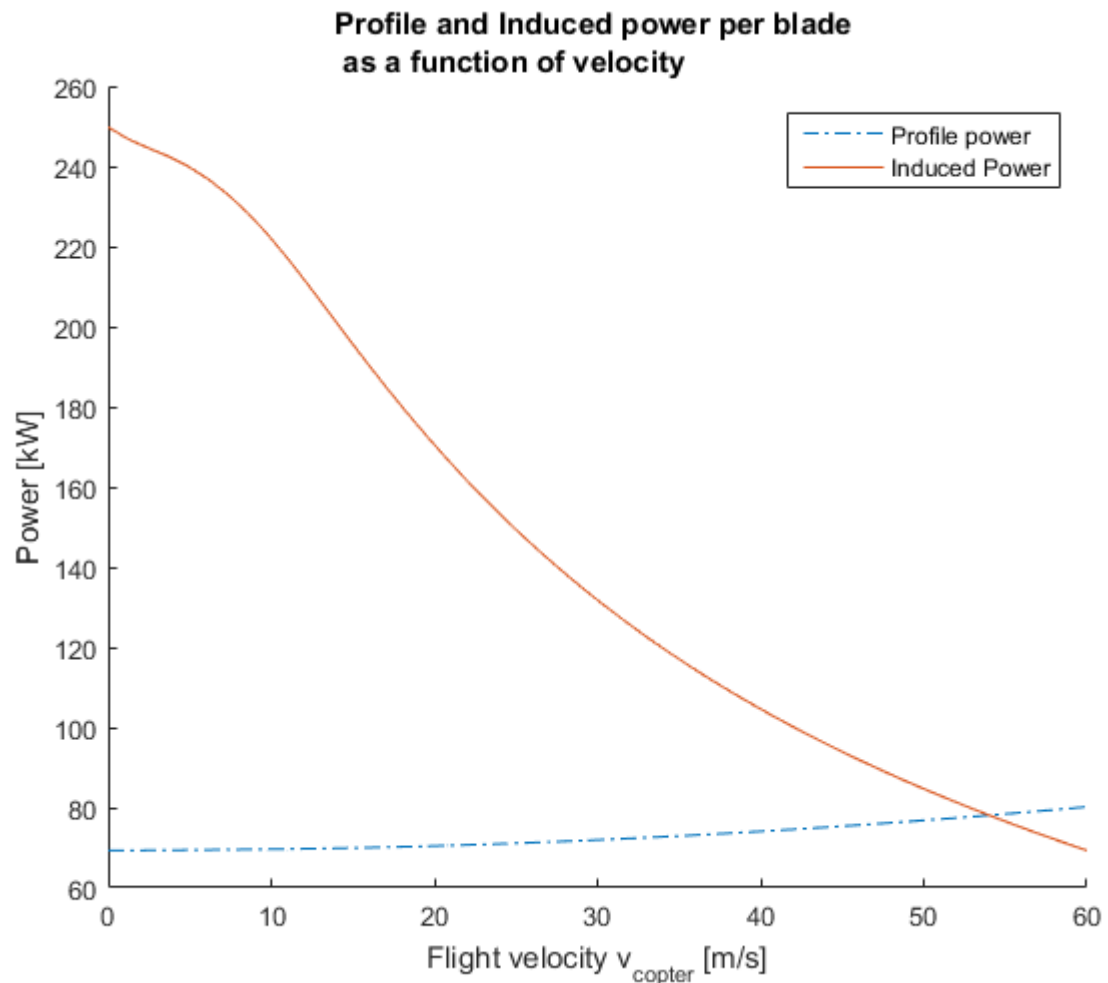


Figure 6.9: Induced and profile power per blade for a lift of 17,500 N

In forward flight there is a difference in the drag between the advancing and retreating blade. This difference will produce a resultant drag opposite to the flight direction. The D_i and D_p of each blade have to be subtracted from each other at every azimuth angle to get this resultant drag. Figure 6.10c gives this drag as a function of azimuth angle. The mean value can be used for the performance of the UAV. At a flight speed of 42 m/s and thrust setting of 17,500 N this drag results in 608.75 N.

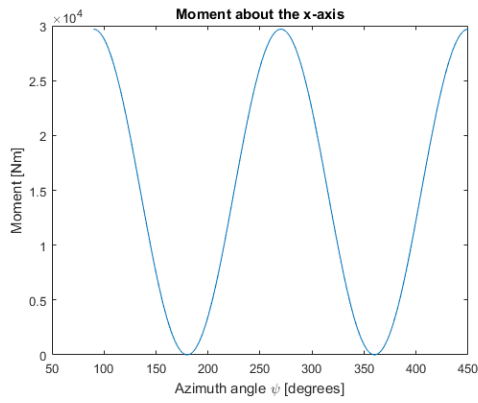
6.2.3. Speed Limitations for the Rotor

In Section 4.2.1 it was shown that the theoretical maximum speed the UAV can reach is 90 m/s. However, only the available power was considered for the calculation of that speed. When taking aerodynamic effects in consideration as well the maximum airspeed will be lower. One of the limits is the Mach number at the tip. This can not reach higher values than 0.84 as mentioned in Section 6.1.1. For flight under extreme conditions, a ground temperature of -30°C and altitude of 2,000 m, the speed of sound is 304 m/s. So for a tip speed at Mach 0.84 a flight speed of 45 m/s will be maximum. The airflow over the retreating blade has to be studied as well. When flying at high speeds a portion of the retreating blade will experience a negative velocity. For an airspeed of 45 m/s stall is only present at the first 30 cm of the retreating blade, at an azimuth angle of 270 degrees. This can be seen in Figure 6.5. However, this portion of the rotor has a negligible contribution to the lift so it will not be the determining factor for the maximum airspeed.

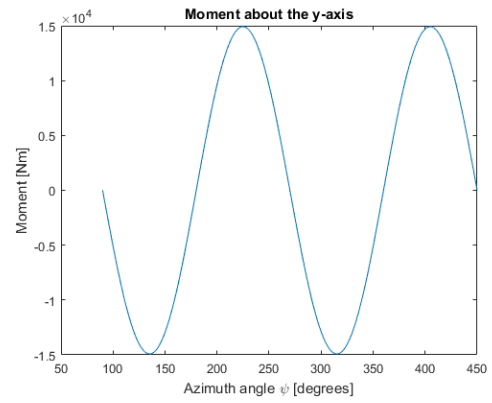
6.2.4. Influence of azimuth variations on the performance of the blade

To get an insight in the forces and moments that act on the rotor the influence of different azimuth angles ψ , the angle of the rotor blade with respect to the x-axis, are researched. The rotor consists of

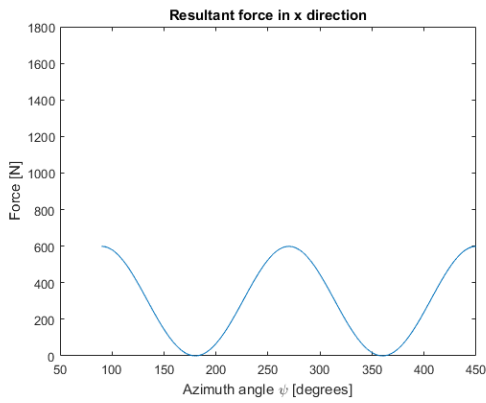
an advancing and a retreating rotor blade. These blades experience different velocities and angles of attack for different azimuth angles. These different angles and velocities result in different lift and drag forces on each blade. It can be seen from Figure 6.10 that these forces have a sinusoidal shape. The amplitude is influenced by the airspeed of the UAV and the period is dependent on the rotational rate of the rotor. It can also be seen in Figure 6.10h that the an area close to the rotor centre of the retreating blade has no contribution to the thrust. It is therefore preferred to install the engine or other structural components near this region. As mentioned in Section 4.1 the rotor has a rotational rate of 500 RPM. The frequency of these oscillations, which can be seen in Figure 6.10, is twice the frequency of the rotor, because the rotor has two blades resulting in 16.7 Hz. For the sizing of the structural components of the UAV the maximum values are taken to ensure structural integrity. For the lift production the mean value will be used, since the period is so short. For the power required to maintain constant rpm the mean value can also be used. This is because the power oscillation only has an amplitude of 5.5 kW and a frequency of 16.7 Hz, read from Figure 6.10g. Also, the blade carries an angular momentum keeping the rotational rate readily constant. Therefore, it will be assumed that the power required by the rotor is azimuth independent.



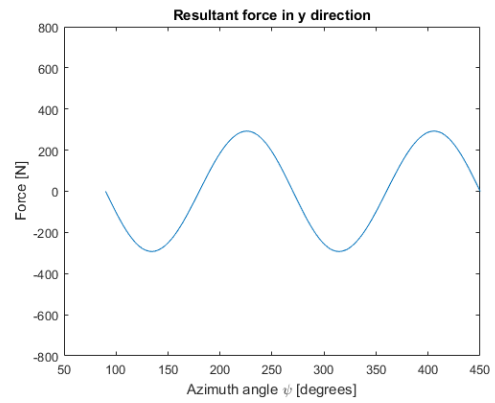
(a) Moment about the x-axis



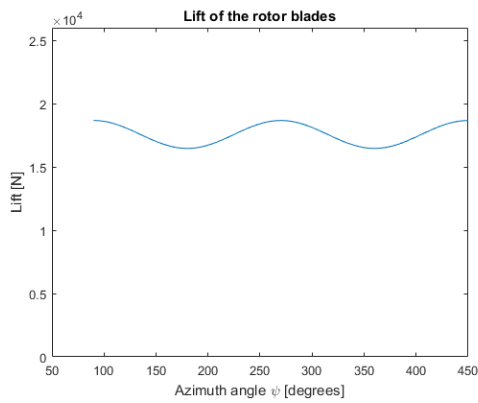
(b) Moment about the y-axis



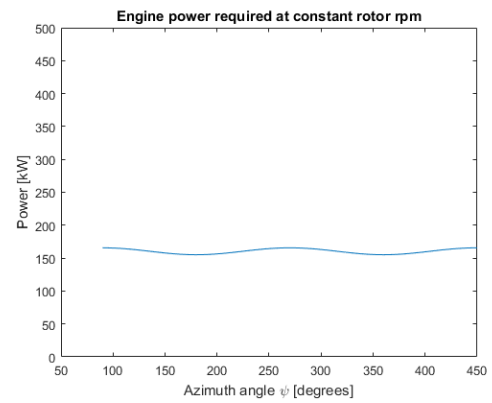
(c) Forces in the x direction



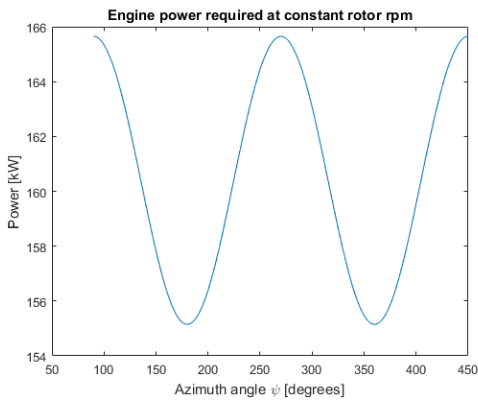
(d) Forces in the y direction



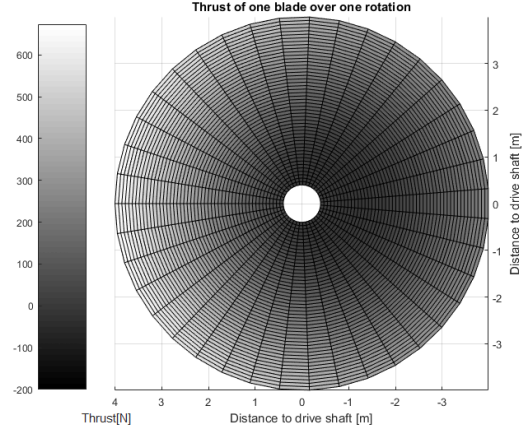
(e) Lift force variation



(f) Power required to keep constant rotor rpm



(g) Close up of power required to keep constant rotor rpm



(h) Thrust delivered by each rotor blade element

Figure 6.10: All figures show the azimuth influence for the rear rotor at the left side at a thrust setting of 17,500 N and airspeed of 42 m/s

6.3. Parasitic Drag Calculations

Drag is the aerodynamic resistance caused by an aircraft moving through the air. The amount of drag depends on the shape of all the components that make up the rotorcraft. The magnitude of these forces can be calculated by Equation (6.11), where ρ is the fluid density, which is assumed to be 1.225 kg/m^3 for air. V is the velocity, A is the reference area and C_D is the drag coefficient. Most of the C_D 's are found in *Fluid-dynamic Drag* [22].

$$F_{drag} = \frac{1}{2} \rho V^2 A C_D \quad (6.11)$$

The rotorcraft is split up in five general components, as shown in Figure 6.11, which all have a different C_D values. The main body structure, the engine block, the supporting cables, the landing gear and the container. The drag calculation for the rotor blades have already been treated in Section 6.2.2. Note that the Reynold's numbers used in this chapter have an assumed kinematic viscosity ν of $1.4 \times 10^{-5} \text{ m}^2/\text{s}$ and the velocity is 42 m/s .

6.3.1. Main Structure Drag

The body drag is divided into three main components. This to show the impact of each component individually. The three components are: beams perpendicular to the flight direction, beams in the flight direction and the landing gear. The aerodynamic impact of these three components are listed in Table 6.5, Table 6.6, Table 6.7 and Table 6.8 respectively. The dimensions of the beams and landing gear is further elaborated in Section 5.4.3.

Beams Perpendicular to Flight Since the beams perpendicular to the flight direction have a frontal area of 15.8 m^2 , they will contribute significantly to the total drag of the structure. Therefore, fairings are added to reduce the drag coefficient. A fairing of elliptical shape is selected for the outer part of these beams with a thickness to chord ratio of 3. Zigzag strips have been installed to make the airflow super-critical in the outer section of the beams. From Figure 6.13 it can be seen that a C_D of 0.3 can be reached. For the inner part a symmetric airfoil shaped fairing is used. This fairing is inclined at an angle θ so it has zero angle of attack in forward flight, shown in Figure 6.12. The implementation of the fairings and trip wires resulted in a drag coefficient of C_D of 0.3 [22] for outer section of the beam and 0.015 for the inner section [21]. The total drag of these beams is 3,319 N.

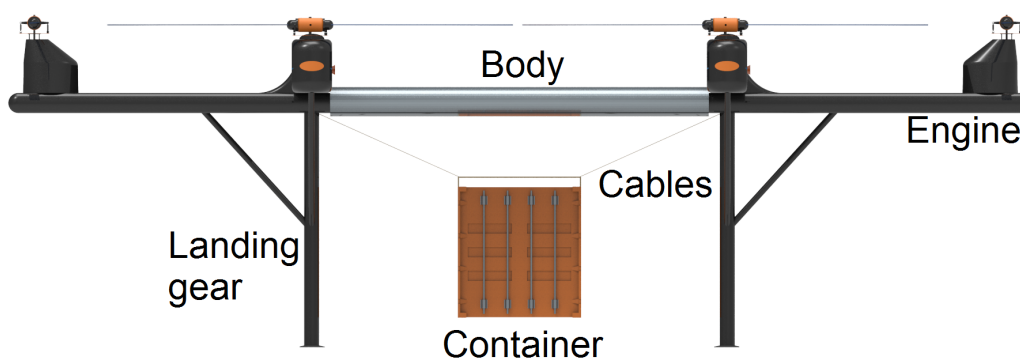


Figure 6.11: Schematic side view of the rotorcraft with its main drag components

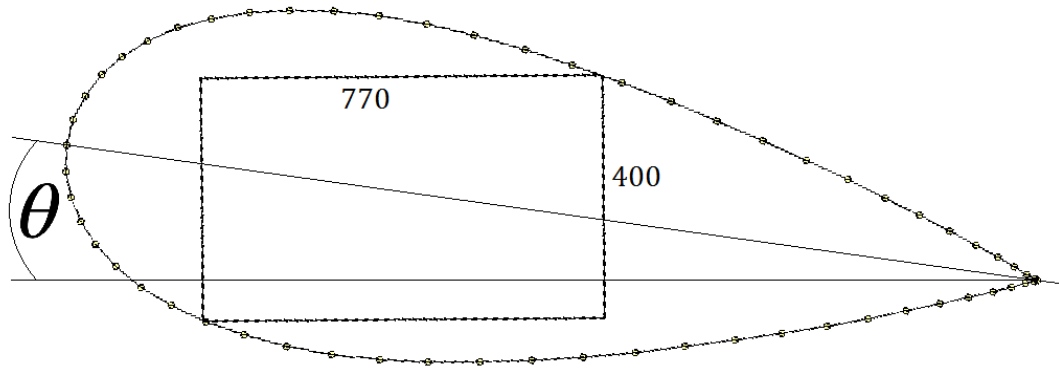


Figure 6.12: NACA 0035 airfoil fairing around the beams perpendicular to the flight direction

Table 6.5: Drag characteristics of inner part of the beams perpendicular to the flight direction

	Value	Unit
Reference area inner section	29.52	m ²
C_D	0.015	-
Equivalent flat plate area	0.443	-
Force	456	N

Table 6.6: Drag characteristics of outer part of the beams perpendicular to the flight direction

	Value	Unit
Reference area outer section	9.28	m ²
C_D	0.3	-
Equivalent flat plate area	2.78	-
Force	2863	N

Beams in Flight Direction The beams in the flight direction only have a surface of 1.12 m² facing the airflow. They are also very long and their shape can be compared to that of a train. According to [22] the drag coefficient of these beams can be set to 0.45. Therefore, the drag of these beams will amount to a total of 519 N.

Table 6.7: Drag characteristics of beams in the flight direction

	Value	Unit
Reference area	1.12	m ²
C_D	0.45	-
Equivalent flat plate area	.504	-
Force	519	N

Landing Gear The landing gear is circularly shaped as stated in Section 5.4.4. Nevertheless the landing gear of the UAV still has a significant effect on the total drag. To decrease this impact trip wires are installed here as well. Together with the trip wires the circularly shaped landing gear struts will have a drag coefficient of 0.4 [20]. Because the landing gear struts are 4.6 m in length and are all perpendicular to the air flow, they produce a total of 1,433 N drag. There are also drag struts that have to be incorporated in the total drag of the landing gear. There are a total of 8 drag struts with a length of 3.18 m each. However, the radius of these struts is only 0.06 m. The drag struts are placed at an angle

of 45 degrees resulting in a drag coefficient of 0.4 for the beams in flight direction and 0.6 for the struts perpendicular to the flight direction, as shown in figure 18 in Hoerner [22]. Note that the landing pads, which are in the flight direction, have been neglected in these drag calculations.

Table 6.8: Drag characteristics of the landing gear

	Value	Unit
Reference area landing struts	5.52	m ²
C_D Landing struts	0.2	-
Equivalent flat plate area	1.10	-
Reference area drag struts flight direction	1.392	m ²
C_D Drag strut flight direction	0.4	-
Equivalent flat plate area	0.557	-
Reference area perpendicular to flight	1.7	m ²
C_D Drag struts perpendicular to flight direction	0.6	-
Equivalent flat plate area	1.02	-
Total equivalent flat plate area	2.68	-
Force	2,760	N

6.3.2. Cable Drag

The supporting cables connecting the container to the HELLCAT have a similar sub-critical aerodynamic drag coefficient as circular cylinders ($C_D = 1.17$). However, there is a steady decrease of the drag coefficient of ropes varying from $C_D = 1.17$ at $Re = 1 \times 10^4$ to $C_D = 1.00$ at $Re = 6 \times 10^4$ resulting in a 1.05 drag coefficient for the given cables[23]. The drag characteristics of the cables can be found in Table 6.9.

Table 6.9: Drag characteristics of the cables

	Value	Unit
Reference Area	1.1378	m ²
C_D	1.05	-
Equivalent flat plate area	1.20	-
Force	1,236	N

6.3.3. Container Drag

The container drag will only be present in half of the mission, as it flies back empty, but has a considerable contribution to the total drag, which can be seen in Table 6.10. The container is modelled as a square box with sharp edges, which has a C_D of 1.05.

Table 6.10: Drag characteristics of the container

	Value	Unit
Reference area	5.76	m ²
C_D	1.05	-
Equivalent flat plate area	6.05	-
Force	6,232	N

6.3.4. Engine Drag

Four engines are housed in the longitudinal beams to get rid of the drag produced by these specific engines, while an elliptic fairing is put over the engine and gearbox on the perpendicular beams to produce a smooth outline and reduce drag. Figure 6.13 shows a plot with the drag coefficients of an elliptical section. The chord to thickness ratio of the designed fairing is assumed to be 2, resulting in a C_D of 0.6. The estimated engine drag can be seen in Table 6.11.

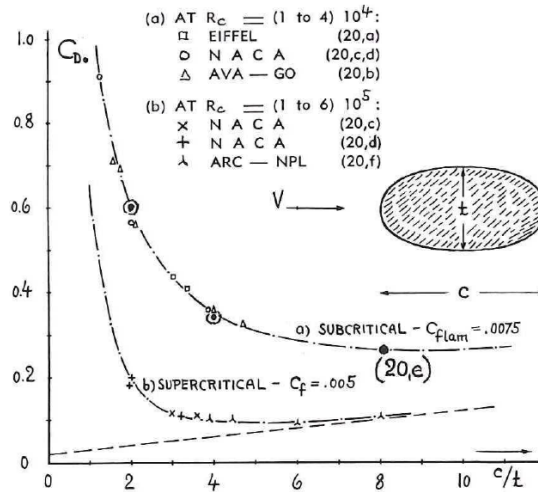


Figure 6.13: Drag coefficients of elliptical sections [22]

Table 6.11: Drag characteristics of the engine fairing

	Value	Unit
Reference area	1.232 x 4	m ²
C _D	0.6	-
Equivalent flat plate area	2.96	-
Force	3,049	N

6.3.5. Vertical Drag Estimation in Hover

A method for making an estimate of the vertical drag in hover is given by Equation (6.12)[25]. Where D_v is the vertical drag output. The inputs are GW , gross weight, A_p and A_d which are the projected area and disc area respectively. Note that the gross weight changes as function of flight time as fuel is being burned and the container is unloaded.

$$D_v = 0.3A_p/A_dGW \tag{6.12}$$

Figure 6.14 schematically shows the projected area. The width of the beams under the rotors are different for the longitudinal and the perpendicular beams, which are 600 mm, and 770 mm respectively. This gives a mean projected area of 2.7636 m², while the disk area is $4^2\pi$

$$D_v = 0.3 \cdot 2.7636/4^2\pi GW \tag{6.13}$$

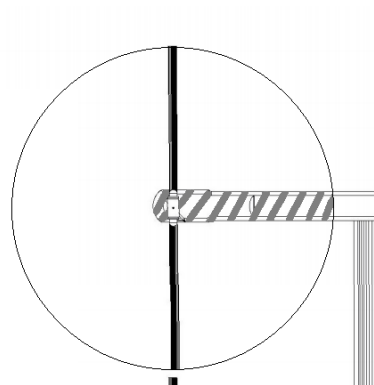


Figure 6.14: Schematic view of the projected area of 1 rotor

These inputs result in the plot given in Figure 6.15. The vertical line is the point where the 5,000 kg payload is unloaded, lowering the gross weight.

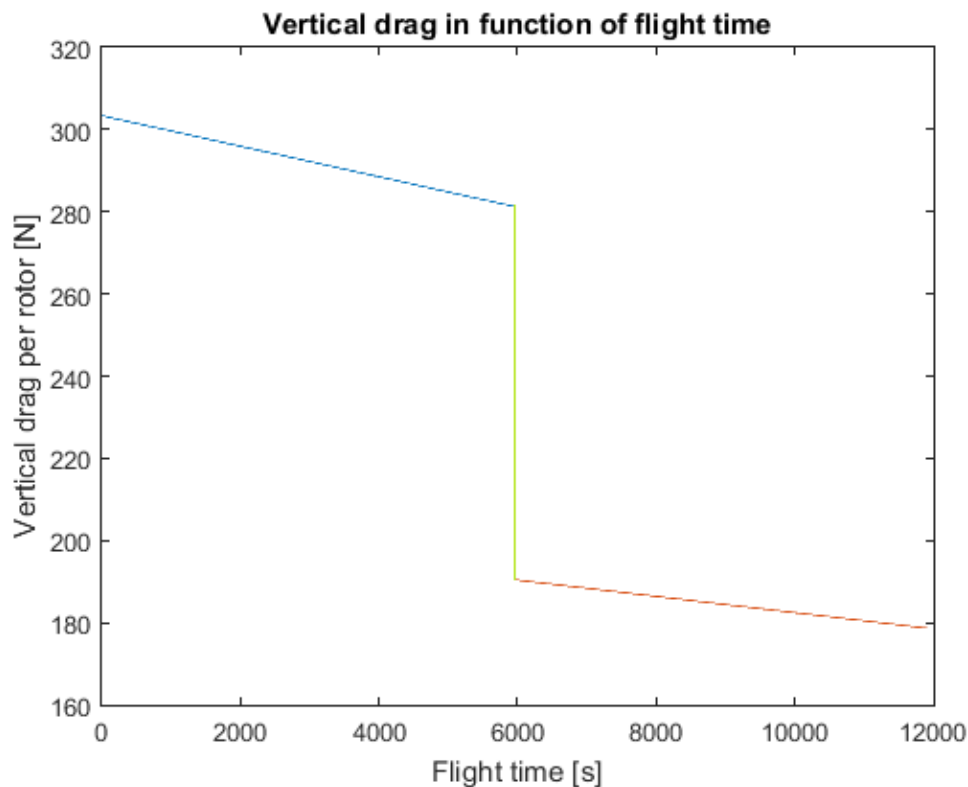


Figure 6.15: Vertical drag estimation in function of mission time

6.4. Aerodynamic Moments

All the drag components calculated in Section 6.3 cause aerodynamic moments on the rotorcraft. As it is symmetric in X- and Y-direction, only the center of gravity in Z-direction is interesting. It is assumed that the fuel is equally distributed and that the container is connected rigidly to the aircraft. A schematic view of the frontal area is given in Figure 6.16.

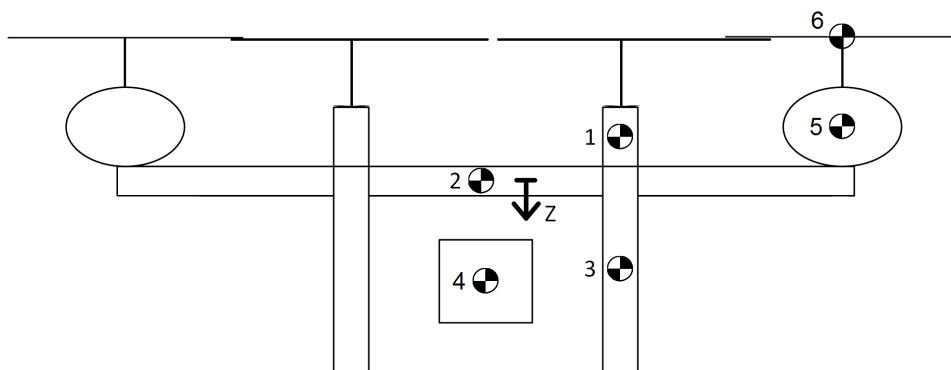


Figure 6.16: Schematic front view of the rotorcraft for center of gravity determination

Table 6.12 shows an overview of all the components with their Z-direction and mass. It is assumed that the mass of the components is distributed evenly so that the center of gravity of the individual components is located in the middle.

Table 6.12: Center of gravity determination

Component	z-location (m)	mass (kg)	Quantity
1 Longitudinal beams	-0.73	427 + 625	2
2 Lateral beams	0	291 + 625	2
3 Landing gear	2.7	164	4
4 Container	2.9	5,000	1
5 Engine	-0.7	460	4
6 Rotor	-2.26	115	8

The sum of the moments divided by the total mass gives the center of gravity in z-direction, which is calculated to be 0.7103m. The aerodynamics moments around the x-axis of the center of gravity are summarised in Table 6.13. Again it is assumed that the drag forces are point forces in the center of gravity of the individual components. The cruise drag from the rotor blades and hub are found in Section 6.2.2. The resulting moment is -0.65645×10^3 N m around the y-axis.

Table 6.13: Aerodynamic moments determination

Component	z-location (m)	Cruise drag (N)	Quantity
1 Longitudinal beams	-1.30	0.2595×10^3	2
2 Lateral beams	-0.57	1.660×10^3	2
3 Landing gear	2.13	0.6675×10^3	4
4 Container	2.33	6.2320×10^3	1
5 Engine	-1.27	0.7622×10^3	4
6 Rotor	-2.83	0.21×10^3	8

6.5. Verification and Validation

The BET relies on dividing the rotor blades in small elements and computes the properties for each blade element individually. The BET model uses 50 blade sections and 200 different azimuth angles at 50 different speeds. v_i from Equation (6.1) can only be calculated numerically, so six iterations are used. When calculating 17 different parameters for each blade at all the different settings 102,000,000 calculations are performed. Therefore, it will become cumbersome to verify the model by hand. It is also very hard to validate the BET model by comparing it to existing helicopters. The blade pitch angle at all the different elements have to be known. Also the power setting of that particular helicopter for as a function of flight speed as well. Because of this the BET model is verified by comparing the power values with the model used in Section 4.2.1. Since that model is verified analytically and validated with reference helicopter in Section 4.2.4 it will be sufficient for the verification and validation of the BET model to compare those results. Figure 6.17 shows the power curves of the model used in Section 4.2.1 and from the BET model. It can be seen that they show great similarities. The BET requires slightly more power to overcome the induced drag, but within an acceptable range for a preliminary design.

The aerodynamic drag calculations were executed by matlab functions, the functions are compared by hand calculations in the beginning to ensure verification of the functions. The values were a complete match, implying that the model works as intended. The center of gravity and aerodynamic moment calculations is verified by plotting the centre of gravity of every individual component to make sure it makes sense, which it did. Together with matching hand calculations this implies that the estimation functions for the centre of gravity and aerodynamic moment work as intended.

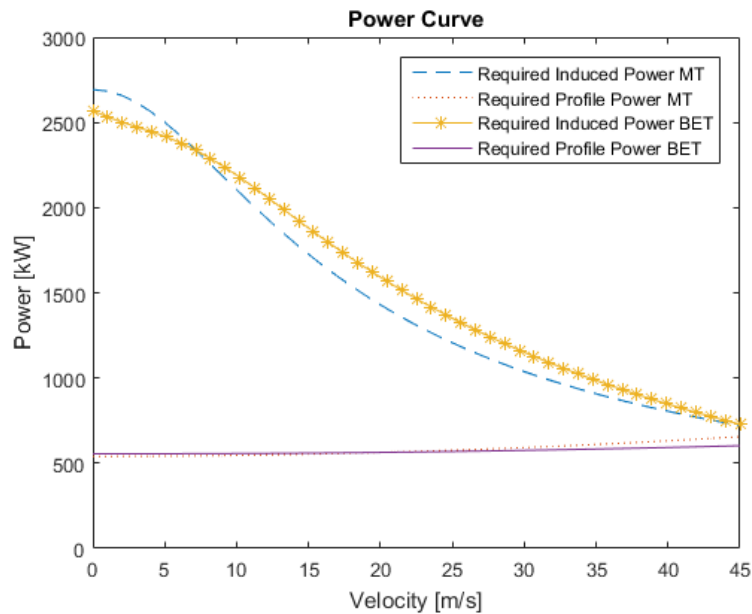


Figure 6.17: Induced and profile power curves from the Blade Element Theory (BET) and Momentum Theory (MT)

6.6. Recommendations

The aerodynamic performance can be further improved to optimise the design. Further research is necessary to see whether taper is possible for the beams of the HELLCAT. Especially taper in the beams perpendicular to the flight direction will reduce the total drag of the HELLCAT. The outer parts of these beams are the highest contributor to the drag, from an ideal aerodynamic point of view a completely tapered beam could half the frontal area and thus reducing the drag by 1431.53 N. A retractable landing gear will be another effective method to reduce the total aerodynamic drag. It is recommended to investigate the wake interactions by using Computational Fluid Dynamics (CFD). This way, the aerodynamic properties will be more accurate and realistic. Also, the shape of the fairing could be optimised for drag reduction by using CFD. For the rotor blades, it should be researched whether the induced and profile power during hovering can be reduced by increasing the rotor blade taper ratio [26]. Finally, a wind tunnel test should be conducted to validate the design.

7 System, Control & Operations

In addition to the previous chapters, this chapter will take a closer look at the stability and control, as well as the operations around the HELLCAT. This is essential for formulating and designing the required systems to fulfil the mission. First, the equations of motion are derived to find the required state variables to be altered to control the HELLCAT. With the variables found, a physical model is built and used in simulation for designing the control systems. Finally, the avionics and navigation systems which play a vital role to achieve safe, unmanned and autonomous flight are discussed.

7.1. Equations of Motion of the HELLCAT

In this section the equations of motion of the HELLCAT will be examined. These are later used to determine control rules for the UAV. First the reference frames in which the vehicle is described are shown, next the rotation around the UAV's axes are considered and finally the translational motion with respect to earth is calculated.

7.1.1. Reference Frames

For the description of the equations of motion, two reference frames are defined. A body fixed reference frame (x pointing forward, y sideways and z down) and an inertial earth fixed (North East Down) reference frame. The body fixed reference frame is used to describe the rotational motion of the aircraft, whereas the inertial earth fixed reference frame is used to describe the translations of the vehicle in space. To transform the angular states from the body frame to the earth-fixed frame, rotation matrices are used. The rotation matrix \mathbf{T} from the body fixed to the earth fixed frame is given by Equation (7.1) [30]:

$$\mathbf{T} = \begin{bmatrix} c_\theta c_\psi & -c_\phi s_\psi + s_\phi s_\theta c_\psi & s_\phi s_\psi + c_\phi s_\theta c_\psi \\ c_\theta s_\psi & c_\phi c_\psi + s_\phi s_\theta s_\psi & -s_\phi c_\psi + c_\phi s_\theta s_\psi \\ -s_\theta & s_\phi c_\theta & c_\phi c_\theta \end{bmatrix} \quad (7.1)$$

In this matrix c denotes the cosine of the subscript and s the sine.

7.1.2. Rotational Equations of Motion

The external forces on the UAV are mainly governed by weight, thrust and aerodynamic drag. The aerodynamic drag calculations are given in Section 6.3 and the resulting moments are described in Section 6.4. The thrust is nearly linear dependent on the rotorblade pitch angle as described in Section 4.2.1, on which the control system described in Section 7.3 is based.

For the rotational equations, first the influence of each rotor is defined. The rotors are numbered 1 through 8 in a clockwise direction. The different rotor contributions are defined as:

$$\begin{bmatrix} L_{control} \\ M_{control} \\ N_{control} \end{bmatrix} = \mathbf{B}\mathbf{u} = \begin{bmatrix} d_2 c_T & d_2 c_T & d_1 c_T & -d_1 c_T & -d_2 c_T & -d_2 c_T & -d_1 c_T & d_1 c_T \\ d_1 c_T & -d_1 c_T & -d_2 c_T & -d_2 c_T & -d_1 c_T & d_1 c_T & d_2 c_T & d_2 c_T \\ -c_m & c_m & -c_m & c_m & -c_m & c_m & -c_m & c_m \end{bmatrix} \begin{bmatrix} u_1 \\ u_2 \\ u_3 \\ u_4 \\ u_5 \\ u_6 \\ u_7 \\ u_8 \end{bmatrix} \quad (7.2)$$

Where c_T is the thrust coefficient of the rotor and c_m the moment coefficient produced by the engine. Note that these coefficients are dependent on the velocity and atmospheric conditions. The inputs in vector \mathbf{u} are defined as a value between 0 and 1, where 0 results in 0 N thrust and a 1 in the maximum

thrust in that flight condition. It is further important to account for gyroscopic effects. In normal conditions these should be negligible, however during some situations they might still influence the results. There are two gyroscopic effects acting on the structure. The first one is caused by the rotation of rotors. The moment contribution of a single rotor, as a result of a pitching velocity, is given as:

$$M = \frac{J_r}{J} \dot{\theta} \Omega_r \quad (7.3)$$

With J_r the moment of inertia of the rotor blade and Ω_r its angular velocity. The second gyroscopic contribution is caused by rotation of the whole structure. Since the structure has three rotational degrees of freedom, as opposed to one for the rotor blade, it results in the moments:

$$\begin{bmatrix} L_{gyro} \\ M_{gyro} \\ N_{gyro} \end{bmatrix} = \begin{bmatrix} (J_y - J_z) \dot{\theta} \dot{\psi} \\ (J_z - J_x) \dot{\phi} \dot{\psi} \\ (J_x - J_y) \dot{\phi} \dot{\theta} \end{bmatrix} \quad (7.4)$$

Finally, a term describing the location of the centre of gravity is added. In most flight dynamics studies the moments are described with respect to the centre of gravity, but for this stability study it is more convenient to take them with respect to the geometrical centre. Especially to study the different loading cases. This results in the following angular relations (in the body frame):

$$\begin{bmatrix} \dot{\phi} \\ \dot{\theta} \\ \dot{\psi} \end{bmatrix} = \mathbf{J}^{-1} \begin{bmatrix} L_{aero} \\ M_{aero} \\ N_{aero} \end{bmatrix} + \mathbf{J}^{-1} m g \mathbf{T} \begin{bmatrix} x_{cg} \\ y_{cg} \\ z_{cg} \end{bmatrix} + \mathbf{J}^{-1} \begin{bmatrix} (J_y - J_z) \dot{\theta} \dot{\psi} \\ (J_z - J_x) \dot{\phi} \dot{\psi} \\ (J_x - J_y) \dot{\phi} \dot{\theta} \end{bmatrix} + \mathbf{J}^{-1} \mathbf{J}_r^T \Omega_r \begin{bmatrix} \phi \\ \theta \\ \psi \end{bmatrix} + \mathbf{J}^{-1} \mathbf{B} \mathbf{u} \quad (7.5)$$

With:

$$\mathbf{J} = \begin{bmatrix} J_x & 0 & 0 \\ 0 & J_y & 0 \\ 0 & 0 & J_z \end{bmatrix} \quad (7.6)$$

7.1.3. Translational Equations of Motion

The translational equations of motion in the earth fixed reference frame are described as:

$$\begin{bmatrix} \ddot{x} \\ \ddot{y} \\ \ddot{z} \end{bmatrix} = \frac{1}{m} \begin{bmatrix} X_{aero} \\ Y_{aero} \\ Z_{aero} \end{bmatrix} - \begin{bmatrix} 0 \\ 0 \\ g \end{bmatrix} + \frac{1}{m} \begin{bmatrix} 0 \\ 0 \\ \mathbf{u} \mathbf{c}_T^T \end{bmatrix} \mathbf{T}_{b \rightarrow e} \quad (7.7)$$

Where the relation $\mathbf{u} \mathbf{c}_T^T$ describes the thrust vector in the body fixed reference frame. As can be seen, there is no direct control in the principle directions of the earth fixed reference frame. The translational control is achieved by means of rotational control, which as shown below can be directly controlled. Note that, since the flight envelope only encompasses relatively small roll and pitch angles (below 30 degrees), the altitude can be directly controlled.

7.1.4. Simplified Equations of Motion

The equations of motion can be simplified for different flight conditions. As already mentioned in Section 7.1.2, the thrust is linearly dependent on rotor pitch, given a constant speed. This means that the equations of motion can be linearised around a certain speed and vehicle attitude.

In most conditions, the gyroscopic effects can be neglected since there are no rotational speeds. This results in the non-linear rotational equation:

$$\begin{bmatrix} \ddot{\phi} \\ \ddot{\theta} \\ \ddot{\psi} \end{bmatrix} = \mathbf{J}^{-1} \begin{bmatrix} L_{aero} \\ M_{aero} \\ N_{aero} \end{bmatrix} + \mathbf{J}^{-1} m g \mathbf{T} \begin{bmatrix} x_{cg} \\ y_{cg} \\ z_{cg} \end{bmatrix} + \mathbf{J}^{-1} \mathbf{B} \mathbf{u} \quad (7.8)$$

and for the translational motion:

$$\begin{bmatrix} \ddot{x} \\ \ddot{y} \\ \ddot{z} \end{bmatrix} = \frac{1}{m} \begin{bmatrix} X_{aero} \\ Y_{aero} \\ Z_{aero} \end{bmatrix} - \begin{bmatrix} 0 \\ 0 \\ g \end{bmatrix} + \frac{1}{m} \begin{bmatrix} 0 \\ 0 \\ \mathbf{u} \mathbf{c}_T^T \end{bmatrix} \begin{bmatrix} -\sin(\theta) \\ \sin(\phi) \cos(\theta) \\ \cos(\phi) \cos(\theta) \end{bmatrix} \quad (7.9)$$

7.2. Simulation

For the model simulation and tuning of the controllers it was chosen to make use of Simulink as part of the MATLAB environment. Making use of the Simmechanics package in Simulink, a multi-body model can be built and simulated. Computer Aided Design (CAD) drawings can be imported and controller tuning can be done using graphical interfaces. This integration of the different components make the use of this program the favoured one.

7.2.1. Physical Model

Due to the concurrent engineering approach a simple geometry is made from the geometry building blocks provided by Simmechanics that represents the final design, as opposed to the importation of the full CAD model since it was not yet available during the start of the simulation design. The geometry blocks represent a density. Combined with the dimensions this results in a mass and inertia. Simulink is able to dynamically derive the EOM's from the geometry and the applied forces on the structure and thereby able to simulate the behaviour of the aircraft. For now, the forces applied are the gravitational acceleration and the thrust and torques on the engine powered blades of which the torques comprise both mechanical and aerodynamic torques.

Making use of the data found in Chapter 4 and Chapter 6 a mathematical representation of the engine and blades can be inserted into Simulink. The thrust and aerodynamic torque of the blades are a function of the incidence angle of the blades as well as a function of the velocity of the aircraft. These forces act as an external force on the body. The blades are rotated through a joint block which is powered by the torque of the engine. This torque of the engine is modelled as a function of the rotational velocity in order to model the accurate spool-up time of the blades to the operating rotational velocity. Furthermore, engine failure is added such that the torque provided by the engine becomes zero instantaneously when in failure mode, while the blade will generate thrust until all the kinetic energy in the blades has been depleted. This is modelled by multiplying the thrust and torque at a specific incidence angle with a fraction. This fraction is the actual rotational velocity divided by the maximum rotational velocity. The remaining thrust provided is used to keep the aircraft in the air while the torque found is used to decelerate the propeller further. When the blade rotational velocity has become zero, no thrust or aerodynamic torque will be generated for the fraction becomes zero.

The controller will be able to input the incidence angle the blade experiences to alter the thrust and torque acting upon the structure per engine. Furthermore, the aircraft model behaviour upon engine failure(s) can be simulated by initiating the engine 'kill-switch'. This too can be done via an input. This combined yields the physical model on which analysis is done.

7.2.2. Physical Model Verification

In order to check whether the displayed behaviour is as expected from an analytical point of view, verification needs to be done. This is done by dividing the physical systems into two stages. The first stage is to check if the behaviour of the engine is as predicted. The second stage is to check if the engines mounted on a frame behaves as expected.

For the first stage, the engine model verification is done in three steps. Firstly, the spool-up time of the blade, as well as the spool-down in the event of engine failure is checked with respect to the torques applied. Secondly, the interaction of the engines on a larger structure are to be examined. For this, two opposing rotating engines are placed on a beam. Now, due to the simulated engine failure of both engines the deceleration of the blades as well as the rotation of the entire structure is analysed. The third test starts out the same as the second test, spooling-up both blades. Only now just one engine is in failure mode. Again, the rotation of the blades and entire structure is examined. The interaction verification tests need to be done to check if the forces in the engine and on the blades are translated to the larger structure correctly as well as in the appropriate direction.

To check whether the torques on the blade are modelled correctly, the engine torque applied the aerodynamic torque is divided by the moment of inertia of the blade to get the acceleration. The acceleration of the blades can be found by dividing the torque by the inertia. It is important to observe that both the model in Simulink and the analytical solution assume an elliptical blade.

$$I_{Blade} = \frac{m_{Blade}d_{Blade}^2}{12} = \frac{35 \cdot 8^2}{12} = 186.67 \text{ kgm}^2 \quad (7.10)$$

This inertia, found through mass m_{blade} and blade diameter d_{blade} is checked against an arbitrary pitch blade setting, taken as 0.79 or 79%. It is found that the net torque applied is:

$$T_{Net} = T_{Engine} - T_{Aerodynamic} = 11130 - 1460 = 9,670 \text{ N m} \quad (7.11)$$

When inserting the inertia and applied torque in the acceleration formula, it can be found that the acceleration is:

$$a_{Blade} = \frac{T_{Blade}}{I_{Blade}} = \frac{9670}{186.667} = 51.80 \text{ rad/s}^2 \quad (7.12)$$

The analytical solution thus yields a value of 51.80 rad/s² while the simulation yields a value of 51.78 rad/s². The behaviour is therefore as expected. The same holds for spooling-down, albeit with different values. Therefore, it can be concluded that the torques act as expected upon the blade.

In the second test, two engines on a rod are spooled-up before killing both at the same time. Since the structure is placed on a circular joint, only the torques on the structure are examined. When executing the test, it is found that the structure will not start to rotate, as expected. During spool-up applied torques of both engines are of opposite sign. Therefore, the net torque is zero. When both engine are in failure mode, the clutch detaches the linkage between engine and blade and no aerodynamic torque on the blades is transferred to the structure. Since both blades are disconnected at the same time, no resultant moment is to be expected. This is verified by the model since the rod will remain stationary while the blades start to decelerate due to the aerodynamic drag which provides a torque which slows down the blades with a rate conform the inertia, torque and acceleration values analytically computed. Therefore it can be concluded that the engine failure mode is appropriately modelled conform expectation.

Finally, one engine is killed while the other remains operational. Now, one torque from one engine remains acting upon the structure. It is therefore expected for the structure to start to rotate. As in the the first test, the inertia and net torque result in an expected acceleration. Again, firstly, the moment of inertia is calculated. Observe that the mass of the beam on which the engines are mounted on either end is taken as 1,000 kg whilst being 20 m long.

$$I_{Structure} = \frac{m_{Beam} \cdot L_{Beam}^2}{12} + \frac{m_{Blade} \cdot d_{Blade}^2}{12} + d_{Blade}^2 \cdot m_{Blade} \quad (7.13)$$

$$= \frac{1000 \cdot 20^2}{12} + \frac{35 \cdot 8^2}{12} + 10^2 \cdot 35 \cdot 2 = 40,706.67 \text{ kgm}^2 \quad (7.14)$$

The torque applied on the entire structure is expected to be the same as the aerodynamic torque at the inserted pitch setting being 1,473 N m at 0° pitch. Then, it can be found that the acceleration is expected to be:

$$a_{Structure} = \frac{T_{Net}}{I_{Structure}} = \frac{1452}{40706.667} = 0.0362 \text{ rad/s}^2 \quad (7.15)$$

As stated above, it is found that the expected acceleration would amount to 0.0362 rad/s². After running the simulation, the acceleration was found to be 0.03618 m/s². Therefore it can be concluded that torques acting upon the structure are correctly applied. The difference in acceleration can be explained due to the change of inertia of the structure. This is due to the the varying position of blades which impose different contributions to the overall inertia; the d_{Blade} changes in Equation (7.13) from 8 m to the chord length of 0.3 m. This proves that the analytical solution is conservative, as was to be expected.

With the engine model passing the above mentioned tests, it can therefore be concluded that the model behaves as expected and is therefore verified.

7.3. Control of the UAV

This section describes the different control algorithms analysed for the stability and control of the system. The main goal of this section is to prove that stability can be achieved by means of an automated control system. To show this, some important mission parts are simulated using the model described in Section 7.2. Anomalies such as engine failures and center of gravity (cg) deviations are also considered.

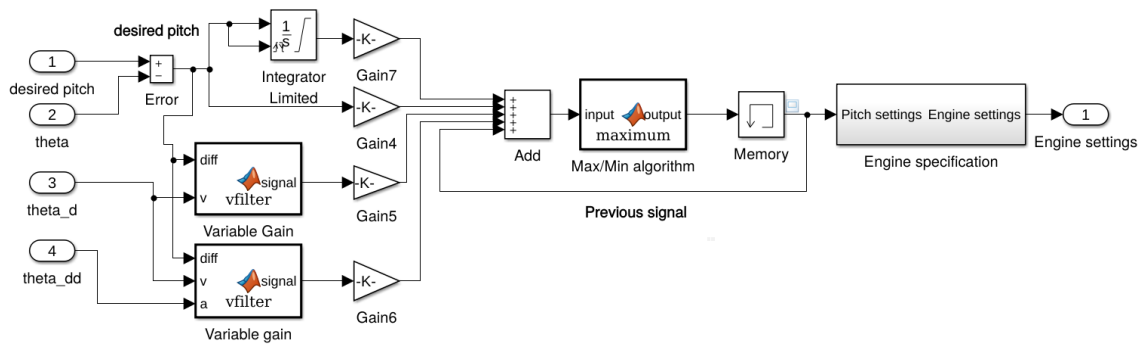


Figure 7.1: Incremental pitch controller

7.3.1. Attitude Control

Attitude control is essential for this design. An octocopter, like the more common quadcopter, is inherently unstable and will flip if not actively controlled. This leads to a problem, especially considering that the engines are not as agile as the small electrical engines known from its smaller brethren. Luckily, the larger inertia of the structure compensates for that, which means that, though slower, stability can be reached by active rotor pitch control. For the design of the control systems there are a few viable control algorithms. The simplest being standard Proportional, Integral and Differential (PID) control. Using this control algorithm for this model, only a stable system can be reached by means of gain scheduling. This technique uses different gains for different flight conditions, to ensure the stability of the nonlinear system. One of the disadvantages of this technique, is that the exact responses of the plant in all different conditions has to be known. A change in the system that affects its dynamics, eg. a change in moment of inertia, means that the whole controller has to be tuned to the new responses of the system. In the 1970s, Non-linear Dynamic Inversion (NDI) was developed to provide control to non-linear systems. [30] This technique however is still dependent on an accurate aerodynamic model. This technique further developed into Incremental NDI (INDI), which solves these dependencies. Instead of calculating the absolute control input, it calculates an increment of the previous input, based on the current and desired state. This is a way to cope with the non-linear control derivatives. Especially for changing geometries this results in a highly adaptive control algorithm. For the case of the octocopter this is an essential property for an eventual controller. Especially since the container loading could vary as well as to cope with possible engine failures. Due to time-constraints it wasn't possible yet to implement such controller on the octocopter model, but [30] and [31] show a very promising control scheme. For the scope of this stability study an incremental PID with second derivative (PIDDD) controller using gain scheduling was implemented, mainly because of the relative ease of tuning and implementation. An example, showing the pitch controller can be seen in Figure 7.1. This controller results in a stable flight system which can rotate around all axes, perform stable step and ramp responses (without overly exciting the engines) and perform all manoeuvres that could be asked by the navigation and position controller.

After the pitch control value is calculated by the controller, they are fed forward and combined with the other control values. The altitude controller assigns a single input value to each engine needed to maintain altitude (or reach it). The pitch controller adds its own value to the front engines, and subtracts it from the rear engines. This results in the same nominal thrust output, however introduces the requested pitching moment. The same procedure holds for the yaw and roll controller which results in the final input vector that is sent to the engines. See Figure 7.2 for a schematic of the control system.

Figure 7.3 shows the response to a 90 degree (0.39 rad) yaw input. The first figure shows the yaw angle and its derivatives in radians, the second figure shows the corresponding engine inputs, with 1 being maximum pitch setting (and thus maximum thrust) and 0 a zero thrust setting.

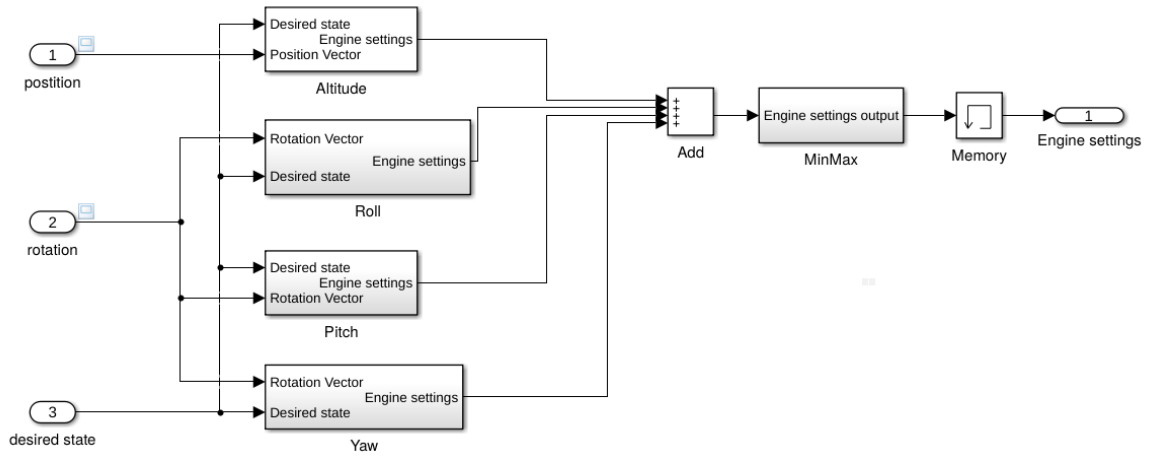


Figure 7.2: Schematic of the attitude and altitude controller

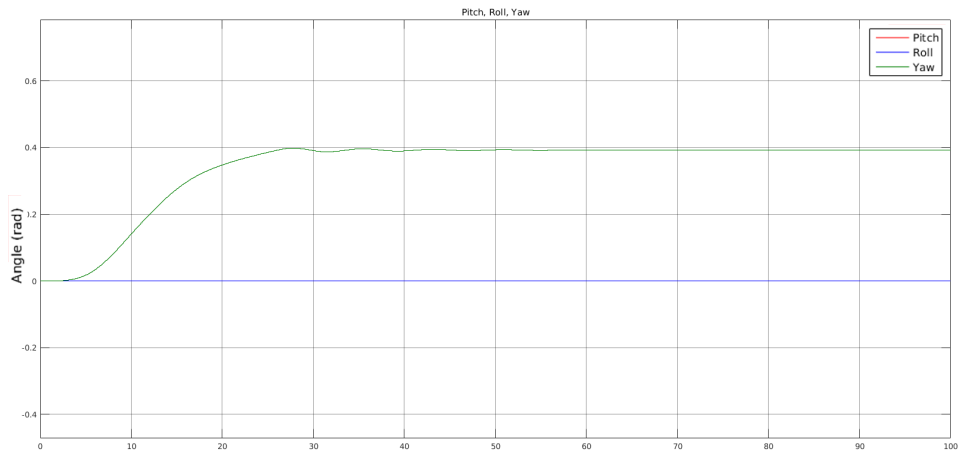


Figure 7.3: Pitch, roll and yaw angles after 0.39 rad yaw input

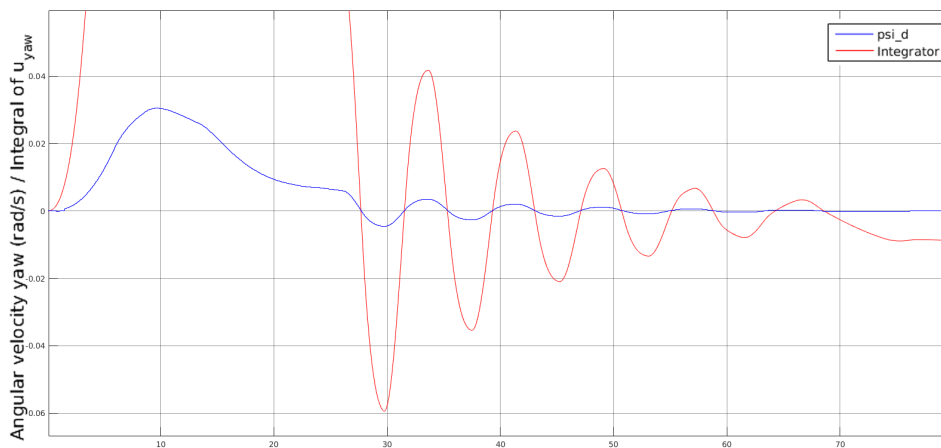


Figure 7.5: Yaw-rate and integral of the yaw input

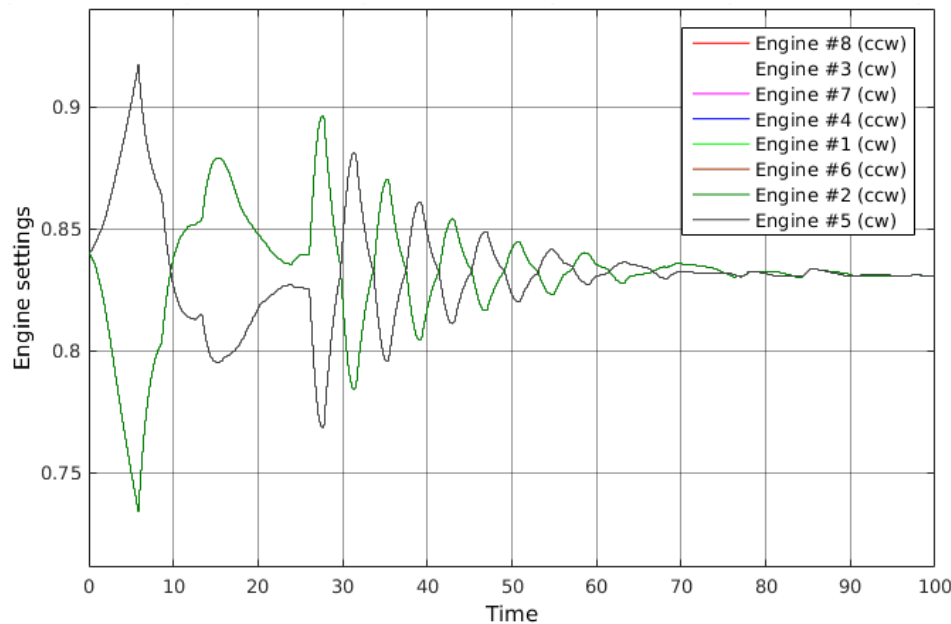


Figure 7.4: Engine response after 0.39 rad yaw input

As can be seen from Figure 7.4, for this tuning it takes around 60 seconds to damp out the oscillatory motion, but the final yaw value is reached within 30 seconds. A more aggressive tuning should reduce these numbers, but further research to find the optimal values would be needed. Note that 4 engines follow the top curve and 4 follow the bottom curve, which explains why only two lines are shown. This is inherent to how the yaw controller works,

7.3.2. Verification Controller

As a way of verifying the response of the controller, the yaw rate was plotted together with the integral of the yaw-controller input. Since the torque acting on the engines is almost linear with respect to the inputs, the results should be that the integral of the input (torque) should change sign at the exact same moment as the velocity. At the moment the total torque over time applied is zero, the angular velocity should be zero. Figure 7.5 shows this expected behaviour exactly. This shows that the inputs of the controller actually result in the requested velocity change.

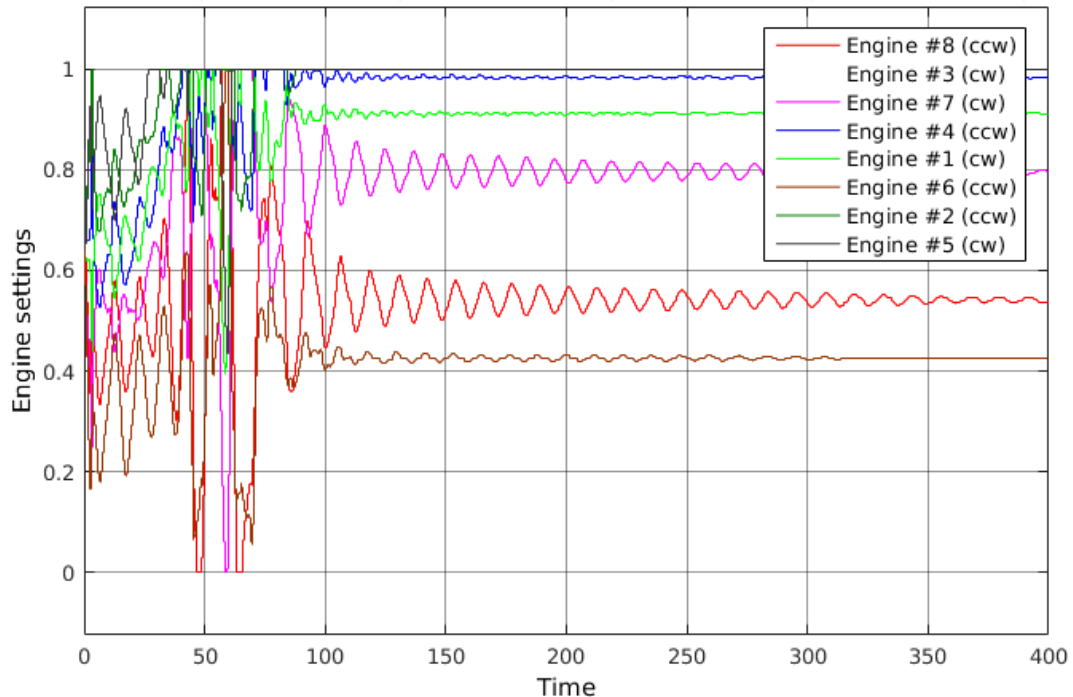


Figure 7.6: Engine responses after failure

7.3.3. Lateral Control

To fulfil a mission, and especially during landing, position control is crucial. Since the thrust vector only lies in the vertical (z) direction, the lateral position has to be controlled using the attitude controller. Changing vehicle pitch results in a different forward velocity. Alternatively, a roll angle results in a sideways force vector. To gain a sense of precision of the uav, a controller for this was written also. Since this controller essentially controls 4 different state variables, (position, velocity, pitch and angular acceleration) tuning for this controller proves very difficult. A similar approach was used as with the attitude controller, making use of incremental PID and gain scheduling. Initial tests showed that reaching the 0.5 m landing accuracy given by the requirements (Chapter 15) is difficult to meet, even given ideal conditions (no wind, single plane of freedom), currently a 4 m accuracy was obtained in ideal conditions. Further optimisation might improve these figures. However, the fact that the system is essentially underactuated, meaning only four degrees of freedom can directly be altered, makes precision in the other two difficult to meet. Wind didn't have to much of an effect on the positioning, with a 20 m/s gust from the side leading to a maximum 8 m displacement. A 0.14 rad roll angle is needed to mitigate its effects.

7.3.4. Engine Failure

With the measurements taken as described in Section 4.1, the effects of engine failure are mostly mitigated. At the moment engine failure is detected by the IMU. When detected the controller automatically ramps up the thrust settings of the engines near the failed engine. It will pitch forward to gain speed increasing its thrust at the cost of a loss of altitude. This loss is in the order of 100 m, however with an updated control algorithm this could still be reduced. Figure 7.6 shows the response and engine settings after engine failure with the current control algorithm. Note that this algorithm is hardly optimised for engine failure, with the exception that the altitude controller is shutdown in the initial few seconds. This shows that the current controller is already responsive enough to cope with a sudden engine failure and remain stable.

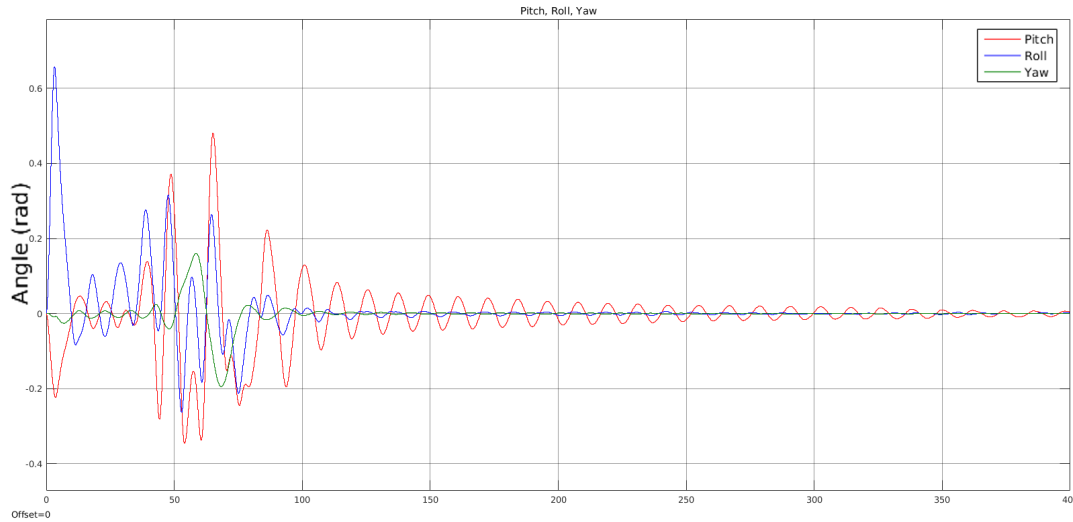


Figure 7.7: Roll angles after engine failure

7.3.5. Centre of Gravity Limits

The centre of gravity of the vehicle could shift due to uneven loading of the container, cable failure or fuel leaks. To check the effects of this cg shift, the equations of motions are used as derived in Section 7.1. A shift in cg only has an effect on the rotational EOM, so only these are considered. If we consider the vehicle in hover (ie. no rotations), these equations become:

$$\begin{bmatrix} \ddot{\phi} \\ \ddot{\theta} \\ \ddot{\psi} \end{bmatrix} = \mathbf{J}^{-1} m g \mathbf{T} \begin{bmatrix} x_{cg} \\ y_{cg} \\ z_{cg} \end{bmatrix} + \mathbf{J}^{-1} \mathbf{B} \mathbf{u} \quad (7.16)$$

To put that to words, in order to remain stable, the 8 engines should be able to counteract the moment generated by the shift in center of gravity. If we take the extreme condition that the container is suspended from only the front cables (ie, the cg of the container shifts 4 meters in positive y direction), the relation in Equation (7.17) can be derived.

$$\begin{bmatrix} \ddot{z} \\ \ddot{\phi} \\ \ddot{\theta} \\ \ddot{\psi} \end{bmatrix} = 0$$

Which gives:

$$\begin{bmatrix} mg \\ 0 \\ y_{cg} mg \\ 0 \end{bmatrix} = \begin{bmatrix} c_t & c_t \\ d_2 c_T & d_2 c_T & d_1 c_T & -d_1 c_T & -d_2 c_T & -d_2 c_T & -d_1 c_T & d_1 c_T \\ d_1 c_T & -d_1 c_T & -d_2 c_T & -d_2 c_T & -d_1 c_T & d_1 c_T & d_2 c_T & d_2 c_T \\ -c_m & c_m & -c_m & c_m & -c_m & c_m & -c_m & c_m \end{bmatrix} \mathbf{u} \quad (7.17)$$

This equation can be made dimensionless, by dividing by d_1 (4 m) and T_{max} (25,000 N). d_2 now becomes 3 — leading to:

$$\begin{bmatrix} 5.72 \\ 0 \\ 1.96 \\ 0 \end{bmatrix} = \begin{bmatrix} 1 & 1 & 1 & 1 & 1 & 1 & 1 & 1 \\ 3 & 3 & 1 & -1 & -3 & -3 & -1 & 1 \\ 1 & -1 & -3 & -3 & -1 & 1 & 3 & 3 \\ -1 & 1 & -1 & 1 & -1 & 1 & -1 & 1 \end{bmatrix} \mathbf{u}$$

Solving this leads to the least squares solution of \mathbf{u} :

$$\mathbf{u} = \begin{bmatrix} 0.76 \\ 0.67 \\ 0.57 \\ 0.57 \\ 0.67 \\ 0.76 \\ 0.86 \\ 0.86 \end{bmatrix}$$

For this worst case scenario of a cg shift, stability can still be reached with enough thrust for the engines to play with (15% for this case). It can be concluded that for this design, even a severe cg shift is not a real risk.

7.4. Navigation and Avionics

In order to perform the mission, as described in Section 3.6, the vehicle is equipped with avionics. In this section, all required avionics are described first. Afterwards, the configuration for the HELLCAT, including numbers and prices of each system, is listed in Section 7.4.5. In Section 7.4.6 an elaboration is given on sensor failing and emergency landings. Finally, recommendations for additional avionics are described in Section 7.4.7. More information about the interaction between the systems can be found in the next chapter, Chapter 8, which includes the communication flow diagram.

7.4.1. Attitude and Accelerations

To determine the vehicle's attitude, velocity and accelerations, it is equipped with an Inertial Measurement Unit (IMU). This unit consists of four components:

Gyroscope (3x): senses the vehicle's angular motion

Accelerometer (3x): senses the accelerations of the vehicle in x, y, and z direction

Magnetometer (3x): measures the magnitude and vectors of the magnetic field

Barometer: measures the pressure to determine the vehicle's height with respect to sea level

Together these systems determine the height, attitude and the accelerations of the vehicle. Assuming that the starting point is known, the current position could be calculated with these measured data. However, a so-called dead reckoning system is sensitive to errors as it solely depends on past data. Every measurement error will be accumulated. To counteract this error, this system is combined with GPS, which is described below.

Temperature sensor Besides the barometric pressure, also the temperature is measured.

Pitot tube To determine the airspeed of the HELLCAT, a pitot tube is installed.

7.4.2. Navigation

Altimeter sensors To determine the altitude of the vehicle directly to the ground below, which is especially useful during the landing, altimeters are installed. A Radio Altimeter (RADALT) works by sending out radio waves and measuring their time required to return to the vehicle after reflection from the ground. The same principle can be performed with laser (LIDAR) or with ultrasonic sound waves (SONAR) commonly used in parking sensors in cars. Based on off-the-shelf reference products, a RADALT appears to be most efficient in terms of cost and range. To provide more precision during the last phase of the landing, additional sensors can be installed in the form of relatively cheap and simple laser altimeters or sonar. Although their range is lower, they are more precise in the final meters. An option would be to install eight smaller sensors, close to each one of the engines. This would result in a better all round vertical distance overview and extra protection for the engines, the most expensive parts of the HELLCAT.

(Differential) GPS receiver To get to a certain destination, a GPS waypoint system is used. The vehicle flies autonomously, following a given set of coordinates, adjustable from the ground segment. To receive its own GPS location, each vehicle is equipped with a GPS receiver. However, the regular

GPS precision is in terms of around 10 m¹. Although this is precise enough to approximately follow the flight path, it is not precise enough to land within the 0.5 m required.

To accommodate for this requirement, and by taking redundancy into account, two measures are taken. The first is to make use of the optical systems, which are described in more detail in the next subsection. The second measure is to set up a differential GPS system, or more specifically a real time kinematic (RTK) GPS system, at the takeoff and landing spot of the UAV. This is done by installing a reference GPS receiver on both landing locations. This beacon sends its position to the vehicle. The vehicle receives both its own GPS signal and the location of the beacon, and positions itself with respect to the beacon. This way the regular GPS error is cancelled out, and the vehicle can land at a certain off-set vector from the beacon with an accuracy of down to 3 cm². This indicates that the beacon GPS system alone can already provide sufficiently precise information about the vehicles' landing spot.

Next to standard GPS not being very precise, another disadvantage is that it is sensitive to jamming. To counter this, anti jamming systems are available. They mitigate the interference by generating so-called nulls in the antenna and sending them in the direction of the jamming source³.

TCAS: Traffic Alert and Collision Avoidance System Another point of attention when operating an autonomous system is the reaction of the individual vehicles to other aircraft and objects. The ground segment traces all vehicles in the system, avoiding collisions between vehicles of the system themselves. To avoid other aircraft, and for other aircraft to avoid the vehicles, a TCAS can be installed. This system operates by identifying other active transponders in a radius around the vehicle. In case two aircraft threaten to collide, one will receive the message to climb, the other to descent. This message can be translated to the desired reaction by the autopilot and the system operates independently of Air Traffic Control. Aircraft without TCAS cannot be detected. Another issue is that this transponder detection by other aircraft might not be desired for certain military operations. In that case, the TCAS can be turned-off and collisions should be avoided by the radar of the air traffic control, by manually sending climb or descent inputs to the vehicle.

7.4.3. Surrounding Awareness

Cameras The most basic optical solution to acquire some surrounding awareness, is by installing cameras. These can be watched by the ground control directly and can be used for optical flow. A vector based motion can be determined by comparing two individual images taken a known time apart. Unique features on the images are marked and compared across multiple images. Using the different positions of the unique features at discrete times enables an algorithm to estimate the motion. Implementing this technique for landing requires a visual landing spot, large enough to spot from approximately 100 m. Although relatively cheap this technique is not applicable in environments with poor lighting conditions. Also, the sand that is expected from the downwash during the landing might block the view of the cameras. This is solved by the IMU of the HELLCAT. Once the exact landing spot is detected, the IMU of the HELLCAT will be able to land within the 0.5 m margin, as long as the landing is sufficiently fast and no unexpected wind gusts are around.

Infrared (IR) To complement the cameras described above, infrared cameras are installed. Infrared sensors measure heat that radiates from objects or persons, convert it to electronic signals, and finally convert those to an image. Although their resolution is lower than the regular cameras installed, the benefit of an IR cameras is that they also work in poor lighting conditions.

7.4.4. Data Processing and Communication

To complete the autonomous system, all outputs of the sensors described above should be collected and processed. This is done by the on board processing computer for avionics. A data storage is used for all collected and processed data. Flight data records should also be stored in the black box. Furthermore, encrypted data has to be communicated between the HELLCAT and the ground segment. As long as the HELLCAT is in line of sight of the ground station, a direct data link can be used. For the rest of the mission the support of satellite communication is required. In typical military operations, communication is performed by ultra high frequency (UHF) radio waves. Commonly used data links in aviation are Aircraft Communications Addressing and Reporting System (ACARS) and Controller Pilot

¹ <http://www.gps.gov/systems/gps/performance/accuracy/> [cited 15 January 2016]

² <https://www.sensefly.com/drones/ebee-rtk.html> [cited 15 January 2016]

³ <http://www.novatel.com/products/gnss-antennas/gajt-anti-jam-antennas/gajt/> [cited 15 January 2016]

Data Link Communication (CPDLC). For military operations there are also Tactical Data Links (TDL). Each vehicle needs to be equipped with a transceiver suitable to the communication system required by the customer.

7.4.5. Avionic Configuration

In Table 7.1 the configuration of the avionics is listed. To keep the development cost as low as possible, only off-the-shelf products should be used. Where possible, a reference product is given that complies with the mission requirements. Their prices are listed as an indication. The systems are relatively light compared to the weight of the entire structure. Thus the system selection was performed based on the price of the systems, not on their weights. The weights of all components can be found in Chapter 12.

Table 7.1: Standard Avionic Configuration

System	Reference product	Price (€)
2 x IMU (incl. GPS)	VN-300 ⁴	9,200
2 x GPS antenna w/ anti jamming	Estimation ^{5 6}	2,000
1 x Atmospheric sensors	BME-280 ⁷	37
2 x RADALT	GRA™ 55 ⁸	11,592
1 x TCAS-I	Garmin GTS855 ⁹	20,050
4 x Camera	SONY FCBEV7500 ¹⁰	5,520
4 x IR	FLIR vue ¹¹	11,040
4 x Autopilot processor	Raspberry Pi 2 ¹²	147
4 x Data Storage	Sandisk Micro SD ¹³	64
2 x Communication	Estimation	9,200
1 x Flight Data Recorder	ERIXX Flight Recorder ¹⁴	350
1 x Emergency beacon	Artex ELT 345 ¹⁵	501
2 x Pitot Tube	APM 2.6 ¹⁶	46
Cables and Wires	Estimation	500
Ruggedisation	Estimation	3,000
Total Price		73,083

7.4.6. Deviations from Standard Procedures

In case an emergency landing is necessary, the vehicle can land relatively fast since emergency landing spots are taken into account when the flight path is defined. As an extra safety measure, the cameras can be used to check the ground below the vehicle. This can be done manually from the ground station, or autonomously by the vehicle with the previously described optical flow method. To find the vehicle back after an emergency landing or even after a serious crash, an emergency beacon is installed that sends out its GPS signals by satellite communication. To protect the systems during emergency

⁴<http://damien.douxchamps.net/research/imu/> [cited 15 January 2016]

⁵<http://www.novatel.com/products/gnss-antennas/gajt-anti-jam-antennas/gajt-ae-n/> [Cited 15 January 2016]

⁶https://www.rockwellcollins.com/Data/Products/Navigation_and_Guidance/GPS_Devices/Digital_Integrated_GPS_Anti-Jam_Receiver-DIGAR.aspx [Cited 15 January 2016]

⁷<https://www.sparkfun.com/products/13676> [Cited 15 January 2016]

⁸<https://buy.garmin.com/en-US/US/in-the-air/avionics-safety/radar-altimeters/gra-55/prod166298.html> [Cited 15 January 2016]

⁹<http://sarasotaavionics.com/avionics/gts855> [Cited 15 January 2016]

¹⁰<https://www.goelectronic.com/SONY20FCB-EV7500.html> [cited 15 January 2016]

¹¹<http://www.oemcameras.com/infrared-thermal-imaging-camera-cores/flir-vue.htm> [cited 15 January 2016]

¹²<https://www.adafruit.com/products/2358> [Cited 15 January 2016]

¹³<http://www.dataio.nl/micro-sd/microsd-16gb/sandisk-16gb-micro-sd-extreme-90mbs-uhs-i-u3/> [Cited 15 January 2016]

¹⁴<http://www.imi-gliding.com/price-list.html> [Cited 15 January 2016]

¹⁵<http://sarasotaavionics.com/avionics/elt-345> [Cited 15 January 2016]

¹⁶<https://store.3dr.com/products/airspeed-kit-with-mpxv7002dp> [Cited 15 January 2016]

landings, but also for protection during regular operations, ruggedisation is used. As can be seen in the table above Table 7.1, most systems are at least installed double. This is done for redundancy reasons, in case one sensor fails, the other one can take over. Furthermore, also for redundancy, some system types fulfil the same function. An example: the IMU, RADALT and the DGPS can all determine the height of the vehicle, so failure of one of the systems will not be catastrophic. More difficult would it be if the external communication is lost for other reasons than sensor failure. In case the connection with the ground segment is lost during the mission, the vehicle is able to follow its waypoints as planned. In case the GPS connection is lost, the vehicle can temporarily follow its flight plan on IMU only. If necessary, the cameras can be used to manually identify its location. Once the GPS signal is back, the potential error can be corrected. In case GPS signal is lost during landing, the vehicle is still able to land with the visual beacon, IMU and its RADALT. When both beacons are unavailable, but the cameras are still available, the cameras can be used to manually select the precise landing spot. In case the cameras are also unavailable, the IMU/GPS combination alone is still be able to land the vehicle within approximately 2.5m¹⁷.

7.4.7. Additional Avionic Systems

To increase the autonomy level of the system, additional surrounding awareness systems could be installed in exchange for a higher total avionics price. A Light Detection And Radar (LIDAR) could be used for precise, real time 3D mapping. It detects the reflection of a sent light pulse of specific wavelength. Using time difference between sending and receiving the pulse, the distance to a reflective surface can be determined. When this is done continuously, a height map of surface can be made. Compared to RADAR, it makes use of higher frequency light, which results in the detection of smaller objects. This 3D mapping would be beneficial for cruise, take-off and landing. It could be used to autonomously identify an emergency landing spot or autonomously fly around encountered buildings during take-off and landing, all making it safer to fly through densely populated areas. Furthermore, 3D maps could be pre-loaded and landing spots could be recognised by the system without the use of beacons. As established by NASA [27], LIDAR is essential for safe autonomous UAV landing as it enables the mapping of the landing spot and helps achieve a positioning accuracy error of less than 10 cm. The disadvantage is that the starting price of off the shelf systems is currently around 55000 USD¹⁸. Especially when more than one LIDAR systems are required, for redundancy or for different angles, this well exceeds the budget set for the avionics of this project. Apart from the cost, it might also be redundant to use real time 3D mapping in a remote area. Therefore, the LIDAR system is currently left out of the configuration, but it is recommended for further investigation if the client desires a higher autonomy level.

¹⁷<http://www.vectornav.com/docs/default-source/documentation/vn-300-documentation/PB-12-0004.pdf?sfvrsn=22>. [Cited 25 January 2016]

¹⁸<http://www.phoenix-aerial.com/news/news2/> [cited 15 January 2016]

8 Interface Definition

This chapter was created to provide a systematic overview of the power elements of the HELLCAT. In the first section of this chapter, all these elements are displayed in the Electric Block Diagram. The second section shows the avionics and engine communication flow diagrams.

8.1. Electric Block Diagram

The electrical block diagram is depicted in Figure 8.1 and it shows all the main elements that require power. As the figure shows the electrical power is generated by three separate alternators each located at a different engine. A single alternator can power the HELLCAT, the other two are for redundancy. The battery is used when the alternator is not producing energy, this is for ground operations or when the engine fails. Each alternator can recharge all three batteries this is also for safety. The power is converted and after passing the engine or avionics bus it reaches the elements. The seven main elements are *Engine*, *Gearbox*, *Hydraulic System*, *Fuel System*, *Rotor System*, *Avionics Subsystem* and the *IMU*.

8.2. Communication Flow Diagram

The purpose of a communication flow Diagram is to illustrate the data flow through the system, flow between the system and its environment. The diagram is divided into two parts, the avionic and the engine communication flow. All elements that are part of the communication chain are depicted in blocks, the arrows illustrate the data flow.

The avionics part of the diagram is subdivided into three categories: the ground system, the external communications and the avionics on the vehicle. The latter part illustrates the interaction between all systems described in the the navigation and avionic section, Section 7.4. The weather system and the flight planning system are located in the ground segment. The flight plan is defined at the ground station and uploaded to an locally stored on the vehicle. The external communications consist of four elements: air traffic control, other aircraft in the area, GPS satellites and the GPS beacon at the landing spot. The data flow between all elements in the avionic part of the communication flow diagram can be found in Figure 8.2.

The following Figure 8.3 shows the engine part of the communication flow diagram. The autopilot square in this figure is the same as the one in Figure 8.2. The left part contains the fuel and oil systems which are all controlled by the *Engine Control Unit*. The right part is about controlling the pitch via the hydraulic system and the gearbox properties.

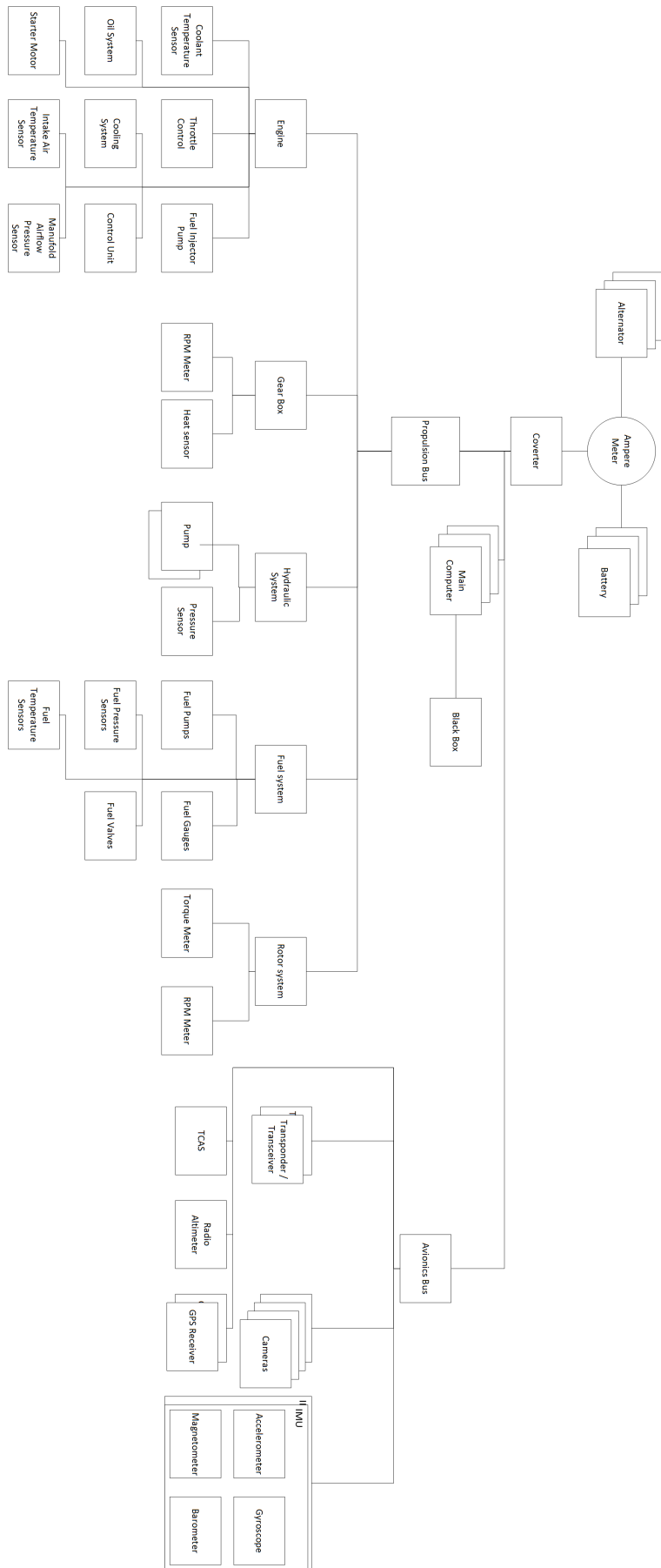


Figure 8. 1: Electrical block diagram

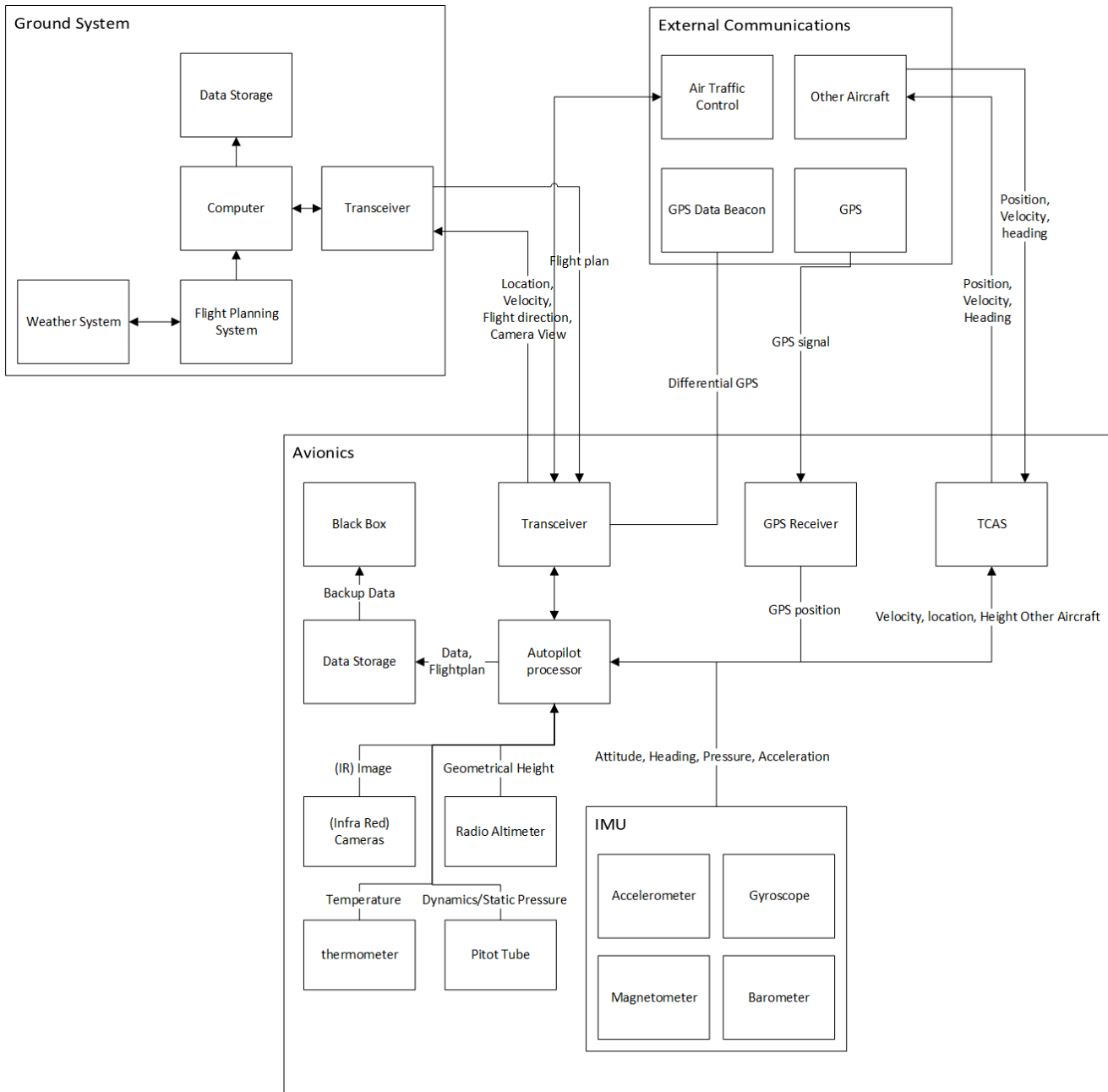


Figure 8.2: Avionics Communications Flow block diagram

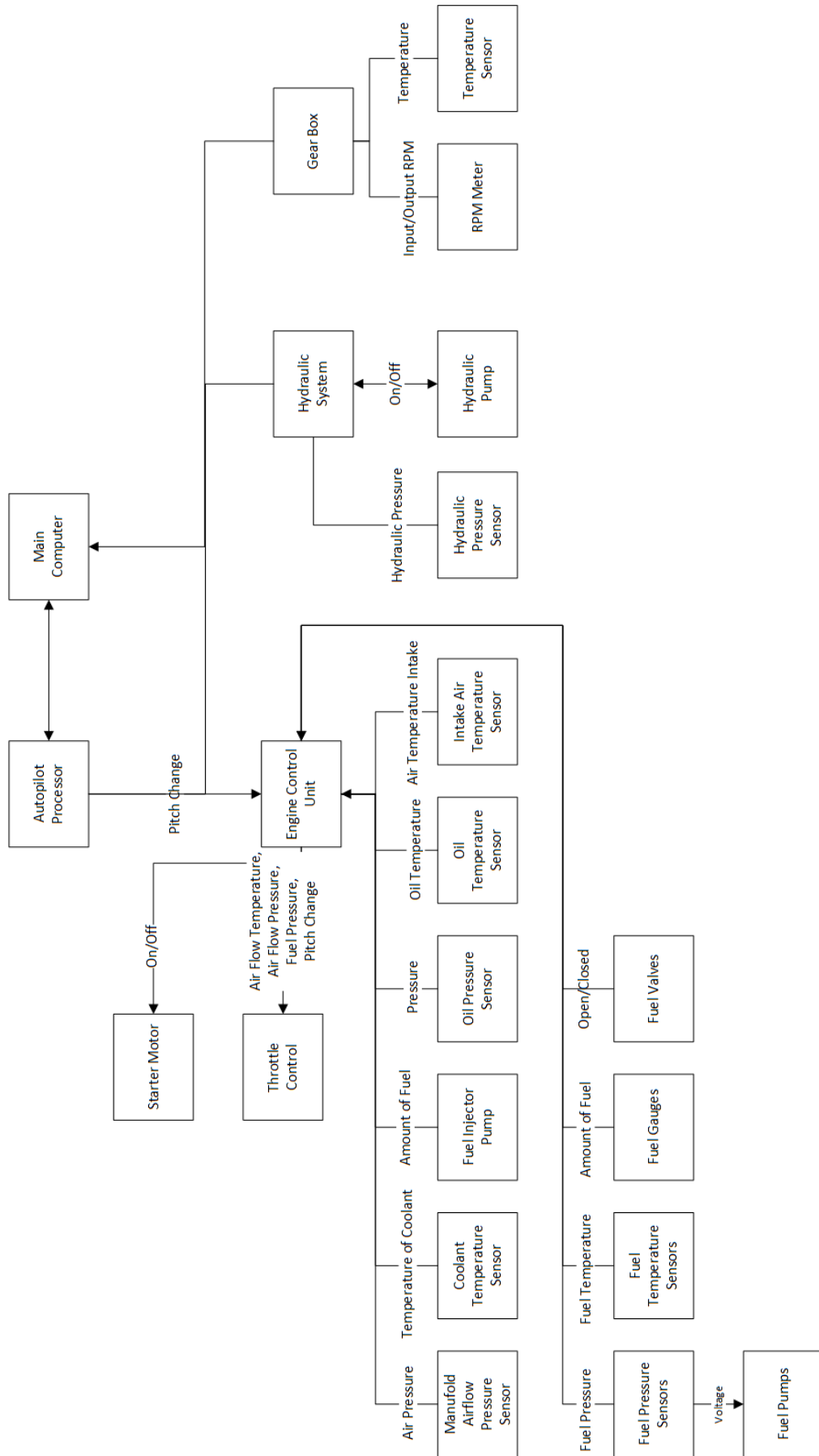


Figure 8.3: Engine Communication flow diagram

9 Risk Management

Project management is applied in the design of the HELLCAT. One of the important aspects of project management is risk management. This chapter will elaborate on the risk identification, risk assessment and risk mitigation. Especially, the mitigation of the critical risks will be discussed. This will show how it is made sure that the risks' likelihood and/or impact will be reduced.

9.1. Risk Identification and Assessment

Tables 9.1 and 9.2 show all conceivable risks divided in several categories. Furthermore, every risk has its own cause and consequence. A summary is found in the risk matrix, Table 9.3. The likelihood and impact of these risks are represented by five different levels, which are visualised by colours and abbreviations:

- Light green, very low (VL) risk.
- Green, low (L) risk.
- Yellow, medium (M) risk.
- Orange, high (H) risk.
- Red, very high (VH) risk.

The risk matrix, which can be seen in Table 9.3, provides a visual representation of the risk register. This matrix helps to quickly identify exactly which possible events pose the highest threat to the project. The possible risks are ordered on their effect (horizontally) and the probability of them actually happening (vertically). By using this matrix it is clearly displayed that catastrophic events are less likely to occur. This gives the design team the ability to engineer the system in such a way that the UAV can cope with these situations or let it behave in a way to limit the consequences. The consequences can vary from a prolonged flight time to mission failure and UAV loss. This shows that risk mitigation is an important task to address.

Table 9.1: Risk register part 1

#	Category	Cause	Risk event	Consequence	Likelihood	Impact	Mitigation	Responsible
1	External	insurgents	enemy fire	structural damage	VH	H	fly higher, structural integrity	user, design group
2		birds	bird strike	structural damage	L	H	bird control, structural integrity	user, design group
3		weather/environment	sand	structural damage	VH	M	more frequent maintenance, material choice, filter in front of engine air intakes	user, design group
4			ice	structural damage	M	M	anti-icing, preflight inspection, more frequent maintenance, material choice	user, design group
5			lightning	circuit damage/structural damage	VL	H	lightning conductor	design group
6		fluctuation energy price	higher energy price	cost increase	M	L	take risk, hedge energy price	production team
7	Commercial	change in leadership	contractual changes	delay/termination project	VL	H	solid contractual agreements	production team
8	Financial	interest rate	interest changes	decrease ROI	L	L	fixed interest rates, take risk	production team
9		currency	currency value fluctuations	increase production costs	M	L	take risk	production team
10	Communication	knowledge monopoly	loss of teammember	loss of essential knowledge	M	H	Two people involved in critical tasks	design group
11	Propulsion	engine failure	loss of lift	rotor shutdown	H	H	preflight checks, if applicable able to operate without 1 engine	user, design group
12		faulty cooling system, oil leakage	Overheated engine	rotor shutdown	M	H	preflight checks and regulated maintenance, if applicable able to operate without 1 engine	user, design group
13		fuel leakage	Fuel shortage	mission failure	M	M	preflight checks and regulated maintenance	user
14		human failure	Wrong fuel	mission failure	L	M	extensive training of ground personnel	user
15		technological dependance	Fuel pump failures	rotor shutdown	L	H	multiple fuel pumps installed	design group
16		technological dependance	Alternator failure	rotor shutdown	L	H	multiple alternators installed	design group
17		faulty cooling system, oil leakage	Gearbox overheating	rotor shutdown	M	H	preflight checks and regulated maintenance, if applicable able to operate without 1 engine	user, design group
18		technological dependance	Clutch failure	rotor shutdown	L	H	preflight checks and regulated maintenance, if applicable able to operate without 1 engine	user, design group

Table 9.2: Risk register part 2

#	Category	Cause	Risk event	Consequence	Likelihood	Impact	Mitigation	Responsible
19	Project management	wrong time assessment	scheduling problems	project delay	H	H	reallocate human resources, increased manhours, early identification of delays	design group, production team
20		driving requirements not met	design doesn't enter production	project failure	L	VH	tight communication, monitor the process	design group
21		some major requirements not met	design has to be revised	project delay, increased costs	M	H	tight communication, monitor the process	design group
22		minor requirements not met	acceptable design is reached	reduced customer satisfaction	H	L	tight communication, monitor the process	design group
23		wrong budget allocation	more expensive product	increased unit costs	H	M	early identification, tight budgetting, take risk	design group
24	Stability and control	unproven technology	RF interference	loss of ground control	L	M	proper shielding of critical components	design group
25			software failure	loss of control	L	H	intensive testing of software	design group
26			wrong flightplan	colision with building/mountain	L	VH	double check flightplan, colision detection	user, design group
27		human failure	instable loading	stability loss	L	H	preflight check, inflight identification and compensation	user, design group
28			positioning system loss	operations failure	VL	M	Choose dependable systems, have backup plan	design group
29			operating system groundstation failure	communication loss	M	H	redundancy, planned safety measures	design group
30			technological dependance	range loss	mission failure	L	M	preflight checks, if applicable able to operate without 1 engine
31	stability loss	crash		L	VH	preflight checks, if applicable able to operate without 1 engine	user, design group	

Table 9.3: Risk matrix

	Effect	VL - Insignificant	L - Minor	M - Moderate	H - Major	VH - Catastrophic
Likelihood						
almost certain to occur - VH				3	1	
H			22	23	11,19	
M			6,9	4,13	10,12,17,21,29	
L			8	14,24,30	2,15,16,18,25,27	20,26,31
rare - VL				28	5,7	

9.2. Risk mitigation

As can be seen in the risk matrix, four risks are in the critical category: the orange and red zone. This means that these risks are likely to happen and that their impact is moderate to catastrophic. Therefore, these risks need to be moved to the yellow or ideally the green zone. In order to do so an improved risk mitigation has been performed, the risk matrix after mitigation is found in Table 9.4. The three risks in the critical category are:

Risk 1: Enemy fire by insurgents

Explanation: Since the UAV will operate in hostile areas it may be subject to enemy fire. Insurgents will try to take the transport system down in order to slow down or prevent the (re)supply of the operating bases.

Mitigation: One way to minimise this is to operate at an altitude of at least 1000 meter wrt. ground, such that the UAV is not within the firing range of small arms. However, if the UAV has to climb to 1000 meter, this takes time. During this time the UAV is vulnerable to bullets. The UAV will take off and climb to 1000 meter vertically in a relatively safe environment, the harbour for example. The landing from 1000 meter altitude will also be performed vertically to fly in a relatively safe area. Use of bullet proof material, use the container as protection, vital parts on top of UAV and self healing materials are also viable options and will definitely be researched.

Risk 3: Wear due to sand

Explanation: The UAV will be operating in areas where sand is present. Therefore, the UAV will be subject to sand. Sand will have a negative impact on the structure when not taken care of. Sand will enter the engine and especially moving parts will deteriorate at a faster pace than without sand being present, because of the friction caused by the sand particles.

Mitigation: Sand filters over the air intakes will be used to prevent sand particles entering the engine. The location of the intake of the engine will be as high as possible from the ground for the same reason. Larger disc area for the rotors will also reduce the sand up-wash. these methods will lead to less wear and tear of the moving parts. Also, maintenance will be held more frequently. This way, wear can be detected at an early stage and can be taken care of. An anti-fouling coating will also be considered for certain engine parts.

Risk 11: Engine failure

Explanation: The UAV powers the rotors by using eight LT4 engines, which are normally used in cars. These engines are not certified to aviation standards. Therefore, engine failure might occur.

Mitigation: Tweaking of the engines lead to a better performance of the engines. The engines are now able to provide more power in case of an engine failure. The UAV will be able to maintain control and fulfil its mission with one failed engine.

Risk 19: Wrong time assessment

Explanation: Team members might underestimate tasks and thus postpone work to the last moment. It can also occur that members take too much time for a certain aspect of the task neglecting other aspects as a result. Difficulties can occur which cause a delay in the schedule.

Mitigation: The Gantt chart provides the allocated time, as well as a time buffer. This time can be used to finish a task that has been underestimated. Also, human resources can be moved from an easier task to the complexer task. Another option is to increase man hours (overtime) but as this puts more strain on the team this will always be a last resort.

The risks that were first in the critical category are moved to the yellow zone. Also, the *M* to *VH* zone in both categories are moved (the box indicated with the bold lines in Table 9.4). The underlined numbers show the risks that were tried to be moved. All risks were handled in this zone and were all successfully managed to either a lower likelihood or impact if not both.

Table 9.4: Mitigated risk matrix

Effect	VL - Insignificant	L - Minor	M - Moderate	H - Major	VH - Catastrophic
Likelihood					
almost certain to occur - VH			3		
H		22	1,19,23		
M		6,9	4,13	10,11,12,17,21,29	
L		8	14,24,30	2,15,16,18,25,27	20,26,31
rare - VL			28	5,7	

10 Sustainability

Considering sustainability is an important aspect during the DSE, it is covered in every aspect of the design. Additionally, special attention is paid to the End Of Life (EOL) disposal and recyclability of the materials used for the UAV treated in Section 10.1. Furthermore, topics where sustainability is considered are fuel emissions and noise reduction, which are treated in Section 10.2 and Section 10.3, respectively.

The total energy use and total CO₂-emission are also calculated using the Audit tool from the CES EduPack[12]. The results can be seen in Table 10.1 and Figure 10.1. As can be seen, a breakdown of total energy and CO₂ usage is included. They are divided into material, manufacturing, transport (of materials and parts needed for manufacturing), use (of the product) and disposal. For these computations, it is assumed that 50 products are manufactured, each having a life span of 10 years. The main structure is designed for a total of 10,000 cycles (or equivalent 5,000 flights), see Chapter 5.

10.1. End of Life Disposal and Material Recyclability

The main structure of the UAV is constructed out of aluminium. This material has some advantages when it comes to recyclability. According to [28] aluminium can be recovered easily and in near full quality. Also, the energy needed for recycling is less for aluminium compared to steel. To preserve the quality of the recycled material alloy variation is kept to a minimum. There are only a few sections on the structural beams that have joints or reinforcements of other material.

Also, when it comes to the EOL disposal of the HELLCAT, it has several unique properties. A large portion of the propulsion system elements are off the shelf. Therefore, those elements can easily be re-used in other systems. For instance: the engine used to propel the rotor blades can be refurbished and used in cars.

Using the CES EduPack tool, it can be seen that energy and CO₂ can be saved by roughly 30% if a typical mixture of recycled and virgin material is used for manufacturing the product. A recycling End-of-Life solution is able to reduce the material energy cost by 65.4% and the CO₂ emission by 59.9%.

10.2. Fuel Emissions

Minimising fuel consumption is one of the goals in a sustainable design. Not only does this conserve the limited amount of fossil fuels available on the planet, but it also reduces the emissions produced by the aircraft. Therefore, during the design constant attention is paid to minimise engine power needed.

Engine emissions are strongly linked to fuel consumption. With a chemical burning reaction fuel and oxygen react to create energy. As a consequence the fuel is, ideally, converted into carbon-dioxide and water. Even under these ideal conditions 1 kg of gasoline produces 3.07 kg of carbon-dioxide (CO₂). When comparing the SFC of the engines of the HELLCAT (GM-LT4), 0.20 Section 4.2, with an engine of a Chinook (T55-L-714A), 0.232¹, if the HELLCAT was fitted with a Chinook engine it would use 16% more fuel. For the typical mission defined in Section 3.5 the HELLCAT will consume 2,000 kg fuel producing 6,140 kg of CO₂ compared to 7,251 kg if the T-55-L-714A engine was used as the powerplant. This is an increase of 18.1% of CO₂ emission.

This increase is the result of the poorer SFC as well as the higher CO₂ emission of kerosene with respect to gasoline, 2.5 compared to 2.3 kg/L. With the use of a car engine the availability of an exhaust system including a catalytic converter is also possible. Catalytic converters can reduce NO_x concentrations over 70% in the exhaust emissions [29], thus lowering the emissions considerably.

It can be seen that the energy usage and CO₂ emission during use of the HELLCAT is the main contributor to the totals, see Figure 10.1. Only the material, use and End-of-Life are included, since the other contributions are smaller than 0.4%. All contributors are shown in Table 10.1. It can be concluded that regarding use, sustainable design is most important. Although the car engine solution already is a more sustainable solution in terms of CO₂ during use, a lot of progress can be made in this area. More

¹URL: http://www51.honeywell.com/aero/common/documents/myaerospacecatalog-documents/Helicopters-documents/T55-L-714A__CH47_Engine_.pdf [cited 8 January 2016]

sustainable fuels are recommended to investigate in the future, in order to restrict this major contributor even more.

The CO₂ emission during use of the product according to this tool is 5,820 kg per mission. This tool does not take loiter into account. However, it does take the CO₂ emission during shipment of the HELLCAT to the region of usage into account. This CO₂ emission is less than 0.6% of the total CO₂ emission during 10 years of use. If loiter time would be taken into account, this would result in a CO₂ emission of 6,693 kg. This is a good estimation, since it is almost equal to the 6,140 kg calculated earlier. It shows this tool is accurate enough, also for energy calculations.

10.3. Noise

Noise pollution is one of the aspects in a sustainable development approach. Excessive noise may affect the health and behaviour of humans and wildlife. As this project designs a VTOL vehicle with rotors it is important to look at helicopter noise reduction. The main source of helicopter noise is aerodynamic noise from the rotors, other contributors are engine noise and transmission noise.

Considering aerodynamic noise, main rotor noise control is being accomplished by careful selection of rotor blade configurations and its rotational tip speed. To achieve an acoustically desirable rotational tip speed the blade chord can be adjusted accordingly together with the number of rotor blades. Blade Vortex Interaction (BVI) noise can be the most important contributor and is the sound generated when the aerodynamic forces from a rotating blade rapidly fluctuates when interacting with the vortices developed from the tip. Diffusing or reducing the tip vortex is a method of controlling BVI noise, this is done by designing an optimal non-square tip shape that modifies the vortex structure. Other BVI noise mitigation is done by altering the distance between the vortices and blade or varying the effective blade angle of attack. [6]

Table 10.1: Table depicting the contributors to the energy and CO₂ usage.

Phase	Energy (J)	Energy (%)	CO2 footprint (kg)	CO2 footprint (%)
Material	1.02e+13	2.4	7.33e+05	2.4
Manufacture	1.25e+12	0.3	9.54e+04	0.3
Transport	9.51e+10	0.0	6.75e+03	0.0
Use	4.1e+14	97.3	2.91e+07	97.2
Disposal	5.59e+10	0.0	3.91e+03	0.0
Total (for first life)	4.22e+14	100	3e+07	100
End of life potential	-6.67e+12		-4.39e+05	

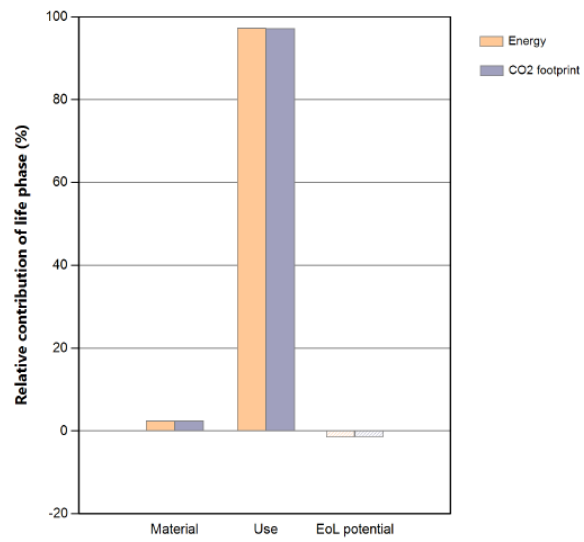


Figure 10.1: Bar chart depicting the main contributors to the energy and CO₂ usage.

11 RAMS

This chapter covers the RAMS, which stands for Reliability (Section 11.1), Availability (Section 11.2), Maintainability (Section 11.3) and Safety (Section 11.4). As is determined throughout the entire project, the engines are the most critical factor for every part of the design. This also holds for the RAMS. All the parts that are bought off-the-shelf are certified for aviation, except the engines. The structural design must also be thoroughly tested to get certified for aviation. Since certification mainly depends on the RAMS, it is added to this chapter in Section 11.5.

11.1. Reliability

The reliability of the UAV will mainly rely on the reliability of the engines, since the engines are the weakest link in the design. There is not much data available of piston engine tests, most companies that produce piston engines keep their test data classified. Therefore it is hard to estimate the engines performance over its life-time. If the engine however gets certified according to military certification standards, if necessary with some modifications, the engine is assumed to be sufficiently reliable to perform a certain amount of operating hours. And especially since the UAV is able to complete its mission and land safely when one engine fails, the reliability is assumed to be minimally as high as a standard helicopter. Actual reliability data can be gained when the engine is fully tested under circumstances that simulate this mission.

11.2. Availability

The availability of the UAV will be lower than an average helicopter. This is because the piston (car) engines should be checked more often than turboshaft engines, especially due to the larger amount of moving parts. So the expected availability will be relatively low due to a higher maintenance time and interval.

Other parts of the UAV will have the standard availability, compared to other military helicopters. The availability is limited to environmental conditions. Due to safety reasons the UAV will remain grounded during extreme cold conditions (below -30°C ground temperature), extreme heat conditions (above 45°C ground temperature), extreme winds (above 20 m/s), sand storms and thunderstorms. These constraints are purely based on the required performance characteristics of the UAV during these conditions. The effect of extreme conditions on the engine itself is unknown at this point in the design phase. The benefit of an unmanned, autonomous systems is that the UAV is significantly less dependent on availability of pilots and ground personnel.

11.3. Maintainability

The maintainability of the UAV is relatively easy compared to a standard helicopter. It has a very simple structure, namely four beams in a 'tic-tac-toe structure'. The aerodynamic fairing around the beams is easy to remove. Therefore it is easy to inspect the structure. The fairing around the engine will also be easily removable. The engine control unit will communicate with the control systems, so if there is something wrong with the engine or when scheduled maintenance is necessary the control systems will communicate that information with the ground station. The more complex part to perform maintenance on, as for every helicopter, is the rotor hub. The rotor hub requires extra attention, because of the many moving parts. However the hub for this design is relatively simple, since it only uses a collective pitch system, compared to the cyclic pitch system that most helicopters have.

The control systems are equipped with an automatic failure detection system. This system checks for failure during the entire mission, including the warm-up and cooling down of the engines. If something is wrong, the control system will automatically send a signal to the ground station. The ground station will then inform the maintenance team about the failure, such that it can be checked immediately. The control systems and their wiring are placed inside the frame of the vehicle. The sensors that require a line of sight to the ground or to the sky can be placed on under or on top of the beam. Easy access for

maintainability will be taken into account when the exact locations are determined.

The exact cost for maintaining the UAV are unknown at this point in the design stage. However a significant budget is set in the operational cost, to account for the relatively low durability of the engines. This is because most parts that are used to design this UAV are already certified for aviation use, except the engines and the structure. Therefore it is expected that the engines must be regularly checked and revised, especially compared to certified turboshaft engines.

When the UAV has encountered significant problems during flight the entire system must be revised, for example an engine failure. This is due to overloaded engines, the other engines must deliver extra power. And a significant shock load to the structure (especially the landing gear), due to a 'rough' landing.

11.4. Safety

Safety is one of the main aspects of this project. The reason to perform the mission by an autonomous aviation solution, instead of a road vehicle convoy, is because of the safety of the army personnel. Transportation over road brings a lot of risks in enemy territory. Especially nowadays, Improvised Explosive Devices (IED's) are used often by terrorists to attack ground personnel and vehicles. That makes the UAV-system solution a significantly safer option than the current way that the mission is performed.

The UAV has, for safety reasons, a lot of redundancy in its design. There are at least two parts of each separate control system built in, such that when one system completely fails, the UAV can easily switch to the other system and perform the mission as planned. Also the fuel systems are designed in such a way that when one part of it fails, the mission can still be completed.

The control systems are designed in a way such that in an emergency situation, the UAV can always land in a safe (unpopulated) area. And that it can avoid obstacles that are in its way. Also the electrical systems properly are insulated, such that they are protected from damage or wear.

Another important aspect of safety is the ground procedures. Safety procedures must be set up to guarantee the safety of the ground personnel. For example ground personnel is not allowed to be under the rotors, when they are driven by the engines. The ground personnel is only allowed at the lift-off area when all mechanical systems are shut down. This creates a safe environment for the container attachment and for the maintenance and system checks.

11.5. Certification

Certification depends mainly on the failure rate of the engine. Since there is no data available to determine the engine failure rate under the operational conditions of this mission, it cannot clearly be stated whether the UAV will get certified. Therefore the next step in the development of the HELLCAT must be testing the engines on the certification requirements. The main focus of these tests must be on the durability under hot and humid environmental conditions. These tests must determine whether the car engines can be used in the mode necessary for the HELLCAT, which is unusual compared to normal automotive use. There is no data (publicly) available to estimate the GM LT4s performance under these conditions. All other components are relatively easy to gain certification (structure) or are already certified for aviation. The control and navigation system should be designed in order to meet the military regulations. The HELLCAT is able to fly completely autonomous, including a detection and avoidance system for safety. The costs for the certification process are unknown. It is however expected that these costs will significantly contribute to the development cost.

12 Mass Breakdown of the UAV

After designing the subsystems, the mass breakdown of the entire UAV will be covered in this chapter. It provides a summary of all the masses of the different elements that are present in the HELLCAT. The breakdown is given per subsystem and the payload, fuel plus container, is added in the end. No contingency budget is needed for the payload since the container mass is constant of 5,000 kg and for the fuel calculations there are already mass reservations made. For the other subsystems a contingency value of 5%, 10%, 4% and 10% is given to the Aerodynamic, Propulsion and Power, Control and Stability and Structural subsystem respectively. This is to ensure that additional unforeseen mass contributions are still budgeted. The subsystems that make up the UAV consist of: Aerodynamics, Power and Propulsion, Structure and Control and Stability. Table 12.5 gives the total masses per subsystem. The complete mass breakdown per subsection is then given in Section 12.1, Section 12.2, Section 12.3 and Section 12.4 .

12.1. Mass Breakdown of the Aerodynamic Subsystem

The aerodynamic subsystem consists of only three main elements: the rotor blades, rotor hub and fairings. The mass contributions of these elements are depicted in Table 12.1. The sources of these masses can be found in more detail in Chapter 6.

Table 12.1: Mass breakdown of the aerodynamic subsystem

Element	Budgeted mass (kg)	Actual mass (kg)
Fairings		204
8 Rotor hubs		640
16 Rotor Blades		259
Total	900	1103

The aerodynamics subsystem mass totals at 203 kg above the budgeted mass. This unforeseen increase is mainly due to the aerodynamic fairings around the beams perpendicular to the flight direction. These fairings were larger than expected because the beams were estimated to be less high. The rotor hubs were less heavy than expected since the HELLCAT uses simple rotor hubs that only have a collective pitch control.

12.2. Mass Breakdown of the Propulsion and Power Subsystem

In Table 12.2 the individual mass contributions of the elements in the Power and Propulsion subsystem are presented. The total mass for this subsystem is 50% higher than originally budgeted. The reason for this difference lies in the fact that automotive engines were used instead of aircraft engines. The engines fitted in the UAV take up almost all the mass budget of this subsystem. Whilst car engines have a significant cost advantage over aircraft engines they are much more heavy. Also, because eight engines are used there are more elements needed as well. This also adds to the total mass.

Table 12.2: Mass Breakdown of the Power and Propulsion subsystem

Elements	Budgeted mass (kg)	Actual mass (kg)
8 engines		2,361
8 gearboxes		544
8 sprag clutches		128
8 starter engines		32
3 alternators		18
4 fuel tanks		250
16 fuel pumps		21.8
16 fuel filters		0.7
24 fuel valves		7.2
fuel line		30
8 KN air filter		8
8 high flow catalytic converter		50
8 oil system		96
Total	2400	3602.7

12.3. Mass Breakdown of the Control and Stability Subsystem

The masses of the elements necessary for stable flight, control and communication with the ground segment are listed in Table 12.3. Because this is a UAV no heavy equipment for the pilot has to be on board. The monitoring systems can be on the ground. This greatly reduces the mass of this subsystem on the HELLCAT. The most weight contribution comes from the electrical wiring and the ruggedisation of the electrical elements. For safety redundancy is applied to most of the elements. Also special attention is given to the ruggedisation to ensure the systems will not be damaged during their, potentially, rough lifetime. The total mass for this subsystem is much lower than previously estimated. This makes up for the Power and Propulsion system which is over weight.

Table 12.3: Mass breakdown of the Stability and Control subsystem

Elements	Budgeted mass (kg)	Actual mass (kg)
2 IMU (with GNSS) sensors		0.06
2 GPS antennas with anti jamming		10
4 IR sensors		0.4
4 Cameras		2.081
2 Radar altimeters		3.2
TCAS-I system		5.13
2 Communication antenna's		10
1 Data recorder/blackbox		0.12
4 Data storage devices		0
4 Autopilot computers		0.2
Ruggedisation		30
Electric wiring		10
1 Emergency beacon		0.9
2 Pitot tubes		0.1
2 Temperature sensors		0.04
Total	750	72.2

12.4. Mass breakdown of the UAV Structure

Finally the different subsystems of the UAV have to be combined in one structure. In Chapter 5 the geometry of the different elements comprising the structure are further elaborated. This section focuses on the mass breakdown of the different elements that make up this structure. Table 12.4 can be used

as an overview of individual masses of those elements. These elements are also divided in more detail in Chapter 5.

Table 12.4: Mass breakdown of the main UAV structure

Elements	Budgeted mass (kg)	Actual mass (kg)
2 Beams perpendicular to flight		729.26
2 Beams in flight direction		486.92
4 Landing gear struts		96.7
4 Shock Dampers		20.4
8 Drag struts struts		27.1
2 Landing skids		110.7
4 Connection links		19.2
4 Slugs		112
Attachment wire ropes		47.5
Total	2700	1649.8

The dimensions of the beams perpendicular and along the flight direction vary in weight, as can be seen from Table 12.4. This is mainly done to minimise their impact on the total drag of the UAV. The beams perpendicular to flight direction contribute the most to the body drag, this is further described in Section 6.3.1. To limit this drag they were given a maximum height. However this did lead to an increase in weight. It is also good to note that the beams are also subject to different loading conditions. The loads produced by the rotor are visualised in Figure 6.10 and the structural loads are mentioned in Chapter 5. Because of the lower drag impact of the members in flight direction they are allowed to be much wider and higher than the beams perpendicular to the flight direction. This lead to a lighter design for those beams.

12.5. Mass Breakdown of the UAV per Subsystem

When adding all the different elements of each subsystem together a mass breakdown per subsystem can be made. This mass breakdown is given in Table 12.5.

Table 12.5: Total mass per subsystem

Subsystem	Budgeted mass (kg)	Actual mass (kg)
Aerodynamics	900	1103
Power and propulsion	2400	3602.7
Structure	2700	1649.8
Control and Stability	750	72.7
Payload (Container + Fuel)	8250	7000
Total	15000	13744.8
Total including contingency	15000	14734

From Table 12.5 it can be concluded that the mass budget breakdown made in [2] is not consistent with the actual mass breakdown. This shows how little knowledge is available in the field of heavy lifting UAV's. However the total mass of the HELLCAT, with a contingency value of 15%, is close to the value set at 15,000 kg. This is mainly due to a lower mass for the Control and Stability subsystem. Also because a very lightweight structure could be made, the total mass, including 15% contingency was kept under the budgeted mass.

13 Cost Analysis

This chapter provides the cost analysis of the HELLCAT. This cost analysis summarises all the costs that must be made in order to create a fully functional UAV. The costs of each (sub-) part of the UAV are listed first in Section 13.1. Afterwards, this chapter gives an overview of all the costs combined, including the maintenance, development and production cost. The operational costs are summarised in Section 13.2. The development and production cost are treated together in Section 13.3. The estimated unit price is compared to the market Section 13.4.

13.1. Cost Breakdown

In this section, all estimated costs for materials and off-the-shelf subsystems are listed in a cost breakdown, Table 13.1. Subtotals are listed for the Structures (Chapter 5), Propulsion and Power (Chapter 4), Aerodynamic (Chapter 6) and Control and Operations (Chapter 7) subgroups. The total budget is set at 570,000 EUR, the estimated unit costs from the Mid-Term report. To provide room for additional unforeseen costs, a contingency factor of 15% is added to the estimated costs.

Table 13.1: Cost Breakdown

Group	System	Budget (€)	Estimated cost (€)
Aerodynamics	16 x Rotor blade		16,952
	8 x Rotor hubs		40,000
	Fairings		554
	Subtotal Aerodynamics	114,000	57,506
Propulsion	8 x Engine		114,342
	8 x Gearbox		28,000
	8 x LT4 starter		1,088
	16 x Fuel pump		4,000
	4x Fuel Tank		8,000
	8 x Engine Controller		16,000
	8 x KN air filter		600
	8 x Exhaust system		2,400
	8 x Sprag clutch		1,760
	3 x Alternator		2,700
	3 x Battery		1,200
	16 x Fuel filter		160
	24 x Fuel valve		600
	Fuel line (200m)		1,200
	8 x Oil system + Acce		6,400
8 x Performance kit		23,960	
	Subtotal Propulsion	228,000	212,410
Control	2 x IMU (with GNSS)		9,200
	2 x GPS antenna with anti jamming		1,840
	4 x Cameras		5,520
	4 x IR sensors		11,040
	2 x Radar altimeter		11,592
	2 x Atmospheric sensors		37
	2 x Communication		9,200
	1 x TCAS-I		20,046
	Cables and wires		500
	1 x Data recorder / black box		350
	4 x Auto Pilot		147
	4 x Data storage		64
	Ruggedisation		3,000
	1 x Emergency beacon		501
	2 x Pitot tube		46
	Subtotal Control	114,000	73,083
Structures	Attachment rope		2,350
	Slugs		503
	4 x Connection link		202
	Estimation total structure (material cost)		14,711
	4 x Shockdampers		1,487
	Production estimation		73,555
	Subtotal Structures	114,000	92,808
	Total	570,000	435,808
	Total including 15% contingency	570,000	501,179

13.2. Operational Cost

The operational costs are mainly determined by the fuel costs. These are calculated in Section 4.2.3. Since the maintenance costs are not exactly known, a certain budget is left in the operational cost breakdown which is expected to be sufficient. Compared to the operational cost breakdown from the Baseline Report, the percentages have changed. This is because the cost for fuel are estimated to be significantly lower due to an optimised performance model. This leaves more budget for maintenance.

Table 13.2: Operational Cost Breakdown

Cost Driver	Percentage (%)	Cost per Mission (€)	Operational Cost (€/kg/100kg)
Fuel	45	1,125	0.09
Scheduled Maintenance	12.5	312.5	0.025
Unscheduled Maintenance	12.5	312.5	0.025
Spare Parts	30	750	0.06
Total	100	2500	0.20

13.3. Development and Production Cost

Cost estimations in general are called Cost Estimating Relationships (CER). To estimate the costs of the entire project, the DAPCA IV model from the book *Aircraft Design A Conceptual Approach* [7], is used. This is a statistical model that uses known data from aircraft. In general the DAPCA method is the most accurate CER, especially for military aircraft, because it uses data from the widest range of aircraft.

The model consists of the Research, Development, Test and Engineering costs (RDT&E) and the production costs. In the DAPCA model, both are combined in the different cost drivers. This is because it is hard to make a clear distinction between the two, especially in the areas of engineering and prototyping. Because the RNLAf has made a clear distinction between the two, estimations have been made in the DAPCA model for this design, to what extent certain cost drivers contribute to development or production cost. Therefore the Production Development Factor (PDF) is added. This factor is the amount of hours in a certain cost driver, that is spent on development in that area. This factor is applied to the manufacturing-, tooling- and quality control hours. For the engineering hours, $(1 - \text{PDF})$ is applied.

DAPCA estimates the hours that are needed for engineering, tooling, manufacturing and quality control groups. These are multiplied by the estimated hourly rates for each specific process. Then the development support, flight test and manufacturing costs are estimated directly. The input values for the DAPCA IV model are stated in Table 13.3. The production development factor is an estimation which part of the production costs, are part of the RDT&E cost. The results of the DAPCA IV model are shown in Table 13.4.

Because this design is less complex than a full size aircraft, another factor is added to the model. This is called the Product Complexity Factor (PCF). This factor compensates for the simplicity of this design and is applied to the material-, manufacturing-, tooling- and quality control costs. The estimated hourly rates of the different groups are the estimated salaries (before taxes) of the employees, times three. These rates are tripled to account for other costs of the employer and for supporting personnel, like managers and administrative support.

Table 13.3: Input Variables DAPCA IV method

Variable	Value	Cost Driver	Value
Operational Empty Weight	7,500 kg	Engineering rate	100 €/hr
Maximum velocity	45 m/s	Tooling rate	60 €/hr
Production quantity	50	Quality control rate	60 €/hr
Number of flight test prototypes	5	Manufacturing rate	60 €/hr
Number of engines per vehicle	8	Engine cost	€ 29,000
Production Development Factor	0.2	Avionics cost	€ 80,000
Product Complexity Factor	0.2	Material cost	€ 50,000

Table 13.4: Results of the DAPCA IV method

Cost Driver	Hours Spent	Value
Engineering	920,000	€ 92,300,000
Tooling	140,000	€ 8,400,000
Manufacturing	450,000	€ 26,800,000
Quality Control	34,000	€ 2,000,000
Development support		€ 6,600,000
Flight tests		€ 7,900,000
Materials		€ 2,500,000
Avionics		€ 48,000,000
Engine		€ 11,600,000
Total		€ 162,000,000
RDT&E		€ 96,000,000
Unit Cost		€ 1,300,000

The unit cost will decrease when the production quantity is larger. When this method is applied for different quantities, the results are shown in Figure 13.1. It can be seen that the more UAVs are produced, the lower the unit cost will be. Also the development costs will be relatively lower (per unit). A change in the value for the PDF will not change the total cost. But the higher this value, the higher the unit cost and the lower the development cost. For example when the PDF is set at 0.4, the unit cost is € 1.55 million and the development cost is € 85 million. When the PCF is changed, the total cost do change. The results for this can be seen in Table 13.5.

PCF	Development Cost (million €)	Unit Cost (million €)
0.1	92	1.0
0.2	96	1.3
0.3	100	1.6
0.4	103	1.9
0.5	107	2.2

Table 13.5: Sensitivity PCF

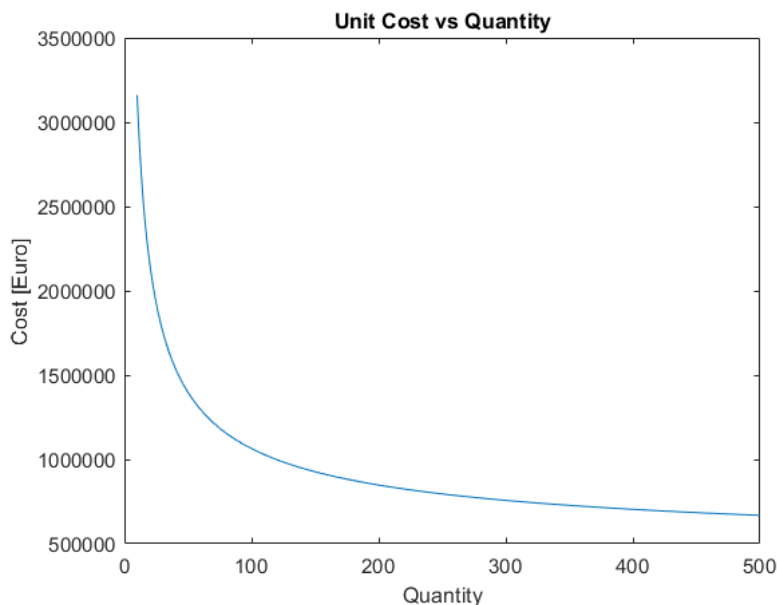


Figure 13.1: Unit Cost vs Production Quantity

13.4. Market Analysis

When this project will actually be realised, the RNLAf will not be the only user. To make the entire project profitable, the UAV must be sold to other governments. In the Baseline Report an extensive market analysis has been done. By analysing the payload, range and the unit price of competitive aircraft, the market price was estimated at 8.84 million euros.

After the detailed design phase, the unit price including the production cost is currently estimated to be 1.3 million euros for a production volume of 50. To see how this compares to the competition, all produced aircraft from the Baseline Review are listed in Table 13.6. The conceptual aircraft are left out, since their data is less reliable. Furthermore, it should be noted that in order to compare the HELLCAT with the competitors, its range in this section is set at 500 km, the distance it can fly without refuelling.

From Table 13.6 it can be concluded that the closest competitor of the HELLCAT is the Kamov Ka-32A. From the competitive aircraft, the Kamov Ka-32A has the lowest unit price and the lowest unit price per payload range. Comparing the HELLCAT to the Kamov shows that the HELLCAT's unit price is more than 4 times as low, while having an almost equal payload and range. This indicates that the HELLCAT is a relatively cheap alternative to current vehicles that are capable of air transporting cargo in combination with VTOL.

Table 13.6: Market Analysis

Name	Load (kg)	Range (km)	Unit price (€ million)	Unit price / (Payload x Range) (€/(kg x km))
HELLCAT	5,000	500	1.3	0.52
Kamov Ka-32A	5,000	538	5.94	2.21
K-max	2,722	500	7.31	5.37
Sikorsky CH-54 Tarhe	9,072	370	11.88	3.54
(Unmanned) UH-60L Black Hawk	4,100	511	15.54	7.42
Eurocopter AS532 Cougar	4,650	573	19.19	7.20
CH-47 Chinook	10,886	370	27.24	6.76
NHindustries NH90	4,200	1,000	38.39	9.14
Bell-Boeing V-22 Osprey	6,800	792	65.81	12.22
Sikorsky CH-53K King Stallion	15,900	852	84.82	6.26

14 Post DSE

After the Design Synthesis Exercise has ended, there is still some work to be done in order to get the Octocopter flying. This chapter shows a possible scenario to accomplish a fully working fleet of Octocopters. Section 14.1 covers the project design development logic and Section 14.2 shows the Gantt chart.

14.1. Project Design Development Logic

Figure 14.1 shows the project design development logic. It contains the steps that need to be taken in order to get a fully operational rotorcraft. The next design step has three main phases. In the first phase all subsystems are designed more in-depth. The design up to this phase was to examine the feasibility of this concept. It is also important that the engines are properly tested, as these are the most critical part of the system. The development of the autopilot system is the next important step. There does not exist a rotorcraft that is similar to this design and therefore an extensive study to the stability of the UAV must be done. In order to reduce the development cost, the RNLAf could incorporate other countries or businesses at this stage. After ordering and manufacturing all the parts the next phase is assembly and testing of all the subsystems and eventually the prototype. After all the testing there should be a design review. This review must evaluate the (sub-)systems and the overall design. If necessary changes have to be made. After all the test flights and component-testing is done, the UAV should get a proper certification. Also from this point the properties and characteristics are known so the UAV could be marketed. During the post development phase the craft is in its operational life, but should still be monitored, reviewed and possibly receive upgrades.

14.2. Gantt Chart

The Gantt Chart shows the steps that need to be taken, in order to finish the design. It is shown in Figure 14.2. The chart shows the estimate time to finish certain parts. The days in the chart show the maximum time that may be spent on the tasks.

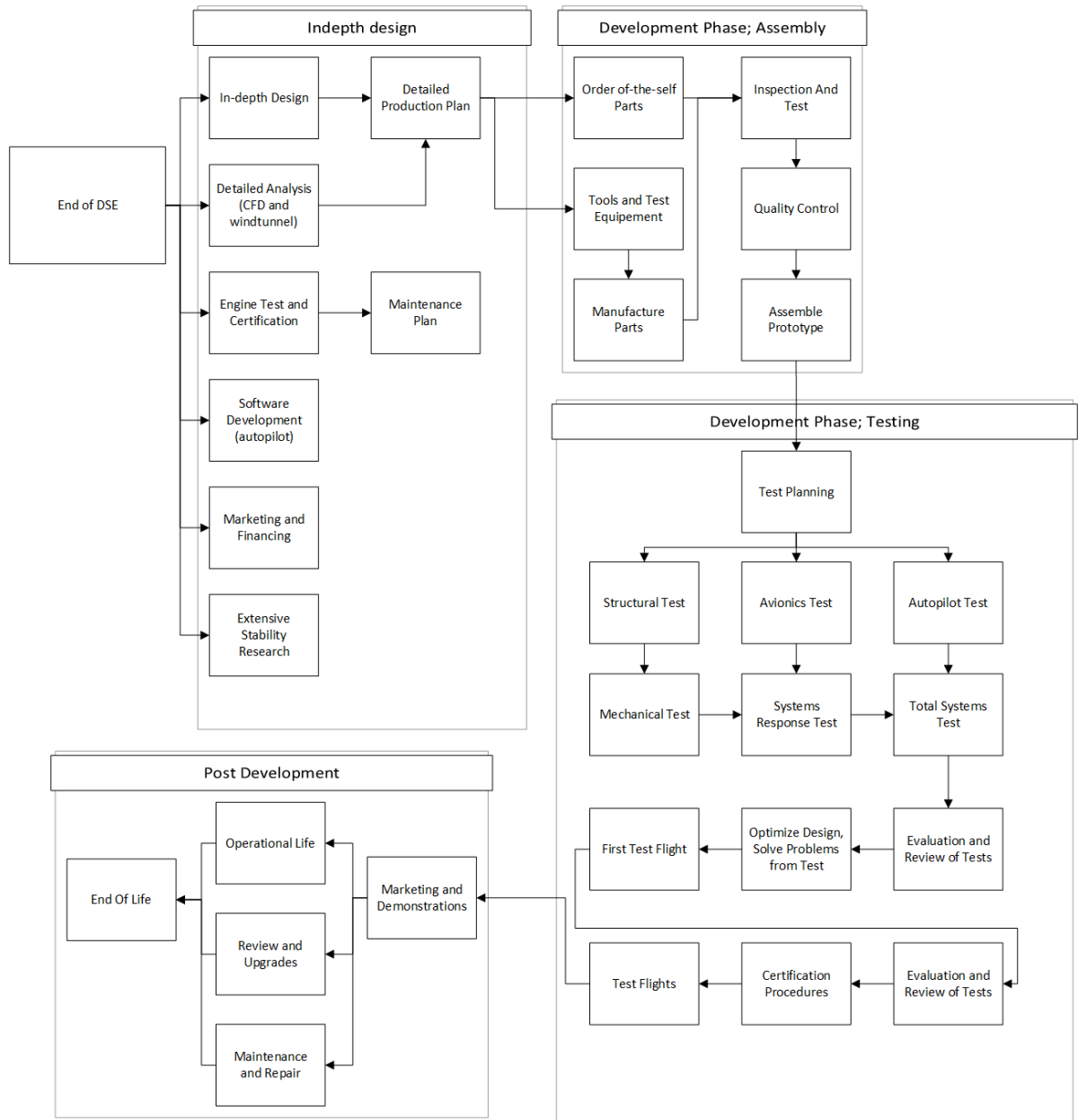


Figure 14.1: Project Design Development Logic, showing the steps after the DSE has ended

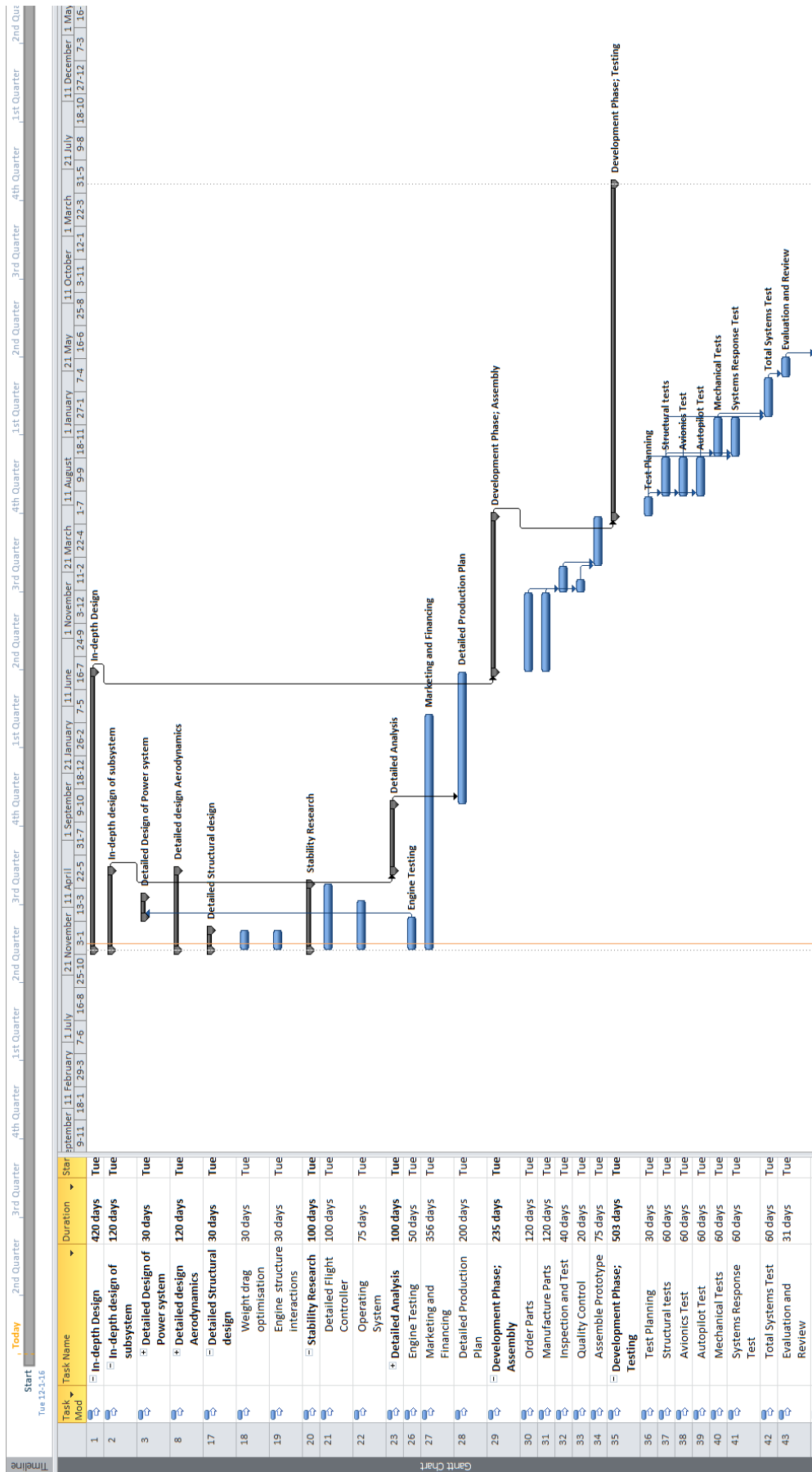


Figure 14.2: Gantt chart showing the tasks to be done after the DSE

15 Compliance Matrix and Feasibility Analysis

The compliance matrix is provided in Tables 15.1 to 15.5 and shows whether a requirement is met or not. If relevant, the table shows the actual value the design meets. The comment section is used to explain why the requirement is not met.

Table 15.1: Requirements Compliance Matrix 1

Category ALC-	Requirements	Actual value	Compliance	Comment
PLO-WEI-01	The aircraft shall be able to lift 5,000 kg of payload		✓	-
PLO-WEI-02	The aircraft shall be able to lift non-uniform loaded containers		✓	-
PLO-CON-01	The aircraft shall be able to attach a 20 ft standard container		✓	-
PLO-CON-02	The aircraft shall be able to attach the payload within 120 s		✓	Attachment can be done quickly with lifting lugs
PLO-CON-03	The aircraft shall be able to detach the payload within 60 s from threshold height		✓	Detachment can be done quickly with lifting lugs
FLC-FDY-01.1	The aircraft shall be longitudinally stable		✓	-
FLC-FDY-01.2	The aircraft shall be laterally stable		✓	-
FLC-FDY-02	The aircraft shall be able to perform a rate one turn		✓	-
FLC-FPE-01	The aircraft shall have a ground speed of at least 40 km/h during cruise	151 km/h	✓	-
FLC-FPE-02	The aircraft shall provide enough forward thrust to sustain at least 40 km/h		✓	-
FLC-FPE-03	The aircraft shall have a minimum service ceiling of 2,000 m	4,450 m	✓	-
FLC-FPE-04.1	The aircraft shall be able to transport a payload over 250 km and return without		✓	-
FLC-FPE-04.2	The aircraft shall be able to fulfil the mission without refuelling		✓	-
FLC-FPE-05	The aircraft shall have a rate of climb of at least 8 m/s		✓	-

Table 15.2: Requirements Compliance Matrix 2

Category ALC-	Requirements	Actual value	Compliance	Comment
FLC-FPE-06	The aircraft shall have a minimum lift of 147150 N		✓	-
FLC-FCO-01	The aircraft shall be able to take off vertically		✓	-
FLC-FCO-02	The aircraft shall be able to land vertically		✓	-
FLC-FCO-03	The aircraft shall be autonomous		✓	Cable attachment is not autonomous
FLC-FCO-04	The aircraft shall be unmanned		✓	-
FLC-FCO-05	The aircraft shall have a landing accuracy of 0.5 m		X	4 m with the current autopilot, can be improved by tuning the controller
FLC-FEN-01	The aircraft shall have a geometric cruise altitude of at least 1,000 m		✓	-
FLC-FEN-02	The aircraft shall be able to climb to 1,000 m from ground level within 200 s		✓	-
FLC-FEN-03	The aircraft shall be able to descent from 1,000 m within 200 s		✓	-
RAM-SAF-01	The aircraft shall have a loiter time of 900 s		✓	-
RAM-SAF-02	The aircraft shall have a collision warning system		✓	-
RAM-SAF-03	The aircraft shall have a manual override capability		✓	-
RAM-SAF-04	The aircraft shall be able to withstand lightning strikes		◦	Not yet investigated, but can easily be solved
RAM-SAF-05	The aircraft shall have an emergency beacon lasting for 7 days		X	Emergency beacon active for at least 50hours
RAM-SAF-06	The aircraft shall have predefined emergency landing locations		✓	-
RAM-MAI-01	The aircraft shall be maintainable in remote locations		✓	-
RAM-AVA-01	The aircraft shall have an availability of 95%		X	Depends on engine reliability

Table 15.3: Requirements Compliance Matrix 3

Category ALC-	Requirements	Actual value	Compliance	Comment
RAM-REL-01	The aircraft shall have a redundant altitude determination		✓	-
RAM-REL-02	The aircraft shall have a redundant attitude determination system		✓	-
RAM-REL-03	The aircraft shall have a redundant navigation system		✓	-
SYS-NAV-01	The aircraft shall have a navigation system		✓	-
SYS-NAV-02.1	The positioning system shall be accurate within 10 cm during payload delivery		✓	-
SYS-NAV-02.2	The positioning system shall be accurate within 10 m during cruise		✓	-
SYS-COM-01	The aircraft shall have a communication system		✓	-
SYS-COM-02	The aircraft shall be able to communicate telemetry		✓	-
SYS-COM-03	The aircraft shall have continuous communication during mission		✓	-
SYS-DAT-01	The aircraft shall have a data handling system		✓	-
SYS-DAT-02	The aircraft shall have a system check		✓	-
SYS-DAT-03	The aircraft shall provide atmospheric properties data		✓	-
SYS-ATT-01	The aircraft shall have an attitude control system		✓	-
SYS-ALT-01	The aircraft shall have an altitude control system		✓	-

Table 15.4: Requirements Compliance Matrix 4

Category ALC-	Requirements	Actual value	Compliance	Comment
SYS-POW-01	The aircraft shall have a power system		✓	-
SYS-POW-02	The aircraft shall provide enough electrical power for systems		✓	-
SYS-POW-03	The aircraft shall provide enough mechanical power for systems		✓	-
SYS-THE-01	The aircraft shall have a thermal control system		✓	Only the engines have thermal control
SYS-THE-02	The thermal control system shall maintain a temperature within the operational range		✓	-
ENV-WEA-01	The aircraft shall be able to maintain control during a wind gust of 12.5 m/s		✓	
ENV-WEA-02	The aircraft shall be able to operate during precipitation		✓	-
ENV-WEA-03	The aircraft shall be able to cope with sandy conditions		✓	-
ENV-WEA-04	The system shall be able to cope with ice accumulation		✓	-
ENV-WEA-05	The aircraft shall be able to withstand temperatures ranging from -50 °C to 60 °C		X	Yes for -30 °C to 60 °C
COS-01	The unit price shall be no more than € 500,000		X	Cost breakdown estimates unit price at 1.3 million
COS-02	The operational costs shall be no more than 0.25 €/kg/100 km	0.20 €/kg/100 km	✓	-
COS-03	The development costs shall be within the Royal Netherlands Air Force development budget		◦	development cost estimated at 96 million. It is up to them if it is within budget
REG-EMA-01	The aircraft shall comply with EMACC		◦	Not within the scope of this project
REG-STA-01	The aircraft shall comply with STANAG 4586		◦	Not within the scope of this project

Table 15.5: Requirements Compliance Matrix 5

Category ALC-	Requirements	Actual value	Compliance	Comment
SST-01	The aircraft shall have an end of life solution		✓	-
SST-02	The system shall have an operational life of 15 years		◦	Depends on number of flights. Structure is designed for 5000 missions
SST-03	Materials used shall not be hazardous to the environment		✓	-
SST-04	Materials used shall be recyclable		✓	The main structure is made from aluminium and is easily recyclable
SST-05	Materials shall be durable		✓	-
SST-NOI-01	The Noise level shall be less than 120 dB during take-off and landing		◦	Not within the scope of this project
SST-NOI-02	The Noise level shall be less than 100 dB during cruise.		◦	Not within the scope of this project
SST-EMI-01	The aircraft shall have a CO_2 emission less than 7,774 kg per mission	6,140 kg	✓	-
SST-EMI-02	Shall comply to EU Emissions Trading System for aviation		✓	-
SCH-LOA-01	The aircraft shall not exceed a load factor of 3g in magnitude		✓	-
SCH-DIM-01	The aircraft shall have a maximum length of 35 m		✓	-
SCH-DIM-02	The aircraft shall have a maximum width of 35 m		✓	-

16 Conclusions

This report presents the process of the detailed design, which results in an airborne solution exclusively designed to autonomously transport a standard 20 ft. container. The designed aircraft will be used in military operations to save time and increase the safety of transportation.

The final design features a tic-tac-toe structure in combination with eight V8 powered rotors. The structure is designed to be simple and light, while still being able to attach the containers. It consists of four beams with an engine at each end. All engines are equally spaced, which leads to the advantage of being able to maintain control more easily in case of an engine failure. Another advantage of this structure is that a single engine failure will not lead to a large torque, because the single beam is intersected twice with at least 2 times the rotor radius of length in between them. The simplicity of the structure also leads to a decrease in cost. The attachment of the container is done by using four cables, which are connected at the intersection points of the beams. The advantages are a lightweight and low cost connection system. Furthermore, cables are easy to use by ground personnel and can be replaced quickly. Each rotor system has two composite rotor blades, which have a radius of 4 m and a chord length of 0.3 m. The rotor blade consists of the Boeing VR-12 airfoil inboard, while the thinner VR-14 airfoil is used near the tip. Collective pitch is used to change the pitch angle of a rotor blade. Fairings are used to reduce the drag of the perpendicular beams and the engines.

The engines used to power the rotors are eight LT-4 General Motor Generation V Small-Block 6.2L supercharged V8 engines, each generating 650 hp and weighing 295 kg. The fuel for the engines is stored in four separate bladder fuel tanks on the intersection points of the beams. The fuel used is premium gasoline. An exhaust system is connected to the engine to reduce the harmful emissions. The service ceiling is 4450 m. The aircraft will be able to fly even higher when the forward velocity is increased. The Hellcat will have a speed of 42 m/s during cruise. The contribution of the fuel costs to the operating costs is 0.10 €/kg/100 km. The HELLCAT has a maximum ferry range of 700 km.

Simulink, which is part of the MATLAB environment, is used to simulate the HELLCAT. Stability of the HELLCAT is achieved by using active rotor pitch control. For the scope of this stability study an incremental PID with second derivative (PIDD) controller using gain scheduling was implemented, mainly because of the relative ease of tuning and implementation. This controller results in a stable flight system which can rotate around all axes, perform stable step and ramp responses (without overly exciting the engines) and perform all manoeuvres that could be asked by the navigation and position controller. The current controller is responsive enough to cope with an engine failure and remain stable. To avoid collisions a Traffic Alert and Collision Avoidance System is used.

It can be concluded that the HELLCAT is a very innovative design. Its main strengths are a low unit cost made possible by the simplicity of the design, as well as its operational ease of use. It is something that has never been done before and therefore a great opportunity for the future of military transportation.

17 Recommendations

Throughout the initial design phase, a lot of obstacles were tackled and a lot of details were analysed. However in each design process but even more so in the short time window this design was created in, some properties have to be left for further research. This chapter will discuss the properties that weren't thoroughly analysed and the further research that should be conducted to improve upon the HELLCAT design.

It is recommended to rigorously test the engine in order to get the HELLCAT certified. This testing is not within the scope of this design phase. However, it should be prioritised in the next phase, as this design depends on these powerful but relative cheap engines. The fuel system should be worked out in a more detailed manner. The aerodynamic performance can be further improved by investigating the wake interactions using Computational Fluid Dynamics. This way, the aerodynamic properties will be more accurate and realistic. Also, the shape of the fairing could be optimised for drag reduction by using CFD. Research should be done to see if tapering can be applied to the beams in order to reduce the drag. It will have to be evaluated what effect this has on parameters like structural weight, manufacturing costs and fuel costs. A retractable landing gear will also be a highly effective method to reduce the total aerodynamic drag. Induced and profile power during hovering might be reduced by increasing the rotor blade taper ratio[26], which should be investigated in the next phase. Furthermore, a wind tunnel test should be conducted to validate the design.

Furthermore, an autopilot, capable and certifiable to perform all required missions, manoeuvres and emergency operations should be developed. Additional surrounding awareness systems could be installed to further increase the autonomy level of the system. This will result in a higher total avionics price. A Light Detection And Radar (LIDAR) could be used for precise, real time 3D mapping. This would be beneficial for cruise, take-off and landing. The LIDAR system can be used to autonomously identify an emergency landing spot or fly around encountered buildings. Furthermore, 3D maps could be pre-loaded and landing spots could be recognised by the system without the use of beacons.

Bibliography

- [1] Aalbers, H., Doedijns, A. D., Dutrieux, S. C. M., Van Kester, J. A. M., Krijnen, H. H., Nieuwenhuisen, K. B. E., Star, J. Q., Van Steijn, F. P., Van der Sommen, R. P. M., Tluk, A. J. and Wiskie, R. A. A., "Project Plan AE3200 DSE," Faculty of Aerospace Engineering, TU Delft, Delft, Nov. 2015.
- [2] Aalbers, H., Doedijns, A. D., Dutrieux, S. C. M., Van Kester, J. A. M., Krijnen, H. H., Nieuwenhuisen, K. B. E., Star, J. Q., Van Steijn, F. P., Van der Sommen, R. P. M., Tluk, A. J. and Wiskie, R. A. A., "Baseline Report AE3200 DSE," Faculty of Aerospace Engineering, TU Delft, Delft, Nov. 2015.
- [3] Aalbers, H., Doedijns, A. D., Dutrieux, S. C. M., Van Kester, J. A. M., Krijnen, H. H., Nieuwenhuisen, K. B. E., Star, J. Q., Van Steijn, F. P., Van der Sommen, R. P. M., Tluk, A. J. and Wiskie, R. A. A., "Mid-term Report AE3200 DSE," Faculty of Aerospace Engineering, TU Delft, Delft, Dec. 2015.
- [4] Torenbeek, E. "Synthesis of Subsonic Airplane Design," Delft University Press, Kluwer Academic Publishers, 1982.
- [5] Johnson, W., "Helicopter Theory," Dover Publications Inc., 1980.
- [6] Edwards, B. and Cox, C., "Revolutionary Concepts for Helicopter Noise Reduction - S.I.L.E.N.T. Program", Bell Helicopter Textron Incorporated Report 699-099-529, 23 Feb 2001.
- [7] Raymer, Daniel P., "Aircraft Design: A Conceptual Approach," American Institute of Aeronautics and Astronautics, 1992.
- [8] Hendricks, E. S. , Tong, M. T., "Performance and Weight Estimates for an Advanced Open Rotor Engine," NASA Glenn Research Center, Cleveland, Ohio, 2012.
- [9] MATLAB, Mathworks, Software Package, Version R2015b (64-bit), 2015.
- [10] Van Holten, Th. and Melkert, J.A., *Helicopter Performance, Stability and Control*, TU Delft, Delft, Nov. 2002.
- [11] Ashby, M. F., *Material Selection in Mechanical Design*, 4th ed., Elsevier Ltd, Burlington, 2011, Chap. 5.
- [12] CES EduPack, Software Package, Ver. 15.3.10, Granta Design, Cambridge, 2015.
- [13] Python, Anaconda Python 3, Software Package, Ver. 2.4.1 (64-bit) Python 3.5.1, Continuum Analytics, Austin, 2015.
- [14] CATIA, Software Package, Ver. V5 R21, Dassault Systèmes, Vélizy-Villacoublay, 2013.
- [15] Military Airworthiness Authorities Forum, "European Military Airworthiness Certification Criteria (EMACC)," European Defence Agency, Edition: 2.1, Oct. 2015.
- [16] Przemieniecki, J. S., *Aircraft Landing Gear Design: Principles and Practices*, Third printing, AIAA Education Series, American Institute of Aeronautics and Astronautics, Inc., Washington, D.C., 1988.
- [17] Megson, T. H. G., *Aircraft Structures for Engineering Students*, Fourth Edition, Elsevier Aerospace Engineering Series, Elsevier Ltd., Oxford, 2007
- [18] Kania, W., Stalewski, W., Zwierzchowska, B., "Design of the Modern Family of Helicopter Airfoils," Institute of Aviation.
- [19] Lin, T., Lee, J., Lwin, T., "Integrated approach for rotor blade manufacturing cost estimate," *Aircraft Engineering and Aerospace Technology*, Vol. 83 Iss 4 pp. 235 - 244.
- [20] Rosko, A., "Experiments on the flow past a circular cylinder at very high Reynolds number," Guggenheim Aeronautical Laboratory, California Institute of Technology, Pasadena, California, November 1960.
- [21] Rosko, A., "Tests of the NACA 0025 and 0035 Airfoils in the Full-Scale Wind Tunnel," National Advisory Committee for Aeronautics. Langley Aeronautical Lab.; Langley Field, VA, United States, Report No. 708 1941.
- [22] Hoerner, S. F., "Fluid-Dynamics Drag," Hoerner Fluid-Dynamic, Vancouver, 1965.
- [23] Crosek, "Theory of Sailing," Spring, 1925.
- [24] "Helicopter Flying Handbook," Federal Aviation Administration, Oklahmoa City, 2012.
- [25] Wahab, A. A., Hafiz Ismail, M., "Estimating Vertical Drag on Helicopter Fuselage during Hovering," Aeronautical and Automotive Dept., Faculty of Mechanical Engineering, Universiti Teknologi Malaysia, 81310 Skudai, Johor, Malaysia.

- [26] Walsh, J. L., "Performance Optimization of Helicopter Rotor Blades," NASA Langley Research Center, Hampton, 1991.
- [27] Amzajerjian, F., Pierrottet, D., Petway, L., Hines and G., Roback, V., "Lidar systems for precision navigation and safe landing on planetary bodies," NASA Langley Research Center, NF1676L-12532, Hampton, VA, May 2011.
- [28] Daniel Carle, Gordon Blount., "The suitability of aluminium as an alternative material for car bodies," *Materials and Design*, Vol. 20 1999 pp. 267 - 272.
- [29] Norbert V. Heeb, Anna-Maria Forss, Christian Bach, Peter Mattrel, "Velocity-dependent emission factors of benzene, toluene and C2-benzenes of a passenger car equipped with and without a regulated 3-way catalyst," *Atmospheric Environment*, Vol. 34 2000 pp. 1123-1137.
- [30] P. Simplicion , M.D. Pavel, E. van Kampen, Q.P. Chu, "An acceleration measurements-based approach for helicopter nonlinear flight control using Incremental Nonlinear Dynamic Inversion," Delft University of Technology, Faculty of Aerospace Engineering, 2011.
- [31] S. Sieberling, Q. P. Chu, and J. A. Mulder, "Robust Flight Control Using Incremental Nonlinear Dynamic Inversion and Angular Acceleration Prediction," Delft University of Technology, Faculty of Aerospace Engineering, 2010.